SCUOLA DI DOTTORATO
UNIVERSITÀ DEGLI STUDI DI MILANO-BICOCCA

Department of Surgery and Translational Medicine

PhD program in Neuroscience Cycle XXIX

CHRONIC PAIN EVALUATION IN ANIMAL MODELS OF OSTEOARTHRITIS: BEHAVIOURAL AND PHARMACOLOGICAL CONSIDERATIONS.

Surname: Comi Name: Eleonora

Registration number: 720663

Tutor: Lanza Marco

Coordinator: Cavaletti Guido Angelo

ACADEMIC YEAR 2015/2016

Table of contents

1. LIST OF ABBREVIATIONS 4
2. ABSTRACT 9
3. INTRODUCTION 12
3.1. OSTEOARTHRITIS 13
3.1.1 Definition and classification 13
3.1.2 Epidemiology and risk factors 15
3.1.3 Knee osteoarthritis 17
3.1.4 Diagnosis 20
3.1.5 Immunopathogenesis of osteoarthritis 22
3.1.6 Pain in osteoarthritis 26
3.1.6.1 Pain definition and mechanisms 26
3.1.6.2 OA pain 29
3.2 ANIMAL MODELS OF OSTEOARTHRITIS 32
3.2.1 The MMT model 34
3.2.2 The MIA model 35
3.3 OSTEOARTHRITIS THERAPY 36
3.3.1 Non-pharmacological therapies 37
3.3.2 Pharmacological therapies 38
3.4 IMIDAZOLINE RECEPTORS 41
3.4.1 Imidazoline-2 receptors ligands and analgesia 43
3.5 CR4056 45
3.5.1 IN VITRO pharmacology 46
3.5.1.1 Binding to imidazoline-2 receptors 46
3.5.1.2 Binding and functional activity assays on monoamine oxidases 47
3.5.2 IN VIVO pharmacology 48
3.5.2.1 EX-VIVO evaluation of endogenous norepinephrine release 48
3.5.2.2 Analgesic activity in different animal models of pain 49
3.5.3 Safety pharmacology 55
3.5.4 Animal pharmacokinetics 55
4. AIM 57
5. MATERIALS AND METHODS 60
5.1 ANIMAL SUBJECTS 61
5.2 MIA MODEL OF OSTEOARTHRITIS 61

5.3 MMT MODEL OF OSTEOARTHRITIS 62
5.4 PHARMACOLOGICAL TREATMENTS 62
5.5 BEHAVIOURAL ASSESSMENTS 63
5.5.1 Mechanical allodynia 63
5.5.2 Primary mechanical hyperalgesia 65
5.5.3 Secondary mechanical hyperalgesia 66
5.5.4 Static weight bearing 66
5.5.5 Dynamic weight bearing 67
5.5.6 Locomotor activity 68
5.5.7 Motor function 68
5.6 LUMBAR DRGs AND SC COLLECTION. 69
5.7 WESTERN BLOT ANALYSIS OF DRGs AND SC SAMPLES. 71
5.8 IMMUNOFLUORESCENCE STAINING OF LUMBAR SC SECTIONS 72
5.9 STATISTICAL ANALYSIS 73
6. RESULTS 75
6.1. MIA MODEL OF OSTEOARTHRITIS 76
6.1.1 Effect of CR4056 acute administration 81
6.1.2 Effect of CR4056 sub-acute treatment 87
6.1.3 Neuronal and glial MAPKs activation in lumbar spinal cord 91
6.1.4 Microglial cells activation in lumbar spinal cord 92
6.2. MMT MODEL OF OSTEOARTHRITIS 95
6.2.1 Effect of CR4056 acute administration 101
6.2.2 Effect of CR4056 sub-acute treatment 102
6.2.3 Satellite glial cells activation in L4 and L5 DRGs 104
6.2.4 Microglial cells activation in lumbar spinal cord 106
7. DISCUSSION AND CONCLUSIONS 109
7.1 PAIN BEHAVIOURS AND CENTRAL SENSITIZATION IN OA ANIMAL MODELS 111
7.1.1 MIA model of osteoarthritis 113
7.1.2 MMT model of osteoarthritis 116
7.1.3 Conclusions 118
7.2 CR4056 ANALGESIC EFFICACY IN OA PAIN ANIMAL MODELS 120
7.2.1 CR4056 in MIA model of osteoarthritis 120
7.2.2 CR4056 in MMT model of osteoarthritis 122
7.2.3 Conclusions 122
8. REFERENCES 123
9. ACKNOWLEDGEMENTS 137

1. LIST OF ABBREVIATIONS

2-BFI – 2-(2-benzofuranyl)-2-imidazoline

ACL – Anterior cruciate ligament

ACLT – Anterior cruciate ligament transection

ADAMTS – A disintegrin and metalloproteinase with thrombospondin motifs

ANOVA – Analysis of variance

AP-1 – Activator protein 1

ARRIVE – Animal Research: Reporting of In Vivo Experiments

ATP – Adenosine triphosphate

BDNF – Brain-derived neurotrophic factor

BK – Bradykinin

BMI – Body mass index

BSA – Bovine serum albumin

BU224 – 2-(4,5-dihydroimidazol-2-yl) quinoline hydrochloride

CCL5 – C-C motif chemokine ligand 5

CD11b – Cluster of differentiation molecule 11b

CFA – Complete Freund's adjuvant

CGRP – Calcitonin gene-related peptide

CNS – Central nervous system

COX – Cyclooxygenase

CR4056 – 2-phenyl-6-(1H-imidazol-1yl) quinazoline

CT - Computed tomography

CX3CR1 – C-X3-C motif chemokine receptor 1

CYP450 – Cytochrome P450

DAMPs – Damage-associated molecular patterns

DAPI – 4',6-diamidino-2-phenylindole

DMM – Destabilization of the medial meniscus

DMOAD – Disease modifying osteoarthritis drug

DRGs – Dorsal root ganglia

DWB – Dynamic weight bearing

ECL – Enhanced chemiluminescence

ECM – Extracellular matrix

ERKs – Extracellular receptor kinases

ESCEO – European Society for Clinical and Economic Aspects of Osteoporosis and Osteoarthritis

EULAR – European League Against Rheumatism

FDA – Food and Drug Administration

GABA – Gamma-aminobutyric acid

GDNF – Glial cell-derived neurotrophic factor

GFAP – Glial fibrillary acidic protein

GI – Gastrointestinal

HA – Hyaluronic acid

HPMC – Hydroxyl-propyl-carboxymethyl cellulose

HPWD – Hind paw weight distribution

HRP – Horseradish peroxidase

i.a. – Intra-articular

i.p. – Intraperitoneal

i.v. – Intravenous

I1Rs – Imidazoline-1 receptors

I2Rs – Imidazoline-2 receptors

I3Rs – Imidazoline-3 receptors

IASP – International Association for the Study of Pain

IB4 – Isolectine B4

Iba-1 – Ionized calcium-binding adapter molecule 1

IBS – Imidazoline binding sites

IC_{50} – Half-maximal inhibitory concentration

IL – Interleukin

IRAS – Imidazoline receptor antisera-selected protein

IRs – Imidazoline receptors

JSN – Joint-space narrowing

JSW – Joint space width

K-L – Kellgren-Lawrence

LCL – Lateral collateral ligament

MAOs – Monoamine oxidases

MAPK – Mitogen-activated protein kinase

MCL – Medial collateral ligament

MIA – Monosodium iodoacetate

MMP – Matrix metalloproteinase

MMT – Medial meniscal tear

MOAKS – Magnetic resonance imaging osteoarthritis knee score

MRI – Magnetic resonance imaging

NE – Norepinephrine

NF-kB – Nuclear factor kappa-light-chain-enhancer of activated B cells

NGF – Nerve growth factor

NHS – Normal horse serum

NMDA – N-methyl-D-aspartic acid

NO - Nitric oxide

NOS-2 – Nitric oxide synthase-2

NRM – Nucleus raphe magnus

NSAIDs – Non-steroidal anti-inflammatory drugs

OA – Osteoarthritis

OARSI – Osteoarthritis Research International Society

OD – Optical density

ON – Overnight

p.o. – Per os (orally)

PAG – Periaqueductal gray matter

PAM – Pressure Application Measurement

PBS – Phosphate-buffered saline

PBST – Phosphate-buffered saline with triton-X

PCC – Pearson's correlation coefficient

PCL – Posterior cruciate ligament

pERKs – Phospho-extracellular receptor kinases

PET – Positron emission tomography

PGE_2 – Prostaglandin E_2

pp38 – Phospho-p38

PRRs – Pattern-recognition receptors

PTOA – Post-traumatic osteoarthritis

PVDF – Polyvinylidene difluoride

QD – Quaque die (daily)

ROA – Radiographic osteoarthritis

RT – Room temperature

s.c. – Subcutaneous

SC – Spinal cord

SEM – Standard error of the mean

SGCs – Satellite glial cells

SNRIs – Selective serotonin-norepinephrine reuptake inhibitors

SOA – Symptomatic osteoarthritis

SP – Substance P

TBS – Tris-buffered saline

TBST - Tris-buffered saline with Tween 20

TENS – Transcutaneous electric nerve stimulation

TGF-β – Transforming growth factor-β

TLRs – Toll-like receptors

TNF-α – Tumor necrosis factor-α

T-PER – Tissue protein extraction reagent

Trk-A – Tropomyosin receptor kinase-A

TRPV1 – Transient receptor potential vanilloid 1 channel

VEGF – Vascular endothelial growth factor

WHO – World Health Organisation

2. ABSTRACT

Aim: Osteoarthritis (OA) is a disabling and painful condition very common in the elderly. Pain is the earliest symptom of OA. To date there are still no curative drugs for this condition. Moreover, the chronic use of first-line pharmacological treatments to handle OA pain is frequently associated with side effects. CR4056 [2-phenyl-6-(1H-imidazol-1yl) quinazoline], an imidazoline-2 receptor ligand, is a promising analgesic drug that has been reported to be effective in several animal models of pain.

The aims of my project were to analyze and compare the time-related progression of OA pain and to evaluate the efficacy of CR4056, in comparison with a standard non-steroidal anti-inflammatory drug (NSAID), i.e. naproxen, in two well-established rat models of OA, able to mimic the painful and structural components of the human pathology.

Methods: Knee OA was induced either by single intra-articular injection of 1 mg/50 µl monosodium iodoacetate (MIA) or by medial meniscal tear (MMT) in the right knee of male rats. The local injection of MIA produces cartilage degeneration, through the local inhibition of glycolisis, while the transection of both the medial collateral ligament and the medial meniscus leads to joint destabilization, resulting in cartilage degeneration and subchondral bone alterations. The withdrawal threshold to mechanical stimulation was assessed both as allodynia and either as primary or secondary hyperalgesia, in MIA and MMT model, respectively. Moreover, in both OA models, pain behaviour was further evaluated as static and dynamic hind paw weight distribution (HPWD) asymmetry between the ipsilateral and the contralateral limb, and as changes in motor function and/or locomotor activity. Pain-related proteins (i.e. glial fibrillary acidic protein [GFAP], phospho-p38 [pp38], phospho-extracellular receptor kinases [pERKs] and ionized calcium-binding adapter molecule 1 [Iba-1]) expression was assessed in either ipsilateral and contralateral lumbar L4-L5 spinal cord or ipsilateral L4 and L5 dorsal root ganglia (DRGs), in either MIA or MMT model.

CR4056 (2, 6 and 20 mg/kg) and 10 mg/kg naproxen were administered as acute and sub-acute treatments in both models, with different experimental design according to previous reports in literature.

Results: MIA model was characterized by the significant development of primary mechanical hyperalgesia, mechanical allodynia and asymmetry in both static and dynamic HPWD. No changes were detected in locomotor activity after MIA injection. 6 and 20 mg/kg CR4056 significantly and dose-dependently reduced both allodynia and hyperalgesia, after acute (7 and 14 days after MIA) and especially after repeated treatment (from 14 to 21 days post-MIA), whereas naproxen was

effective after sub-acute treatment only. Both compounds had no significant effect on static and dynamic HPWD changes. No difference was detected in pp38 and pERKs expression in ipsilateral lumbar spinal cord, between MIA and sham group. On the other hand, a significant increase in the number of Iba-1 positive, morphologically identified, activated microglia in ipsilateral L4-L5 spinal cord dorsal horn occurred, 21 days after MIA injection. Sub-acute treatment with 6 mg/kg CR4056 and naproxen reversed MIA-induced microglia activation.

MMT model was characterized by the significant development of a progressive asymmetry in static HPWD and a long-lasting secondary mechanical hyperalgesia. Conversely, neither mechanical allodynia nor changes in dynamic HPWD, motor function and locomotor activity were detected after MMT surgery. 20 mg/kg CR4056 and naproxen promoted a mild but significant anti-hyperalgesic effect, after acute treatment (28 days post-surgery) only. Conversely, repeated treatment (from 28 to 42 days post-surgery) with 6 mg/kg CR4056 significantly reduced the progression of static HPWD asymmetry, whereas naproxen had no effects. No difference in either GFAP or Iba-1 expression was detected, in either ipsilateral L4 and L5 DRGs or ipsilateral L4-L5 spinal cord dorsal horn, between MMT and sham group.

Conclusions: Both MIA and MMT OA models display a pain behaviour comparable to human OA, with however different relative contribution of peripheral and central pain mechanisms. Moreover, the data obtained herein showed that the imidazoline-2 receptor ligand CR4056 might represent a new effective treatment option for OA pain.

3. INTRODUCTION

3.1. OSTEOARTHRITIS

3.1.1 Definition and classification

Osteoarthritis (OA), the most common form of arthritis, is a degenerative chronic disease that affects several million individuals worldwide.

OA comprises a heterogeneous group of syndromes that involves the whole synovial joint in a pathological dynamic process that can result from the dysregulation of a complex set of biomechanical and biochemical interactions between multiple structures, which can disrupt the normal homeostasis of the joint *[Loeser et al., 2012].*

OA implies primarily the local progressive degeneration of joint hyaline cartilage, the connective avascular and aneural tissue that covers the opposing articulating bony surfaces.

Hyaline cartilage protects the joint bones from compressive joint loads and provides flexibility and support through its property of high resiliency and deformability *[Buchanan et al., 2002]*.

OA articular cartilage changes result from the disruption of the normal balance between anabolic and catabolic processes influenced by biomechanical forces, as well as abnormalities in autocrine, paracrine, and endocrine regulation at a cellular level, leading to a disequilibrium in normal tissue turnover within the joint *[Beaumont et al., 2009].*

However, recent observations suggest that OA should be approached as a failure of the entire joint organ *[Lories et al., 2011].* As a matter of fact, OA is also characterized by concomitant changes in the underlying bone, including development of marginal outgrowths, osteophytes, and increased thickness of the bony envelope (bony sclerosis). Soft-tissue structures within and around the joint, such as synovium, ligaments, menisci and periarticular muscle are also affected *[Felson et al., 2000; Loeser et al., 2012]*.

The main clinical symptoms of OA are joint pain, tenderness, stiffness and dysfunction, crepitus, occasional effusion and variable degrees of localized inflammation *[Kean et al., 2004; Lane et al., 2011]*.

This disease is associated with a substantial negative impact on the patient's quality of life as well as on healthcare costs, and therefore represents a massive worldwide healthcare and financial burden *[Buchanan et al., 2002; Poulet et al., 2016]*.

Historically, two major systems have been proposed for the classification of OA: etiological and articular.

According to the first one, OA can be divided in primary or secondary. Primary OA is defined as an idiopathic condition developing in previously undamaged joints, in the absence of an apparent triggering event. On the other hand, secondary OA is defined as being caused by several well-recognized predisposing disorders, which can be divided into four main categories: metabolic conditions (e.g. haemochromatosis and calcium crystal deposition), anatomic abnormalities (e.g. epiphyseal dysplasias), trauma (e.g. major joint trauma or joint surgery) and inflammatory disorders (e.g. any inflammatory arthropathy).

Nevertheless the distinction between these two OA forms is not always clear, since it has been proved that a significant proportion of subjects who develop secondary OA have some generalized predisposition to the disorder *[Arden et al., 2006].*

An additional aetiological classification of OA was proposed by Beaumont and colleagues, based on the strong role of genetic factors and the crucial influence of aging and estrogen deficiency related to menopause in OA pathogenesis and development. According to this system, primary OA is divided into three distinct subsets: type I OA, genetically determined; type II OA, estrogen hormone dependent; and type III OA, aging related *[Beaumont et al., 2009]*.

The articular classification of OA into localized (monoarticular or oligoarticular) or generalized (polyarticular) is based on the number and distribution of joint sites affected.

The individual synovial joints most commonly affected by OA are knees, hips, hands (distal interphalangeal joints) and spine (intervertebral facet joints). The generalized form involves three or more of these joint groups *[Arden et al., 2006].*

An additional system for OA classification widely used in clinics distinguishes between radiographic (ROA) and symptomatic OA (SOA), since the association between joint pain and radiographic features of OA is not constant *[Arden et al., 2006].*

The most commonly used radiologic grading system for knee, hip and hand OA is the Kellgren-Lawrence (K-L) grade, which determines the severity of radiographic OA on the basis of the presence and degree of osteophytosis, joint-space narrowing (JSN), sclerosis, and deformity affecting the joint, irrespective of clinical symptoms *[Suri et al., 2012]*. This system assigns one of five grades (0–4) to an increasing severity of the disease, based on the assumed sequential appearance of osteophytes, joint space loss, sclerosis and cysts *[Kellgren et al., 1957; Kean et al., 2004].* These criteria have been adopted by the World Health Organisation (WHO) to define radiographic OA in epidemiologic studies *[Litwick et al., 2013]*.

Conversely, symptomatic OA is defined as the presence of radiographic OA in combination with characteristic symptoms of OA, including pain, aching, or stiffness in the affected joint *[Suri et al., 2012].*

3.1.2 Epidemiology and risk factors

The prevalence and incidence of OA vary according to the definition of OA, the specific joint(s) under investigation, and the characteristics of the study population *[Zhang et al., 2010]*.

In particular, recent literature data have shown that OA prevalence varies from 12.3% *[Palazzo et al., 2014]* (self-reported in the ‘‘Disability-Health’’ 2008 population-based survey in France) to 21.6% *[Helmick et al., 2008]* (physician-diagnosed OA in the USA estimated by the 2003–2005 US National Health Interview Survey).

The prevalence and incidence of hand, hip and knee disease increase with age, occurring after the age 40 to 50 years *[Palazzo et al., 2016].*

Both hand and knee diseases appear to be more frequent among women than men, especially after the age of 50 years, although the female-to-male ratio varies between 1.5 and 4.0 among studies. A leveling off occurred for both groups at all joint sites around the age of 80 years *[Arden et al., 2006; Palazzo et al., 2014]*.

Moreover, OA seems to be greater in developed than developing countries *[Cross et al., 2014]*.

The etiology of OA is multifactorial, but still largely unknown. It can be considered the product of the interplay between systemic and local factors. The relative importance of risk factors may vary for different joints, for different stages of the disease, for either the development or the progression of the disease, and for radiographic as opposed to symptomatic OA *[Zhang et al., 2010].*

The risk factors of OA can be divided into systemic and local risk factors, which either increase overall susceptibility to joint degeneration or impair the optimal functioning of a joint, respectively. Moreover, both systemic and local factors may operate in a joint-specific way to influence whether a reparative response is normal or aberrant, and whether it succeeds or fails in providing protection from further degeneration *[Arden et al., 2006].*

The main systemic risk factors that have been identified for knee, hand and hip OA are:

- Age: Age is one of the strongest risk factors for OA of all joints. The increase in the prevalence and incidence of OA with age is probably due to a cumulative exposure to

various risk factors and biological changes that occur with aging, such as oxidative damage, thinning of cartilage, muscle weakening and reduction in proprioception, which may make a joint less able to cope with adversity *[Zhang et al., 2010; Palazzo et al., 2016]*.

- Gender: The prevalence of hip, knee and hand OA is higher in women than men, and the incidence increases around the time of menopause *[Palazzo et al., 2016]*. This evidence has led to the hypothesis of a possible role for sex hormones, particularly estrogen deficiency, in the systemic predisposition to OA. However, results on effect of estrogen, either endogenous or exogenous, on OA from observational studies have been conflicting *[Zhang et al., 2010].*
- Obesity: Obesity can be classified as having both systemic and local mechanical effects on OA *[Suri et al., 2012].* Obesity, defined as body mass index (BMI) > 30 kg/m^2, is strongly associated with knee OA, whereas the relationship between overweight (BMI > 25 kg/m^2) and knee OA is lower but still significant. Moreover, obesity is positively associated also with hand OA. This finding emphasizes the metabolic and inflammatory systemic effects of obesity and strengthens the hypothesis of an association between OA and metabolic syndrome *[Palazzo et al., 2016]*.
- Genetics: The development of OA is driven by a complex interplay of genetic and environmental factors *[Suri et al., 2012].* Genetic factors account for 60% of hand and hip OA and 40% of knee OA. The main candidate genes that have been implicated in OA development include the ones encoding for type II collagen, vitamin D receptor, insulin-like growth factor 1 and growth differentiation factor 5 *[Palazzo et al., 2016]*.
- Diet: Low intake of several dietary factors, such as vitamins D, C and K, is suspected to have a role in the development of OA. However, further studies are needed to better define the association between this disease and these dietary factors *[Palazzo et al., 2016]*.
- Bone density and osteoporosis: Several studies have proved that a high bone density is associated with an increased risk of developing radiographic OA of the knee, hip and hand. However, the relationship between skeletal status and OA is complex. Additional evidences have shown that, while OA development seems to be linked with high bone density, the disease progression may be related with both local and systemic bone loss *[Arden et al., 2006].*

Local biomechanical risk factors of OA seem to determine mainly the exposure of individual joints to injury and to excess loading conditions, which eventually lead to joint degeneration.

The main local risk factors for knee OA are:

- Joint injury: Joint injuries frequently lead to a progressive process of severe debilitating condition known as acute post-traumatic osteoarthritis (PTOA). Several studies have reported that ranges from 20% to more than 50% of patients who had joint trauma develop OA and represent ∼12% of all OA cases *[Punzi et al., 2016].* In particular, either anterior cruciate ligament or meniscal injury seems to be mostly related to the increased incidence of knee OA *[Suri et al., 2012].* Moreover, repeated injuries and excess body weight are known to further increase the risk for PTOA. The hypothesis is that OA development in the injured joints initiates during the initial traumatic event by intra-articular pathogenic processes, such as apoptosis of articular chondrocytes, subchondral bone remodeling, cellular infiltration and the release of inflammatory mediators in synovial fluid *[Punzi et al., 2016].*
- Joint alignment: Malalignments may be related to genetic, developmental, or traumatic causes and may be either a cause or consequence of OA. Knee varus and valgus malalignments have been associated with progression of radiographic knee OA in multiple longitudinal studies *[Suri et al., 2012].*
- Abnormal joint loading: Several data suggest that repetitive joint use linked to occupation is associated with the development of OA. Moreover, also repetitive and excess joint loading that accompanies specific physical activities seems to increase the risk of developing OA in the stressed joint *[Arden et al., 2006; Palazzo et al., 2016]*.

3.1.3 Knee osteoarthritis

Knee osteoarthritis is the most common type of OA (6% of all adults). Several studies have shown that knee osteoarthritis in men aged 60 to 64 is more commonly found in the right knee (23%) than in the left one (16.3%), while its distribution seems to be more evenly balanced in women (right knee, 24.2%; left knee, 24.7%) *[Michael et al., 2010].*

The knee is a diarthrodial or synovial joint, which is characterized by a complex internal structure and, in particular, by the presence of a synovial cavity that separates the opposing bony surfaces.

The knee is composed of three functional compartments: the femoropatellar articulation, which consists of the patella and the patellar groove on the front of the femur, and the medial and lateral femorotibial articulations, linking the femur with the tibia. In particular, the lateral and

medial condyles of the upper extremity of the tibia (tibial plateau) articulate with the distal lateral and medial femoral condyles. These bony surfaces are separated by a thin layer of hyaline cartilage, which provides a smooth surface that allows an efficient gliding motion during joint movement, in association with a boundary layer of lubricants, provided by lubricin and hyaluronic acid (HA) produced by both chondrocytes and synoviocytes *[Loeser et al., 2012].* Hyaline cartilage is composed of specialized cells, chondroblasts and chondrocytes, and has viscoelastic and compressive properties provided by the extracellular matrix (ECM). The ECM is mainly composed of type II collagen and abundant ground substance, rich in proteoglycans, aggrecans and elastin fibers. Type II collagen is responsible for the tensile strength of the cartilage, while aggrecans endow hyaline cartilage with its compressive strength (i.e. stiffness and elasticity), providing a highly hydrated matrix *[Buchanan et al., 2002].*

A small depression between the condyles of the tibial plateau (intercondylar area) provides attachment for the medial and lateral menisci of the joint, which are crescent-shaped fibrocartilaginous structures that serve to widen and deepen the articulating surface between the femoral condyles and the tibia. The main function of the menisci is to provide structural integrity to the joint during tension and torsion movements, reducing friction and protecting hyaline cartilage from excessive stress.

The joint capsule consists of the external fibrous layer and the internal synovial membrane. The fibrous layer encloses the femoral condyles and the superior articular surface of the tibia, separating the joint from the surrounding structures. The synovial membrane or synovium lines all surfaces of the articular cavity not covered with articular cartilage, attaching to the periphery of hyaline cartilage and menisci. The synovial membrane is composed of synoviocytes, fibroblasts-like cells able to secret and reabsorb synovial fluid. Synovial fluid is an interstitial fluid filtered from the blood plasma, which contains also proteins locally synthesized, such as HA and lubricin, secreted by synoviocytes and chondrocytes, respectively. The main functions of synovial fluid are to provide oxygen and nutrients to the articular chondrocytes and to lubricate the articulating surfaces of the joint, reducing friction during movement.

The main motion of the knee joint is flexion and extension, with limited medial and lateral rotation. The main muscle for knee extension is the quadriceps femoris, which is also the most important muscle in stabilizing the joint, while flexion is produced by the hamstring muscles.

The knee joint is also stabilized by extracapsular and intra-articular ligaments. The main extracapsular ligaments are the medial collateral ligament (MCL), which is firmly attached to the

medial meniscus, and the lateral collateral ligament (LCL). These ligaments ensure the correct flexion and extension movement of the joint, providing restraint to valgus and varus stress, respectively. The main intra-articular ligaments are the anterior cruciate ligament (ACL), which prevents posterior translation of the femur on the tibia (or anterior displacement of the tibia) during flexion-extension of the knee, and the posterior cruciate ligament (PCL), which in turn prevents anterior translation of the femur on the tibia.

Many vessels are involved in forming the arterial anastomosis around the knee joint that supplies the patella, the femoral and tibial condyles, the bone marrow, the articular capsule and the synovial membrane. Branches of the obturator and femoral nerves of the lumbar plexus and the tibial and common peroneal nerves from the sacral plexus innervate the knee joint (***Figure 1***) [*Platzer, 5th edition*].

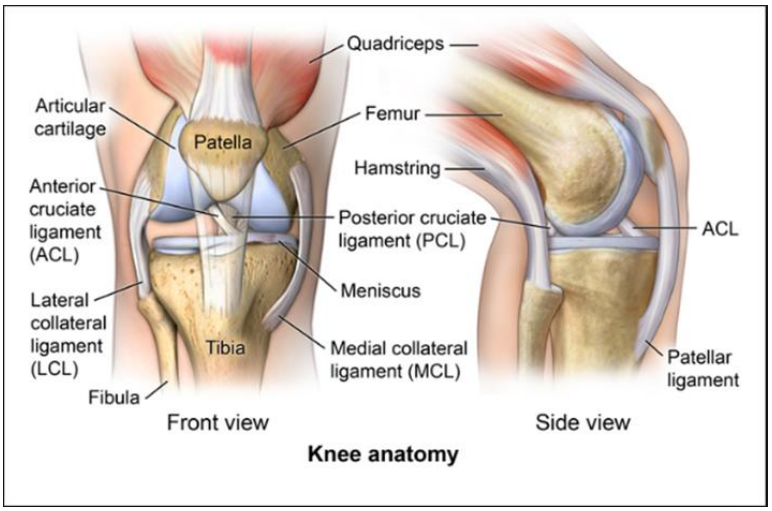

Figure 1: Knee joint.

Knee osteoarthritis involves all structures within the joint in a non-uniform and focal manner, leading to hyaline cartilage degeneration, bony remodeling, capsular stretching, weakness of periarticular muscles, synovitis and, in some patients, laxity of the ligaments and lesions in the bone marrow, which may represent trauma to the bone. Moreover, with a large enough area of cartilage loss or with bony remodeling, the joint becomes tilted, and malalignment develops, leading to a further structural deterioration of the joint *[Felson, 2006].*

Knee OA frequently presents as a unilateral problem and the medial femorotibial compartment of the knee is the most commonly affected, compared with the lateral femorotibial and femoropatellar compartments.

Patients suffering from osteoarthritis often complain of pain during movement, typically related to activity and occurring when movement is initiated. Pain of knee OA is often described as a dull ache and is usually felt in the medial and lateral joint compartments and retropatellar area. Additional knee OA symptoms are morning joint stiffness, which usually lasts less than 30 minutes, reduced range of motion in knee flexion and extension, crepitus and crunching sensations and joint instability. As osteoarthritis progresses, the pain becomes continuous, and the functionality of the joint is severely impaired. Therefore, knee OA is a leading cause of impaired mobility that prevents OA patients from engaging in their usual activities.

Moreover, the radiological demonstration of typical signs of osteoarthritis of the knee does not correlate with symptoms. Only about 15% of patients with radiologically demonstrated knee OA complain of knee pain.

The evolution of knee OA tends to be slow, both clinical and radiological findings can remain unchanged for years *[Kean et al., 2004; Felson, 2006; Michael et al., 2010].*

3.1.4 Diagnosis

In clinical practice, the major elements of the diagnostic evaluation of knee OA are the clinical history, physical examination, imaging studies, and, in some cases, laboratory testing.

Joint pain, exacerbated by activity and relieved by rest, and limitation of range of motion are common symptoms to all forms of OA; however, each joint and each stage of the disease has its own characteristic physical examination findings *[Sinusas, 2012].* The physical examination for knee OA diagnosis consists in joint inspection and palpation, testing of the range of movement, and special functional tests, such as meniscus tests, gait analysis and either varus/valgus stress or drawer tests for lateral or anterior and posterior ligaments stability, respectively *[Michael et al., 2010].*

Nowadays, the increasing importance of imaging for OA diagnosis and follow-up is well recognized.

Radiography is the simplest, least expensive and most commonly employed imaging technique for OA. This imaging modality enables the detection of OA-associated bony features, i.e. osteophytes, subchondral bone sclerosis and cysts.

The presence and severity of the disease are typically determined by using the semiquantitative K-L grading system *[Hayashi et al., 2016].* Radiographic OA of the knee is usually defined as a K-L

grade of 2 or higher *[Suri et al., 2012]*. However, K-L grading has its limitations, therefore individual grading systems for the different OA radiographic features, including osteophytes and JSN, have been developed. These grading systems categorize the femorotibial joint space width (JSW) and osteophytes, separately for each compartment of the knee, according to their severity, based on published atlases (e.g. the Osteoarthritis Research Society International atlas), which provide image examples for grades for specific features of OA *[Hunter et al., 2012; Hayashi et al., 2016].*

Nevertheless, radiography is characterized by a poor sensitivity and a relatively large precision error that do not allow early detection of joint degradation *[Rousseau et al., 2012].*

Magnetic resonance imaging (MRI) is a more sensitive imaging method with several advantages for monitoring the progression of OA. MRI allows a three dimensional joint evaluation as a whole organ and the assessment of OA pathological changes in joint structures not visualized by radiography, i.e. articular cartilage, menisci, ligaments, synovium, capsular structures and bone marrow.

Several semiquantitative MRI scoring systems for knee OA are available; the most recently published is the MR Imaging Osteoarthritis Knee Score (MOAKS). Moreover, quantitative or compositional MRI analysis allows either the direct quantification of cartilage volume, surface areas and thickness, or the visualization of the biochemical properties of different joint tissues, respectively.

However, MRI is still not routinely used in clinical management of OA patients due to its high cost and limited availability.

Ultrasonography enables real time, multiplanar imaging of joint soft tissues at relatively low cost. This imaging technique allows a reliable assessment of OA-associated features, such as osteophytes, peripheral cartilage lesions and synovial inflammation, without contrast administration or exposure to radiation.

The major advantage of ultrasound imaging, compared with conventional radiography, is the ability to detect synovial pathology. However, ultrasonography has several limitations, including its limited ability to detect deep articular structures and the subchondral bone, due to the physical properties of ultrasound. Moreover, it remains an operator-dependent technique *[Hunter et al., 2012; Hayashi et al., 2016].*

Nuclear medicine imaging with radiotracers, such as scintigraphy and positron emission tomography (PET), enables imaging of active metabolism and visualization of osteophytes

formation, subchondral bone sclerosis and cysts formation, bone marrow lesions and sites of synovitis. However, this technique is not commonly used in a routine clinical setting for OA diagnosis *[Hayashi et al., 2016].*

Computed tomography (CT) is ideal for the evaluation of bone morphometry, but its clinical application for OA imaging is limited by its poor ability of soft tissue evaluation, along with ionizing radiation exposure *[Hunter et al., 2012].*

Finally, especially for OA early diagnosis, there is a considerable interest for the identification of specific biological markers in serum, urine and synovial fluid of OA patients that reflect quantitative and dynamic variations in joint tissue remodeling, and therefore disease progression. Nowadays, even if several candidate biomarkers for diagnosis of OA have been identified, since their circulating levels are significantly modified before radiographic damages can be detected, none of them can still be considered a valid tool in routine clinical practice *[Rousseau et al., 2012].*

3.1.5 Immunopathogenesis of osteoarthritis

Osteoarthritis is a whole-organ disease of the joint. Knee OA induces pathologic changes in all joint structures, including fibrillation and degradation of articular cartilage, thickening of the subchondral bone, osteophytes formation, inflammation of the synovium (synovitis), degeneration of ligaments and menisci and hypertrophy of the joint capsule *[Loeser et al., 2012].*

During the development of OA, the normal, quiescent articular chondrocytes are activated, in relation to the exposure to abnormal environmental insults, e.g. high-magnitude mechanical stress, inflammatory cytokines or altered amount or organization of matrix proteins. The activated chondrocytes undergo a phenotypic shift characterized by cell proliferation, cluster formation, and increased production of both matrix proteins and matrix-degrading enzymes, resulting in fibrillation and degradation of cartilage matrix. In particular, chondrocytes in OA cartilage, especially those in clonal clusters, express cytokines, chemokines, pattern-recognition receptors (PRRs) and other receptors for ECM components.

The activation of stress- and inflammatory-induced signaling (e.g. nuclear factor kappa-light-chain-enhancer of activated B cells [NF-Kb] and mitogen-activated protein kinase [MAPK] pathways) and transcriptional and posttranscriptional events in chondrocytes during OA results in imbalanced homeostasis and aberrant expression of catabolic and inflammation-related genes. These include nitric oxide synthase (NOS)-2, cyclooxygenase (COX)-2, and several cytokines, chemokines and

ECM degrading enzymes. In particular, matrix metalloproteinase (MMP)-1, -3 and -13 and a disintegrin and metalloproteinase with thrombospondin motifs (ADAMTS)-4 and -5 are the enzymes major involved in type II collagen, aggrecans and others ECM components degradation. The upregulation of cartilage-degrading proteinases produces matrix degradation products, which can further promote, along with pro-inflammatory mediators, the catabolic activation, the aberrant, hypertrophy-like differentiation and the apoptosis of chondrocytes *[Goldring et al., 2011; Goldring, 2012; Loeser et al., 2012].*

Synovitis has now been recognized as a common finding both in early and late stages of OA. Indeed, many OA patients have symptoms of joint inflammation, such as morning stiffness, warmth, pain and joint effusions. Moreover, OA tissue and synovial fluid of OA patients are frequently characterized by high levels of pro-inflammatory mediators, such as inflammatory plasma proteins, complement components and cytokines *[Robinson et al., 2016].*

Synovitis is characterized by both the hyperplasia of the synovial lining cells and the infiltration of inflammatory cells, consisting primarily of macrophages and mast cells, but also a smaller but quantifiable number of T and B cells. The inflammation of the synovium is present in OA joints well before the development of significant radiographic changes *[Scanzello et al., 2012; Sokolove et al., 2013].* Moreover, recent epidemiological studies in patients with knee OA have demonstrated a correlation between synovitis and both symptoms, such as pain, and progression of cartilage damage *[Ayral et al., 2005; Hill et al., 2007]*. Therefore, synovial inflammation has now been strongly implicated in OA pathogenesis. Synovitis in OA is generally chronic and low-grade and is likely a secondary process induced by an immune response, primarily innate and to a lesser degree adaptive, which occurs following cartilage damage *[Sokolove et al., 2013; Robinson et al., 2016].*

Innate immune mechanisms involved in OA include the activation of both PRRs on behalf of damage-associated molecular patterns (DAMPs), and the complement system, which promotes the inflammatory responses of innate immune cells, such as macrophages and mast cells, as well as synoviocytes and chondrocytes in the joint.

DAMPs are endogenous molecules produced during tissue damage that trigger an inflammatory response through the interaction with their PRRs, located mainly on innate immune cells. In particular, at least four classes of DAMPs have been implicated in the innate immune response within the damaged OA joint. The products from ECM breakdown, which occurs at sites of inflammation (e.g. fibronectin and low molecular weight HA), could promote both inflammation and cartilage loss. In addition, plasma proteins that exude from blood vessels at sites of

inflammation- or damage-induced vascular leakage (e.g. fibrinogen) are capable of acting as DAMPs. Moreover, intracellular alarmins (e.g. the S100 family of proteins) released from stressed, damaged, or necrotic cells can act as a third source of DAMPs. Finally, microscopic inorganic crystals, including basic calcium phosphate and calcium pyrophosphate dehydrate, released from cartilage into the synovial space by injury or wear and tear, promote inflammation through their interaction with various components of the innate immune system [*Robinson et al., 2016].*

On the other hand, Toll-like receptors (TLRs) are one of the main classes of PRRs involved in OA. TLRs activation has been implicated in the development of synovial inflammation and degradation of articular cartilage in OA [*Scanzello et al., 2012].*

An additional innate immune mechanism involved in OA pathogenesis that promotes inflammation and tissue damage is the activation of the complement system, especially mediated by cartilage ECM components (e.g. fibromodulin and aggrecans), calcium crystals and components of apoptotic debris.

Innate immune cells, implicated in OA pathogenesis, which can be activated by either DAMPs or complement, include macrophages and mast cells. Macrophages are recruited and activated in the inflamed synovium of OA joints and contribute to cartilage breakdown and osteophytosis by producing cytokines, such as interleukin (IL)-1β and tumor necrosis factor (TNF)-α. The activation of synovial macrophages is required for the production of MMPs and the subsequent cartilage damage. Moreover, the increasing number and activation of mast cells in OA synovium contribute to inflammation and structural damage, through the release of several mediators (e.g. tryptase) that stimulate the proliferation and cytokines production by synoviocytes and strengthen the recruitment of inflammatory cells within the synovial joint.

Furthermore, synoviocytes and chondrocytes themselves are mediators of OA-associated inflammation and contribute to OA pathogenesis, producing pro-inflammatory cytokines and chondrolytic mediators in response to the activation of innate immune mechanisms.

The main pro-inflammatory mediators implicated in OA pathogenesis, released within the joint mainly by synoviocytes, chondrocytes and resident and infiltrating immune cells, include cytokines, chemokines, growth factors, adipokines, neuropeptides and lipid inflammatory mediators.

IL-1β and TNF-α are the two major pro-inflammatory cytokines responsible for the shift of cartilage homeostasis towards catabolism, which leads to cartilage degradation. IL-1β and TNF-α signaling, mediated by the activation of NF-kB and the activator protein 1 (AP-1) transcription

factors, can induce both autocrine production of IL-1β and TNF-α and the expression of other pro-inflammatory and chondrolytic mediators, including MMP-1, MMP-13, nitric oxide (NO), prostaglandin E_2 (PGE_2) and IL-6. In particular, NO seems to contribute to the cartilage degradation in OA by enhancing expression of MMPs and inhibiting collagen and proteoglycans synthesis.

Several chemokines (e.g. IL-8 and C-C motif chemokine ligand 5 [CCL5]), small secretory molecules responsible for chemotaxis of immune cells, also increase the release of MMP-3 by chondrocytes, thus enhancing the breakdown of cartilage matrix components, and promote periarticular bone remodeling.

Several growth factors have been implicated in OA pathogenesis. Among them, transforming growth factor-β (TGF-β) family, expressed in bone, cartilage and synovium, has been associated to the development of osteophytosis and synovial fibrosis, while vascular endothelial growth factor (VEGF), produced in the inflamed synovium, can promote angiogenesis, contributing to inflammation in OA. Finally, the increased production within the joint of nerve growth factor (NGF) by mast cells, synoviocytes and chondrocytes, induced by cytokines such as IL-1β, TNF-α and IL-6, regulates the autocrine production of cytokines and chemokines, via the high-affinity NGF receptor, tropomyosin receptor kinase-A (Trk-A) *[Haseeb et al., 2013; Sokolove et al., 2013; Robinson et al., 2016].* Therefore, NGF seems to play an important role linking the response of the immune and nervous system during inflammation. As a matter of fact, NGF increases pain in the arthritic joint through several mechanisms, e.g. by promoting the proliferation of terminal nerves, the degranulation of mast cells, and the upregulation of several neuropeptides, such as substance P (SP) and calcitonin gene-related peptide (CGRP). Moreover, NGF is able to sensitize directly nociceptors within the joint *[Raychaudhuri et al., 2011].*

In addition to traditional cytokines, high systemic and synovial fluid levels of adipokines, soluble mediators primarily derived from adipose tissue and released into the bloodstream, have been associated with cartilage degeneration and synovitis in OA. Adipokines are also produced within the OA joint by infrapatellar fat pads, synoviocytes, chondrocytes, osteoblasts and osteoclasts. Several adipokines, such as leptin, adiponectin, resistin, visfatin, and nefastin-1, can promote the production of inflammatory mediators and cartilage-degrading factors. Therefore, in addition to local inflammation within the joint, systemic inflammation might also have an important role in OA pathogenesis.

Lipid mediators, including prostaglandins and leukotrienes, seem to be involved in OA pathogenesis. In particular, PGE_2 promotes inflammation, apoptosis and angiogenesis, which characterize OA disease.

Finally, neuropeptides, such as substance P (SP) and bradykinin (BK), play an active role in OA joint not only in pain modulation, but also in promoting and maintaining synovial inflammation, through the activation of infiltrating immune cells and the induction of pro-inflammatory cytokines production (***Figure 2***) *[Haseeb et al., 2013; Sokolove et al., 2013; Robinson et al., 2016].*

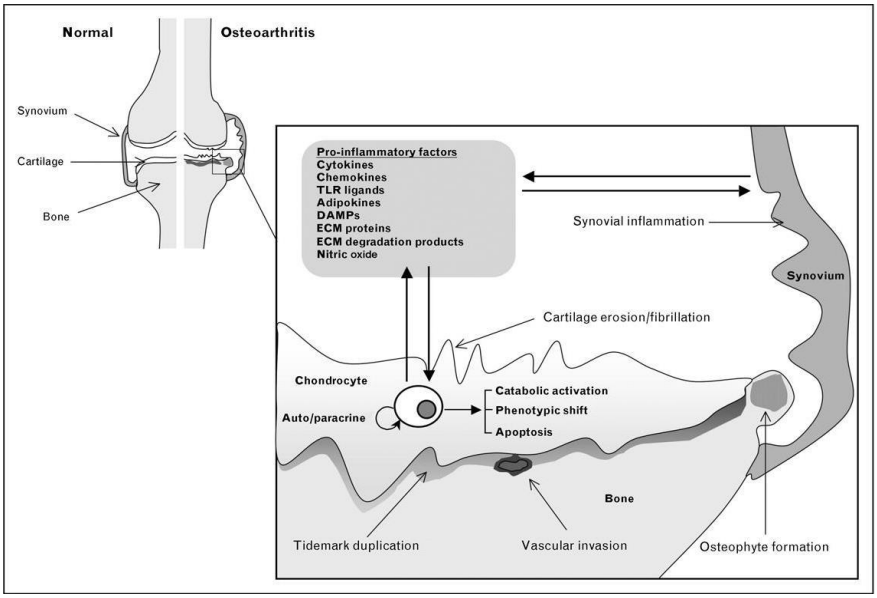

Figure 2: Main mediators involved in pro-inflammatory events in OA *[Goldring et al., 2011].*

3.1.6 Pain in osteoarthritis

3.1.6.1 Pain definition and mechanisms

According to the International Association for the Study of Pain (IASP), pain can be defined as "an unpleasant sensory and emotional experience associated with actual or potential tissue damage, or described in terms of such damage" *[Merskey et al., 1994].*

Pain is currently divided into nociceptive pain (often inflammatory), which results from tissue damage; neuropathic pain, involving nerve damage; and idiopathic pain, which has no identified cause *[Thakur et al., 2014].*

Nociceptive pain arises from the stimulation of peripheral nociceptors, i.e. high-threshold primary afferent fibers able to detect and transduce mechanical, chemical or thermal noxious stimuli.

Nociceptors consist of the medium diameter (conduction velocity of 2-30 m/s) thinly myelinated Aδ mechanoreceptors (type III receptors) and the small diameter (conduction velocity of 0.5-2 m/s) unmyelinated C polymodal (type IV receptors) nerve fibers. On the other hand, thickly myelinated sensory Aβ nerve fibers (type II receptors) normally respond to non-nociceptive mechanical stimuli, including stretch and pressure. The soma of all these sensory nerve fibers is located in the dorsal root ganglia (DRGs) *[Stemkowski et al., 2012; Mantyh, 2014].* DRGs reside near the entrance of dorsal roots into the spinal cord, and represent both the first relay centre for sensory input transmission from periphery and an important site for the processing of neural information *[Hanani, 2005; Mantyh, 2014].*

C-fibers can be further classified as either peptidergic or non-peptidergic nerve fibers, based on their different neurotrophic support. Peptidergic fibers express Trk-A (NGF-dependent), the transient receptor potential vanilloid 1 channel (TRPV1), SP, CGRP and other neuropeptides, and terminate mostly in lamina I, the outer lamina II and lamina V of the spinal cord dorsal horns. Conversely, non-peptidergic isolectine B4 (IB4)-positive nociceptive afferents terminate mostly in the middle third of lamina II of the spinal cord dorsal horns and express glial cell-derived neurotrophic factor (GDNF) receptors, while generally do not express CGRP *[Stemkowski et al., 2012; Mantyh, 2014].*

In the dorsal horns of the spinal cord, the nociceptive afferent fibers innervate both second-order projection neurons and local interneurons, releasing glutamate and several neuropeptides. The nociceptive signal is then transmitted from the spinal cord dorsal horns to the brainstem, to the thalamus, via the spinothalamic tract, and to the medulla and mesencephalon, through the spinoreticular and spinomesencephalic tracts.

Moreover, at the level of the dorsal horns of the spinal cord a modulation of the transmission of the nociceptive signals occurs, through both the local inhibitory and excitatory interneurons and the descending inhibitory and facilitatory pathways, originating in the midbrain and brainstem. In particular, the descending inhibitory pathways include noradrenergic neurons that descend through the dorsal lateral funiculus from brain sites, such as periaqueductal gray matter (PAG) or the nucleus raphe magnus (NRM), to the spinal cord dorsal horns, where they significantly contribute to the modulation of pain, producing analgesia via the local spinal release of endogenous norepinephrine (NE) *[Millan, 2002; Pertovaara, 2006].*

Chronic pain associated with injury or diseases, such as OA, can result from alterations in the properties of peripheral nerves, which lead to peripheral and central sensitization [*Basbaum et al., 2009*].

Peripheral sensitization consists of an increase of both transduction sensitivity and terminal excitability (i.e. reduction of the activation threshold) of nociceptors, triggered by tissue damage and inflammation [*Coutaux et al., 2005*]. Peripheral sensitization of primary afferent nociceptors results also in posttranslational changes of second-order nociceptive neurons within the spinal cord dorsal horns, leading to central sensitization *[Salaffi et al., 2014].*

Central sensitization is a form of nervous system plasticity, consisting of increased membrane excitability, synaptic facilitation, loss of inhibition, reversal of inhibition, and enhancement of excitation of nociceptive central circuits *[Stemkowski et al., 2012].* Central sensitization manifests as an increase in responsiveness to noxious stimuli, a spread of pain sensitivity to areas outside of the tissue damaged area and a development of pain in response to low intensity stimuli *[Ji et al., 2001].*

One possible mechanism for enhanced post-synaptic sensitivity of spinal second-order nociceptive neurons, responsible for central sensitization, involves the upregulation of several second messenger systems activation. In particular, the family of mitogen-activated protein kinases (MAPKs), including the extracellular signal-regulated protein kinase (ERK) 1 and 2 and p38, expressed by neuronal and glial cells respectively, plays a key role in the development and maintenance of central pain sensitization.

Both peripheral and central sensitization lead to a heightened sensitivity to noxious stimuli (hyperalgesia), and to pain in response to non-noxious stimuli (allodynia) *[Coutaux et al., 2005].* Moreover, in chronic pain state, mechanical allodynia seems to be mediated also by Aβ nerve fibers. After tissue damage, Aβ primary afferent nerve fibers undergo both an aberrant sprouting into the lamina II of the dorsal horns, which allows their contact with nociceptive-specific projection neurons, and a change in their pattern of neurotransmitters expression, which includes the novel synthesis of excitatory neuropeptides, such as SP *[Millan, 2002].*

The excitatory amino acid glutamate and the neuropeptide SP are pivotal to the induction of central sensitization *[Coutaux et al., 2005].*

An additional important mechanism in central sensitization is the upregulation of COX-2 *[Dimitroulas et al., 2014]*.

Moreover, spinal glial cells are involved in the establishment and maintenance of central sensitization. Neurons can regulate the activation of microglia and astrocytes through multiple cellular pathways, including a sustained release of neurotransmitters, ATP and neuropeptides. The neuron-to-glia mediators include several chemokines, such as the membrane-anchored and cleavable chemokine fractalkine expressed by neurons, able to activate glial cells through the interaction with its glial receptor C-X3-C motif chemokine receptor 1 (CX3CR1). Microglia activation consists of cellular proliferation, morphological changes, and increased expression of glial markers, such as the ionized-calcium-binding adapter molecule (Iba-1). As a result of their activation, both microglia and astrocytes release pro-inflammatory factors, such as cytokines, prostaglandins or neurotrophins (e.g. brain-derived neurotrophic factor [BDNF]), and secrete inflammatory mediators, such as GDNF, which contribute to sensitization of the spinal neurons *[Gosselin et al., 2010; Ren et al., 2010].*

Neuropathic pain is generally produced by damage to the peripheral or central nervous system. Spinal glial cells have a significant role in neuropathic pain development as well *[Dimitroulas et al., 2014].*

Moreover, recent evidences have proved the involvement of the activation of satellite glial cells (SGCs), the main type of glia within DRGs, in the occurrence and maintenance of inflammatory and neuropathic pain. Indeed, DRGs neurons and their surrounding SGCs form a morphologically distinct functional unit. The crosstalk between neurons and SGCs within DRGs represents a mechanism for neuronal signals modulation in the sensory pathway *[Dublin et al., 2007; Takeda et al., 2009]*. One marker of satellite glial cells is glial fibrillary acidic protein (GFAP). In particular, it has been proved that under resting conditions SGCs display low levels of GFAP, while it increases along with SGCs activation, after nerve injury or inflammation, in several chronic pain models *[Hanani, 2005].*

3.1.6.2 OA pain

Pain is the earliest and most disabling symptom for the patient, of symptomatic OA *[Kean et al., 2004].*

OA pain has multifaceted etiologies, resulting from a complex interaction between local tissues damage, inflammation, and the peripheral and central nervous systems. OA pain is driven by both nociceptive and neuropathic mechanisms.

Within the knee joint, Aδ and C nociceptive fibers innervate the synovial membrane, joint capsule, periarticular ligaments, menisci, adjacent periosteum and subchondral bone, while Aβ nerve fibers innervate the synovial membrane, joint capsule, periarticular bursae, fat pad, ligaments, menisci and adjacent bony periosteum *[Salaffi et al., 2014].*

Osteoarthritis pain has acute or chronic wax-and-wane characteristics. The progression of nociception from an acute to a chronic process is not fully comprehended. The most consolidated hypothesis is that peripheral mechanisms in acute pain and long-term potentiation of neuronal sensitivity to nociceptive inputs in the dorsal horns of the spinal cord may underline the transition from an acute to a chronic process *[Haviv et al., 2013].*

Tissue damage and inflammation within the OA joint induce both a prolonged nociceptors activation and a reduction in their activation threshold, and enhance nociceptors sensitivity, leading to the development of peripheral sensitization of primary afferent nociceptors. Moreover, via peripheral nociceptors activation, perpetuation of the inflammatory process results in posttranslational changes of second-order nociceptive neurons within the spinal cord dorsal horns, responsible for central sensitization *[Coutaux et al., 2005; Salaffi et al., 2014].*

Several algogenic mediators, released by damaged cells, inflammatory cells or nociceptors, promote peripheral sensitization within the OA joint.

Peripheral inflammation, cartilage degradation and bone marrow lesions induce the release of several pro-inflammatory mediators, which cause localized tissue damage and activate peripheral nociceptors. In particular, cytokines, such as IL-1β and TNF-α, can directly activate sensory neurons and indirectly contribute to nociceptors sensitization via the production of kinins and prostanoids, by inducing the upregulation of the B1 receptors of bradykinin and the enzyme COX-2, respectively.

Kinins, such as BK and kallidin, cause a cascade of secondary changes, including prostanoids and NO production, and the sensitization of sensory transducers such as TRPV1 receptor. TRPV1 is a non-selective cation channel activated in the primary sensory neurons by protons (pH< 5.3), capsaicin or intense heat (> 45°C) and regulated by several inflammatory mediators (e.g. kinins, PGE_2, NGF), thus able to enhance the nociceptive stimuli.

PGE_2 exerts its effect via several prostaglandin E_2 receptors present both in peripheral sensory neurons and in the spinal cord, leading to nociceptors sensitization *[Coutaux et al., 2005; Read et al., 2008; Sofat et al., 2011; McDougall et al., 2012].*

In OA, stimulation of primary sensory neurons is further promoted by neovascularization of articular cartilage, mediated by hypoxia, and the production of angiogenic growth factors in the synovium *[Dimitroulas et al., 2014].*

In addition, within the OA joint, the increased release of NGF by inflammatory cells, mast cells, synoviocytes and chondrocytes plays a central role in promoting peripheral sensitization. In particular, the NGF-Trk-A complex, once internalized and transferred to the nociceptive neurons soma in DRGs, leads to altered gene transcription and increased synthesis of several proteins, which are further transported both retrogradely to the peripheral endings and to central endings. In particular, NGF induces an increased production of several neuropeptides associated with joint nociception, such as SP and CGRP, and ion channels (e.g. TRPV1), both within the joint and in the spinal cord dorsal horns. SP and CGRP can stimulate primary sensory neurons by activating ion channel-linked receptors, increase blood vessel permeability and facilitate the release of bradykinin. Moreover, NGF induces the overexpression of BDNF in the peptidergic C fibers. BDNF, after being released in the dorsal horns of the spinal cord, binds to its high-affinity Trk-B receptor, leading to the phosphorylation of N-methyl-D-aspartic acid (NMDA) receptors. NMDA receptors play a pivotal role in central sensitization both within the dorsal horns, mediating a persistent activation of primary afferent neurons, and in the nociceptive central circuits.

Mediators of pain at the DRGs level in OA include NGF, CGRP, TRPV1 and opioid receptors, while chemical mediators of pain in the brain include SP, serotonin and glutamate.[*Read et al., 2008; Sofat et al., 2011].*

Neuropathic pain mechanisms, including spontaneous discharge and amplification of nociceptive impulses, cross excitation and sprouting, and central sensitization, contribute to OA pain for at least a subset of OA patients *[Dimitroulas et al., 2014].* As a matter of fact, several clinical observations have reported that nerves innervating the synovium of OA patients were morphologically abnormal, but enriched in pro-inflammatory neuropeptides *[McDougall et al., 2012].* Moreover, in several preclinical animal models of OA, both the activation of spinal microglia and astrocytes and the upregulation of several neuronal markers of nerve injury in DRGs have been detected *[Sagar et al., 2011; Orita et al., 2011; Ferreira-Gomes et al., 2012b].*

Finally, a portion of the pain experienced by OA patients appears to be sympathetic efferent nerve-mediated.

The joint capsule, synovium and bone are richly innervated by adrenergic and cholinergic sympathetic post-ganglionic neurons. A dynamic interplay exists between sympathetic

innervations and the control of vascular tone, bone turnover, inflammatory status and sensory innervations within the joint *[Read et al., 2010; Mantyh, 2014].*

Moreover, NGF may play an important role in linking sympathetic and C-fiber innervations, as sympathetic activation stimulates NGF secretion from vascular smooth muscle *[Dray et al., 2007]*.

3.2 ANIMAL MODELS OF OSTEOARTHRITIS

An animal model for human disease is defined as a homogenous set of animals, which have an inherited, naturally acquired, or experimentally induced biological process, resembling the human disease in one or more respects [*Pritzker, 1994*].

In vivo preclinical animal models have been employed with the purpose either to study the pathogenesis of the disease or to investigate the therapeutic efficacy of treatment modalities [*Bendele, 2001*].

OA is a heterogeneous disease in humans; therefore, no single animal model should be expected to be relevant for the study of all aspects of the disease process.

The choice of an "appropriate" animal model strongly depends on the aspect or clinical phenotype of human OA of interest for the intended purpose of the researchers *[McCoy, 2015].* In particular, OA clinical phenotypes that may warrant distinct therapeutic strategies include the cause or mechanism of onset of the disease (post-traumatic, age-associated, metabolic/obesity or genetic); the joint structures affected (e.g. cartilage erosion, bone remodeling, synovitis); the disease progression (stage and rate); and the symptoms, in particular pain and disability *[Malfait et al., 2015].* Moreover, cost, availability, housing, and length of the experiment need to be considered, along with the most desirable primary outcomes, for the choice of a suitable OA animal model. In general, smaller animals may be favored for investigations of basic pathophysiology and for early screening of therapeutic interventions, while large animal models should be used for the endorsement of previous findings before human clinical trials *[McCoy, 2015].*

Animal models of OA can be divided into spontaneous and induced animal models.

Spontaneous OA animal models are the hallmark of primary idiopathic human OA and include both naturally occurring and genetic models of the disease. Spontaneous OA models are characterized by a slower progression of the disease, thus mimicking more closely the course of primary OA in humans. On the other hand, these models take more time to develop and tend to be more variable in their outcomes *[McCoy, 2015; Kuyinu et al., 2016].*

The Dunkin Hartley guinea pig has been the most widely used animal to study naturally occurring OA. In addition, particular strains of mice, such as STR/ort, are predisposed to the development of spontaneous idiopathic OA *[Kuyinu et al., 2016].* STR/ort mice develop an age-related spontaneous and progressive condition, associated also to dyslipidemia, obesity and pre-diabetes, which resembles the human senile OA *[Mason et al., 2001].* The underlying mechanisms that drive the development and progression of spontaneous OA in these animal models are however not well defined, and may reflect specific subtypes of idiopathic human OA. In particular, Hartley guinea pig model is characterized by early subchondral bone remodeling, meniscal ossification and ligament changes, while STR/ort mice resemble more the systemic inflammatory/immune response involved in OA *[Malfait et al., 2015].*

Moreover, transgenic mice have been used extensively as genetically modified species to study OA and, in particular, the effects of a particular gene on the development of the disease. The genes selected for manipulation are typically involved in cartilage matrix degradation, chondrocytes differentiation or apoptosis, bone turnover and inflammation *[McCoy, 2015].*

Induced OA animal models are commonly employed to study secondary OA and are obtained primarily by surgical manipulation or intra-articular (i.a.) chemicals injection.

Surgically-induced OA models resemble osteoarthritis that occurs due to an insult/injury to the affected joint (PTOA). These animal models have been used to study both the effect of drugs on the disease process and the pathogenesis of post-traumatic osteoarthritis, e.g. subchondral bone changes *[Kuyinu et al., 2016].* The advantages of surgical models are the repeatability and the rapid onset and progression of the disease, as well as the clear relationship between the disease-triggering event and the development of the pathology *[Fang et al., 2014].*

Surgically-induced OA models include partial or total meniscectomy, destabilization of the medial meniscus, meniscal tear and ACL transection (ACLT). Each model relies on a combination of joint instability, altered joint mechanics (i.e. changes in load bearing or joint congruence), and inflammation to induce OA lesions *[McCoy, 2015].*

The ACLT model is currently used as OA model in small animals such as rats and rabbits in particular. ACL injury causes joint destabilization, inducing mild cartilage destruction and osteophytes formation *[Kuyinu et al., 2016].* The combination of ACLT with other surgical procedures can lead to more severe and rapid damage in the joint than ACLT alone *[Fang et al., 2014].*

A partial meniscectomy in rats and rabbits causes a destabilization of the joint leading to rapid degeneration and a more severe OA than ACLT.

The medial meniscal tear (MMT) OA model in rats and guinea pigs causes joint instability and proteoglycans and chondrocytes loss, leading to cartilage degradation *[Kuyinu et al., 2016].*

The destabilization of the medial meniscus (DMM) is currently the most commonly used surgically-induced OA model in mice, which has been proved ideal for studying OA pathophysiology, molecular mechanisms and pain. DMM surgery is performed by transection of the medial meniscotibial ligament, which causes mild instability, resulting in unbalanced joint biomechanics that lead to cartilage destruction, subchondral bone sclerosis and osteophytes formation *[Fang et al., 2014].*

Chemically-induced OA models involve mostly the intra-articular injection into the knee joint of a toxic or inflammatory compound. In particular, the model currently most employed is obtained by the i.a. injection of monosodium iodoacetate (MIA) in rats. This animal model has a unique pathophysiology, which has no correlation to that of PTOA. Therefore, MIA chemically-induced OA model is mainly used to study the mechanism of OA pain-related behaviours and for the screening of symptom-modifying OA drugs, given its rapidity and reproducibility *[McCoy, 2015; Kuyinu et al., 2016].*

The MMT and the MIA animal models in rats were selected for the present study as most commonly used surgically- and chemically-induced OA models, able to mimic both the painful and structural components (e.g. chondropathy, osteophytosis and synovial inflammation) of the human pathology *[Mapp et al., 2013].*

3.2.1 The MMT model

The MMT model as a surgically-induced OA model is particularly suited for studying the pathophysiology of post-traumatic knee OA and is commonly used to evaluate potential therapeutics *[Mapp et al., 2013; Yu et al., 2015].*

This model is induced by the transection of both the medial collateral ligament and the medial meniscus of the femorotibial rat joint, which leads to joint destabilization and results in a progressive occurrence of degenerative changes within the articular cartilage (e.g. chondrocytes degeneration and apoptosis, loss of proteoglycans and matrix fibrillation), synovitis and

subsequent subchondral bone thickening and osteophytes formation. In particular, degenerative changes occur by 3-6 weeks post-surgery *[Janusz et al., 2002; Bove et al., 2006].*

Moreover, previous studies in this OA model have proved its characterization by primary joint pain and discomfort, defined as changes in hind paw weight bearing distribution, with often concurrent secondary mechanical allodynia *[Bove et al., 2006].* In particular, changes in hind paw mechanical loads caused by deterioration of the articular cartilage seem to trigger osteophytes formation, most likely as a skeleton adaptation aimed to stabilize the injured joint. Osteophytes can further limit joint movement and can be a source of joint pain, thus affecting bone and cartilage metabolism *[Bagi et al., 2015b].*

3.2.2 The MIA model

The MIA model is mostly employed for OA pain studies to assess the efficacy of analgesic drugs *[Bove et al., 2003].*

This animal model is obtained by the intra-articular injection of MIA, an inhibitor of glyceraldehyde 3-phosphate dehydrogenase, in the infrapatellar area of the rat knee joint. Therefore, the local injection of monosodium iodoacetate disrupts chondrocytes metabolism and produces cartilage degeneration, through local inhibition of glycolysis. In particular, MIA injection induces rapid chondral erosion characterized by loss of proteoglycans matrix and, at later stages, subchondral bone remodeling with osteophytes formation, in a dose-dependent manner *[Guzman et al., 2003; Combe et al., 2004].*

Moreover, the local injection of MIA results in acute inflammation, characterized by joint swelling, synovitis and immune cells infiltration within the infrapatellar fat pad, which leads to the local release of pro-nociceptive mediators such as SP, bradykinin and prostaglandins. The inflammatory early phase of this model largely resolves by day 7 and is not expected to play a role in mediating chronic OA pain *[Bove et al., 2003].* Nevertheless, this inflammatory response can induce both a sensitization of peripheral nociceptors leading to a C fiber-mediated decrease in response threshold and an increased input to the spinal cord *[Combe et al., 2004].* As a matter of fact, after MIA injection a pain phenotype rapidly develops in the hind limb ipsilateral to the injected knee, suggesting the presence of central sensitization *[Thakur et al., 2012].* In particular, previous behavioural studies in MIA model have proved the occurrence of an initial transient pain response associated with early inflammatory mechanisms, induced by structural changes, lasting less than 7

days, and a following second greater pain response, resulting from the articular degenerative process, beginning 14 days after the injection *[Bove et al., 2003; Ivanavicius et al., 2007].*

Moreover, after MIA injection, both alterations in hind paw weight bearing *[Pomonis et al., 2005],* and profound secondary mechanical hyperalgesia and allodynia in the injected limb occur *[Fernihough et al., 2004].* In particular, the allodynic response was previously associated with the involvement of central pain mechanisms *[Fernihough et al., 2004, Ferland et al., 2011].*

OA pain pathways associated to central sensitization in MIA model involve enhanced excitability of both neurons and glial cells in spinal cord. As a matter of fact, a time-dependent activation of microglia and astrocytes in the spinal cord has been demonstrated in this model of OA pain *[Sagar et al., 2011].* Moreover, these OA pain pathways in MIA model may overlap, at least in part, with neuropathic pain mechanisms. Several previous studies have suggested the involvement of a potential neuropathic pain component in MIA-induced pain at later stages, with a dose-dependent degree of neuronal injury and/or central sensitization *[Ivanavicius et al., 2007; Im et al., 2010; Ferreira-Gomes et al., 2012b; Thakur et al., 2012].*

Finally, one of the major advantages of MIA model consists of the straightforward manipulation of the severity of the disease, pain in particular, by altering the concentration of monosodium iodoacetate used to induce the pathology *[Pomonis et al., 2005].*

3.3 OSTEOARTHRITIS THERAPY

Although important advances have been made in understanding the pathophysiological processes of OA, there are currently no pharmacological treatments able to modify the disease progression.

At present, OA pharmacological therapies, along with physical treatments, still focus mainly on improving OA symptoms and particularly pain *[Sofat et al., 2014].* As a matter of fact, according to the recommendations of the Osteoarthritis Research International Society (OARSI), the European League Against Rheumatism (EULAR) and the European Society for Clinical and Economic Aspects of Osteoporosis and Osteoarthritis (ESCEO), the optimal management of OA requires a combination of both non-pharmacological and pharmacological modalities.

Conversely, surgical modalities including various types of osteotomy, arthroscopic interventions, and knee arthroplasty are reserved for patients with severe clinical disease (i.e. symptoms and/or functional limitations), associated with a reduced health-related quality of life, despite conservative therapy *[Jordan et al., 2003; Zhang et al., 2008; Bruyère et al., 2014].*

The majority of intra-articular surgeries is performed through an arthroscope with the advantages of a minimal operative trauma and a very low infection rate. Joint-preserving surgical techniques consist of arthroscope lavage, shaving (i.e. chondroplasty) and debridement. Conversely, bone-stimulating surgical techniques include drilling, microfracturing and abrasion arthroplasty. Moreover, joint surface can be restore either by autologous chondrocytes transplantation or by autologous osteochondral transplantation *[Michael et al., 2010].* Finally, total joint replacement/arthroplasty is regarded as the best orthopaedic surgery for advanced OA, since this medical procedure seems to reduce pain and improve joint function *[Zhang et al., 2016].*

3.3.1 Non-pharmacological therapies

Non-pharmacological treatments recommended by OARSI, EULAR and ESCEO include education, lifestyle modification, such as weight loss or minimizing activities that aggravate the condition, and physical therapy *[Jordan et al., 2003; Zhang et al., 2008; Bruyère et al., 2014].*

Provision of information and overall patient education about the disease process, its prognosis, pain mechanisms, treatment options and their objectives and implication, has actually minimal effect on OA symptoms, but results essential for treatment adherence, improving patients quality of life *[Grainger et al., 2004; Bruyère et al., 2014].*

In managing OA, weight reduction should be a key goal. Several studies have proved that weight loss decreases pain, improves physical function, and has structure-modifying effects on the knee cartilage. This goal can be accomplished through an intensive low-calorie diet program *[Grainger et al., 2004; Bennell et al., 2012; Vaishya et al., 2016].*

The aim of physical therapy is to maintain joint mobility and improve joint stability and muscle strength. Water or land-based exercises, aerobic walking, quadriceps strengthening, resistance exercises, and tai chi reduce pain and disability from knee OA *[Vaishya et al., 2016].* Moreover, Transcutaneous Electric Nerve Stimulation (TENS) is also a possible physical intervention, which seems to reduce the need for analgesic medications *[Bruyère et al., 2014].*

Among additional physical remedies for OA patients, the access to walking aids is an important help in providing security to patients. In particular, bracing of the knee or the foot can be a useful non-operative and non-pharmacological treatment for patients with OA that predominantly involves either the medial or lateral femorotibial compartment *[Bruyère et al., 2014; Vaishya et al., 2016].* Finally, acupuncture seems to reduce OA pain and increase functional mobility with

minimal side effects, even if these benefits are small and the mechanism of pain relief is unclear *[Vaishya et al., 2016].*

3.3.2 Pharmacological therapies

Pharmacological therapy for OA should be individualised after a careful assessment of symptoms severity, comorbidity, concomitant therapy, side effects, therapy costs, and patient preferences *[Grainger et al., 2004].*

Most practice guidelines recommend acetaminophen (i.e. paracetamol) as first-line oral analgesic for mild-to-moderate OA, and if effective, as the preferred long-term oral analgesic, due to its relative safety and effectiveness *[Zhang et al., 2016].*

Acetaminophen is an active metabolite of phanacetin, characterized by a significant analgesic and mild anti-inflammatory activity, due to its effect on both COX-1 and COX-2. Acetaminophen is associated with less toxicity than other analgesic drugs, even if overdosing of acetaminophen may induce hepatotoxicity *[Merashly et al. 2012, Vaishya et al., 2016].* Therefore, the daily-recommended maximal effective dosage of this analgesic agent, for OA pain management, is 3000 mg *[Bruyère et al., 2014; Zhang et al., 2016]*.

For patients with severe symptoms or non-responding to acetaminophen, more potent drugs should be considered, such as non-steroidal anti-inflammatory drugs (NSAIDs).

NSAIDs provide significant anti-inflammatory and analgesic effects, by reducing prostaglandins biosynthesis through COX-1 and COX-2 inhibition *[Vaishya et al., 2016; Zhang et al., 2016].* In particular, NSAIDs might have dual sites of action, inhibiting peripheral nociceptors sensitization as well as acting centrally at the level of the spinal cord and brain, since these drugs can cross the blood-brain barrier *[Malfait et al., 2013a].*

NSAIDs are characterized by a better overall efficacy than acetaminophen in terms of pain relief for moderate-to-severe OA, providing however only a short-term pain relief, with a greater incidence of gastrointestinal (GI) side effects *[Vaishya et al., 2016; Zhang et al., 2016].* Therefore, OARSI recommends that NSAIDs should be used at the minimum effective dose, avoiding a prolonged use as much as possible. Ibuprofen, naproxen, diclofenac, nimesulide and acetylsalicylic acid are the most commonly used NSAIDs.

In patients with increased GI risk, either a COX-2 selective inhibitor or a non-selective NSAID with co-prescription of a proton pump inhibitor or misoprostol (i.e. prostaglandin E_1-analogue synthetic compound) may be considered for gastric protection.

COX-2 selective inhibitors, such as celecoxib and etoricoxib, have similar analgesic effects compared with non-selective NSAIDs, with a better GI tolerability. However, COX-2 inhibitors have been associated with increased incidence of cardiovascular adverse effects *[Zhang et al., 2008].*

Therefore, the choice between NSAIDs and COX-2 inhibitors should be made carefully after evaluation of risk factors, considering in particular both GI and cardiovascular risks.

Naproxen is the preferred drug among the NSAIDs regarding cardiovascular safety *[Merashly et al., 2012].*

Topical NSAIDs, ibuprofen and diclofenac in particular, are widely used as adjunctive or alternative therapy to oral analgesic/anti-inflammatory agents for knee OA *[Jordan et al., 2003; Zhang et al., 2008].*

Opioids are used for the management of moderate-to-severe OA pain when NSAIDs and acetaminophen are ineffective or contraindicated. However, the frequent adverse effects associated with opioids, including nausea and vomiting, constipation, respiratory depression, sedation, tolerance and physical dependence, limit their chronic use *[Zhang et al., 2016].*

The analgesic effect of opioids arises from their ability to inhibit directly the ascending transmission of nociceptive information from the spinal cord dorsal horns and to activate pain control circuits that descend from the midbrain to the dorsal horns *[Vaishya et al., 2016].*

Weak opioids, such as codeine, are often combined with acetaminophen for enhanced efficacy *[Merashly et al., 2012].*

Tramadol, a centrally acting analgesic with a weak opioid agonist activity, which inhibits the reuptake of serotonin and norepinephrine, may be used in OA patients that have contraindications to NSAIDs and COX-2 selective inhibitors and/or in the case of the failure of the acetaminophen therapy *[Sarzi-Puttini et al., 2005].*

Additional centrally acting agents that have been recently introduced for chronic pain management are the selective serotonin-norepinephrine reuptake inhibitors (SNRIs) antidepressant drugs *[Martel-Pelletier et al., 2012].*

In particular, the selective SNRI duloxetine has been proved effective in reducing OA pain in two double-blind, placebo-controlled randomized trials *[Chappell et al., 2009; Chappell et al., 2011]*, leading to its approval in the USA by the Food and Drug Administration (FDA) for the treatment of

chronic musculoskeletal pain, including OA. Therefore, duloxetine may be a promising and efficacious way to alleviate OA pain, alternative to opioids, for patients who are not able to take NSAIDs or who have a sub-optimal response to NSAIDs and require adjunctive therapy. Duloxetine is thought to alleviate pain through the increase of local brain levels of serotonin and norepinephrine, i.e. the increased tonic activity of the descending inhibitory pain pathways in the central nervous system *[Malfait et al., 2013a].* However, more large-scale longitudinal studies have to be performed to further investigate its safety and efficacy for OA treatment *[Zhang et al., 2016].*

Medications administered via the intra-articular route for the treatment of OA pain include corticosteroids and hyaluronic acid.

Corticosteroids i.a. injection is recommended by OARSI and EULAR for OA patients with moderate-to-severe pain and/or synovial joint effusion, who do not respond to oral analgesic and anti-inflammatory agents *[Jordan et al., 2003; Zhang et al., 2008].* Their mechanism of action is due to a reduction in prostaglandins, bradykinin and histamine release *[Vaishya et al., 2016].* Intra-articular corticosteroids have a rapid onset of action (few days) and an effect of significant pain improvement lasting for a relatively short period (3-4 weeks) *[Merashly et al., 2012].* However, the repeated use of corticosteroids could facilitate tissue atrophy, joint destruction, or cartilage degeneration *[Vaishya et al., 2016].*

On the other hand, intra-articular HA has a more delayed onset of action and a more prolonged effect (up to 3-6 months) on OA pain, given once every 3-5 weeks, compared with corticosteroids *[Merashly et al., 2012].* HA i.a. injections have the purpose to restore the normal intra-articular content of hyaluronic acid, since OA joints are characterized by HA deficiency *[Vaishya et al., 2016].* The role of i.a. hyaluronic acid injections on OA pain has been controversial, but most meta-analyses have shown a significant benefit for knee OA patients *[Bruyère et al., 2014].*

The aminosugar glucosamine and the glycosaminoglycan chondroitin sulphate are both very widely used as “nutritional supplements” by patients with OA *[Zhang et al., 2008].*

Glucosamine is an endogenously synthesized hexosamine involved in the synthesis of HA, proteoglycans, glycolipids, and glycoproteins of articular cartilage. Glucosamine sulfate has demonstrated a similar effect to placebo on knee OA pain in randomized controlled studies, while evidences for a possible structure modifying effect remain controversial.

Conversely, chondroitin sulfate is a structural component of the ECM, which is essential for pressure resistance by retaining water within the cartilage. Chondroitin sulfate seems to induce a mild improvement in OA pain and function with even an apparent small effect on joint structure. However, further high quality trials for both compounds are required *[Merashly et al., 2012; Vaishya et al., 2016].*

The variety of new drugs for OA pain management that have shown promising results in clinical trials includes tanezumab, a monoclonal antibody against NGF. A proof-of-concept study showed that tanezumab significantly reduced knee pain while walking and improved the patients' global assessment, compared with placebo, in patients with knee OA. However, the FDA suspended all trials of tanezumab after the occurrence of rapidly progressive OA, resulting in request for total joint replacement in some patients. Nevertheless, subsequent assessments have shown that the risk of rapidly progressive OA with tanezumab was lower than that with tanezumab/NSAID combination therapy. Moreover, the rate of joint replacement resulted comparable between tanezumab monotherapy and placebo treatment. Therefore, the FDA has agreed to continue the clinical trials of tanezumab in OA treatment in conjunction with appropriate safety monitoring *[Zhang et al., 2016].*

3.4 IMIDAZOLINE RECEPTORS

Imidazoline receptors (IRs), also called imidazoline binding sites (IBS), represent binding sites that have high affinity for compounds containing an imidazoline structure *[Li et al., 2011].*

The presence of imidazoline receptors was first hypothesized in the 1960s, with the discovery of clonidine, to explain the hypotensive effect of this drug, not fully accounted by its interaction as α2-adrenoceptors agonist.

Since the discovery of IRs, further work has identified three different subtypes of imidazoline binding sites, based upon binding affinity, location and physiological function *[Lowry et al., 2014].*

Imidazoline-1 receptors (I1Rs) are located in plasma membranes of neurons in the brain, at fairly high density in the region of the medulla oblongata, and in the heart, kidneys, liver and pancreas.

I1Rs by definition exhibit a high affinity for clonidine and related compounds, such as monoxidine. The imidazoline-1 binding sites are involved in the central control of blood pressure *[Gentili et al., 2006; Li et al., 2011; Lowry et al., 2014]*. As a matter of fact, clonidine-like drugs cause a decrease in outflow by reducing the release of neurotransmitters (i.e. norepinephrine and, to a lesser

degree, epinephrine) from sympathetic nerve endings in peripheral tissues, resulting in a decrease of peripheral vascular resistance, heart rate, cardiac contractility and blood pressure. Even if clonidine-like drugs exert their pharmacological effect at α2-adrenoceptors, several evidences suggest that I1Rs located within the rostral ventrolateral medulla have the greater role in the antihypertensive effects of these drugs *[Lowry et al., 2014].* The I1 receptor-preferring agonists rilmenidine and moxonidine are currently used to control hypertension and heart failure in the clinic *[Li et al., 2011].*

Recently, an I1 receptor candidate protein, i.e. the non-G-protein-coupled imidazoline receptor antisera-selected protein (IRAS), has been cloned, providing novel insights into the signalling pathways that may be associated with IRs. In particular, IRAS is proposed to work through the integrin-signalling complex, leading to the activation of phospholipase C, and to induce the phosphorylation of ERKs, through the binding of insulin receptor substrate proteins *[Lowry et al., 2014].*

Imidazoline-2 receptors (I2Rs), although have not been cloned, are not-G-protein-coupled IBS located in the outer membrane of mitochondria of peripheral and central tissues and, as allosteric binding sites, on monoamine oxidases A (MAO-A) and MAO-B *[Lowry et al., 2014; Bektas et al., 2015].* As a matter of fact, biochemical and pharmacological studies have suggested a possible structural and functional correlation between I2-IBS and MAOs, two mitochondrial enzymes involved in the oxidative deamination of monoamine neurotransmitters, such as serotonin, norepinephrine, and dopamine *[Sánchez-Blázquez et al., 2000; Gentili et al., 2006]*. Moreover, the imidazoline-2 binding sites on MAOs seem to be allosteric sites, since they are separated from the active domain of the enzyme that recognizes the mechanism-based inhibitors, and are not equally available in all the tissues.

I2 receptors are distributed ubiquitously throughout the brain regions such as the arcuate nucleus, caudate nucleus, putamen, globus pallidus, substantia nigra, interpeduncular nucleus, area postrema, mammillary peduncle, ependyma, lateral mammillary nucleus, and the pineal gland. Low to moderate densities are found in the cerebral cortex, thalamus, hippocampus, amygdala, inferior olivary nucleus, ependymal, and various peripheral regions *[Bektas et al., 2015].* Moreover, I2Rs are found in both neurons and glial cells *[Sánchez-Blázquez et al., 2000].*

I2Rs bind preferentially imidazolines and guanidines, such as idazoxan, a non-selective α2-adrenoceptors antagonist, and have a lower affinity for 2-aminoimidazolines, such as clonidine.

Moreover, imidazoline-2 binding sites are divided into I2A- and I2B-IBS, according to their affinity for amiloride, high or low, respectively *[Bektas et al., 2015].*

Imidazoline-2 receptors have been associated with various neurobiological states or central nervous system (CNS) pathologies, including Parkinson's disease, depression, hyperphagia, tolerance and addiction to opioids and analgesia *[Gentili et al., 2006; Li et al., 2011].*

Finally, imidazoline-3 receptors (I3Rs) are present in pancreatic β-cells and regulate insulin secretion, through the modulation of the adenosine triphosphate (ATP)-sensitive potassium channel *[Lowry et al., 2014].*

3.4.1 Imidazoline-2 receptors ligands and analgesia

I2Rs are present in brain areas involved in pain perception and response to painful stimuli *[Gentili et al., 2006].* Moreover, different studies have suggested that several imidazoline-2 receptors ligands meet all the criteria necessary for a drug to be consider useful for pain treatment (i.e. the drug itself has analgesic property, and/or acts as an adjuvant to facilitate other drugs analgesic action, by enhancing their analgesic activity or by altering their pharmacokinetics, and/or decreases the adverse effects of other analgesics) *[Li et al., 2011].*

Although the I2 receptors and their signalling pathways have not yet been cloned and characterized, respectively, non-selective and selective I2Rs ligands have been used to study this receptor system. The majority of I2Rs is widely accepted as being allosteric sites on MAOs. Therefore, I2Rs ligands are described as allosteric modulators. In particular, I2 receptors agonists can be considered allosteric inhibitors of MAO-A and MAO-B, since they have proved to inhibit monoamine oxidation. This inhibition could explain the pain modulatory effect of imidazoline-2 receptors ligands, since increased levels of monoamines such as serotonin and norepinephrine contribute to pain control, especially in the CNS regions related to pain *[Bektas et al., 2015].*

Agmatine is the most extensively studied endogenous non-selective I2 receptors ligand, with a moderate affinity to α2-adrenoceptors as well as all subtypes of imidazoline receptors. Agmatine exerts a wide range of biological effects, including pain modulation. In particular, agmatine has shown no notable analgesic effects for acute phasic thermal and mechanical pain, after both systemic, spinal (intrathecal) and supraspinal (intracerebroventricular) administration. On the other hand, agmatine has produced consistent analgesic effects in acute tonic pain models, after systemic administration. Moreover, both systemic and spinal agmatine administration has

demonstrated significant analgesia, alleviating hyperalgesia and/or allodynia, in several inflammatory and neuropathic pain models. Agmatine analgesic effects can be generally reversed by the non-selective I2/adrenergic α2 receptors antagonist idazoxan, but not by the selective α2 adrenoceptors antagonist yohimbine, suggesting that agmatine-induced analgesic effects are mediated by I2Rs *[Li et al., 2011; Bektas et al., 2015].*

The development of highly selective I2 receptors ligands (>1500-fold selectivity for I2 BS over α2-adrenoceptors), such as 2-(2-benzofuranyl)-2-imidazoline [2-BFI] and its quinoline analogue 2-(4,5-dihydroimidazol-2-yl) quinoline hydrochloride [BU224], has been instrumental in further characterizing I2 binding sites and their functions *[Garau et al., 2013].* In particular, 2-BFI and other I2Rs ligands are effective for tonic and chronic pain (inflammatory and neuropathic pain) but ineffective for acute phasic pain (nociceptive stimulus-evoked reflexive responses), showing similar effects, compared with agmatine. Differential neurobiological mechanisms of the different pain conditions may explain these different analgesic effects of I2Rs ligands. In particular, I2 receptors ligands differentially modulate Aδ and C fibers, which in turn are differentially involved in phasic pain or chronic pain *[Li et al., 2011].*

BU224 and idazoxan, have been considered putative I2Rs antagonists, since they both attenuate the analgesic effects of several I2 receptors agonists such as 2-BFI, even if these compounds have also demonstrated to have agonist effects in some assays. This suggests that these I2Rs ligands are actually characterized by a low efficacy at I2 binding sites *[Qiu et al., 2014].*

Finally, several studies have shown that I2Rs agonists can potentiate opioid-induced analgesia, even in acute phasic pain models, and attenuate the development of tolerance and dependence associated to opioids. In particular, central (intracerebroventricular) or peripheral (subcutaneous [s.c.]) administration of I2Rs ligands, such as agmatine and 2-BFI, potentiates the morphine-evoked supraspinal antinociception in mice and decreases the adverse effects of opioids (e.g. tolerance, constipation, and physical dependence) *[Li et al., 2011; Bektas et al., 2015].*

Moreover, the I2 binding sites ligands exhibiting no antinociceptive effects by themselves in acute phasic pain models, but able to potentiate the analgesic effect of morphine, have been indicated as agonists, while those, such as idazoxan or BU224, that by co-treatment completely reverse this potentiation, have been considered antagonists *[Sánchez-Blázquez et al., 2000].*

Furthermore, a recent study has shown that opioids with higher efficacy (e.g. morphine) demonstrated additive interactions when studied with 2-BFI for antinociception, while opioids

with lower efficacy (e.g. buprenorphine) demonstrated supra-additive interactions with 2-BFI for antinociception *[Sieman et al., 2016].*

The manner in which I2Rs agonists influence opioid-induced antinociception is unclear. Nevertheless, the modulation of the opioid system by I2Rs ligands may occur at different levels *[Thorn et al., 2012].*

One hypothesis is that also central glial activity may play a role in these interactions. Some adverse effects of chronic opioid treatment regimens, such as tolerance and hyperalgesia, have been hypothesized to be mediated by activated spinal microglia. Moreover, previous reports and unpublished observations by Sieman and colleagues, have suggested that I2Rs ligands are capable of attenuating microglia activation in various experimental scenarios *[Sieman et al., 2016].*

Thus, I2 receptors ligands may be useful for treating certain pain conditions (e.g. chronic pain) when used as monotherapy, or combined with opioids as adjuvant, since these drug are effective analgesics in tonic, inflammatory and neuropathic pain models and they increase the therapeutic (antinociceptive) effects and reduce the development of tolerance and dependence of opioids *[Li et al., 2011].*

3.5 CR4056

2-phenyl-6-(1H-imidazol-1yl) quinazoline or CR4056 is a new synthetic highly selective I2Rs ligand (molecular formula $C_{17}H_{12}N_4$; molecular weight 272.31 Da) (***Figure 3***).

CR4056 interacts competitively with I2 binding sites with a sub-micromolar affinity, and via this interaction inhibits human recombinant as well as rat MAO-A activity, through an allosteric mechanism. Moreover, CR4056 is characterized by a potent analgesic activity in different animal models of inflammatory, chronic and neuropathic pain *[Ferrari et al., 2011; Meregalli et al., 2012; Lanza et al., 2014].*

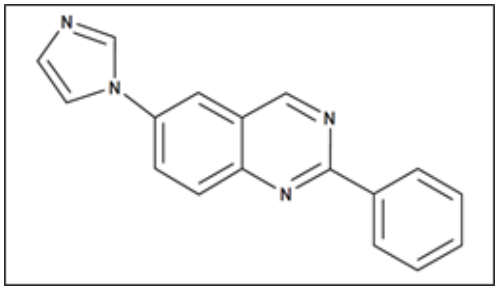

Figure 3: Chemical structure of CR4056.

3.5.1 IN VITRO pharmacology

The activity of CR4056 was first evaluated in vitro, in screening assays to assess its pharmacological selectivity relative to cell-surface receptors, ion channels, transport sites and enzymes, e.g. adrenergic, serotoninergic, dopaminergic, opioid, cholinergic (muscarinic and nicotinic), sigma, imidazoline, gamma-aminobutyric acid (GABA), glycine and glutamate receptors, COX-2, and inducible NOS. CR4056, at the concentration tested (10 µM), was inactive in all assays but inhibited the affinity for I2 receptors and MAO-A by more than 90% *[Ferrari et al., 2011].*
Therefore, additional in vitro pharmacological studies were conducted in order to further evaluate the interactions of CR4056 with I2 binding sites and MAO enzymes.

3.5.1.1 Binding to imidazoline-2 receptors

CR4056 binding to I2 binding sites was investigated using rat whole-brain membranes labeled with the specific radioligand [3H]2-BFI. Aliquots of rat brain membranes were incubated with [3H]2-BFI in presence or absence of different concentrations of CR4056; matching experiments with various reference compounds (2-BFI, BU224, idazoxan, clonidine) were run for comparison. CR4056 inhibited [3H]2-BFI binding with an affinity value (i.e. half maximal inhibitory concentration IC_{50}) of 596 ± 76 nM. The selectivity of CR4056 for I2Rs was confirmed by the absence of activity on I1Rs at concentrations up to 10 µM.
In the standard binding assay protocol, 3 µM CR4056 co-incubated with labeled radioligand, induced a significant inhibition of specific binding to I2Rs (-73% vs. control). Conversely, a modified binding assay protocol was applied to test whether CR4056 binding to I2 receptors was reversible. In particular, in this assay, the pre-incubation of 3 µM CR4056 and I2 receptors (i.e. rat whole-

brain membranes) before starting the equilibrium binding assay in the presence of labeled radioligand, followed by two washes, induced a two-fold decrease of the inhibitory effect of CR4056 (-35% vs. control). These results suggest a reversible binding of CR4056 towards I2 receptors.

Additional experiments were performed to study the effect of CR4056 on equilibrium parameters of [3H]2-BFI specific binding to high and low affinity I2 binding sites. This study showed that CR4056 is a competitive ligand for I2 high affinity binding sites, whereas no significant effects were observed for low affinity binding sites [*Ferrari et al., 2011*].

3.5.1.2 Binding and functional activity assays on monoamine oxidases

Given the structural and functional correlation between I2 binding sites and MAOs, the affinity of CR4056 for MAO-A and MAO-B was studied in receptor binding assays in rat cerebral cortical membranes. The reference agents (i.e. clorgyline and (R)-deprenyl for MAO-A and MAO-B, respectively) were tested concurrently with the test compound in order to assess the assay suitability. CR4056 inhibited MAO-A specific binding with an IC_{50} of 358 ± 12 nM. The inhibition of MAO-B specific binding was achieved at concentrations two orders of magnitude higher. Moreover, the functional activity of CR4056 and reference compounds on the activity of MAO-A and MAO-B was studied on human recombinant enzymes, through a fluorimetric assay. CR4056 selectively inhibited the enzymatic activity of MAO-A, with an IC_{50} value of 202.77 ± 10.3 nM. Similarly to the binding study, CR4056 was about 100 times less active as inhibitor of MAO-B activity *[Ferrari et al., 2011].*

Furthermore, a study on the effect of 1 µM CR4056 on enzymatic kinetic dynamic parameters of MAO-A in rat cerebral mitochondrial membranes, using serotonin as substrate, was performed. The selected concentration of the compound has shown in previous screening assays a full inhibition of human recombinant MAO-A activity and is compatible to IC_{50s} calculated towards rat cerebral and recombinant human MAO-A. The results of this study revealed that CR4056 behaves as an allosteric inhibitor of rat cerebral MAO-A. On the other hand, an analogous study was carried out in order to evaluate the effect of CR4056 on enzymatic kinetic dynamic parameters of human recombinant MAO-A. In particular, CR4056 was tested at 0.3 µM and 1 µM, concentrations that have significantly inhibited human recombinant MAO-A activity in previous screening assays. In this case, the results obtained suggest a mixed (competitive-allosteric) mechanism of action of

CR4056 towards monoamine oxidases A. The different mode of action of CR4056 towards either rat or human recombinant MAO-A may be explained by both the differences in MAO-A structure and activity between the two species and the different inhibitory effects exerted by different I2Rs ligands.

3.5.2 IN VIVO pharmacology

Although I2 binding sites are not fully characterized at molecular level, robust pharmacological evidences have demonstrated an allosteric inhibition of MAOs activity by several I2Rs ligands. Being responsible for monoamines catabolism, MAOs play a pivotal role in pain control and chronic pain state such as neuropathic pain *[Bektas et al., 2015*]. Indeed, pharmacological treatments that increase the synaptic levels of norepinephrine and serotonin have gained prominence in the management of chronic pain, including musculoskeletal and OA pain, with regard to the selective SNRI duloxetine *[Malfait et al., 2013a].*

Another relevant activity of I2 receptors is the modulation of the opioid system, which may occur at different levels*.* In particular, recent evidence has shown that I2Rs ligands are able to increase beta-endorphin secretion in the rat adrenal medulla, mimicking the effect of opioid receptors agonists *[Chang et al., 2010].* Moreover, an interaction between imidazoline ligands and the opioid system was observed in the locus coeruleus neurons *[Ruiz-Durántez et al., 2003].* This interaction is probably involved in the prevention of tolerance and addiction (i.e. attenuation of the hyperactivity of locus coeruleus neurons during opiate withdrawal) to opioids *[Wu et al., 2011].*

Therefore, the in vivo pharmacological characterization of CR4056 was performed focusing on both these modes of action of I2Rs ligands: the inhibition of MAOs activity and the interaction with the opioid system.

3.5.2.1 EX-VIVO evaluation of endogenous norepinephrine release

The levels of endogenous norepinephrine were measured in parieto-occipital cortex and lumbar spinal cord (L4-L6) of male rats orally administered with 20 mg/kg CR4056, after either acute or sub-acute (4 days, daily [QD]) treatment, in order to evaluate the efficacy of the compound as regards the increase of NE release, as a result of MAO-A inhibition. The acute 20 mg/kg CR4056 oral (p.o.) administration induced an increase of NE levels, which resulted significant in the

parieto-occipital cortex only. On the other hand, the 4-days sub-acute CR4056 oral treatment significantly increased NE levels, both in cerebral cortex and in the lumbar spinal cord *[Ferrari et al., 2011].*

3.5.2.2 Analgesic activity in different animal models of pain

CR4056 administered by oral route has been proven effective in reducing experimental pain in several animal models.

The acute oral administration of 6, 20 or 60 mg/kg CR4056 promoted a complete reversion of secondary mechanical hyperalgesia, associated with either inflammation or neurogenic inflammation, induced by the sub-plantar injection in the rat paw of either Complete Freund's adjuvant (CFA) (***Figure 4***) or capsaicin (***Figure 5***), respectively. In particular, the 6 and 20 mg/kg doses were highly effective against pain perception, whereas 60 mg/kg CR4056 caused hypoalgesia (i.e. increase of the pain threshold above the mechanical threshold of sham animals) *[Ferrari et al., 2011].*

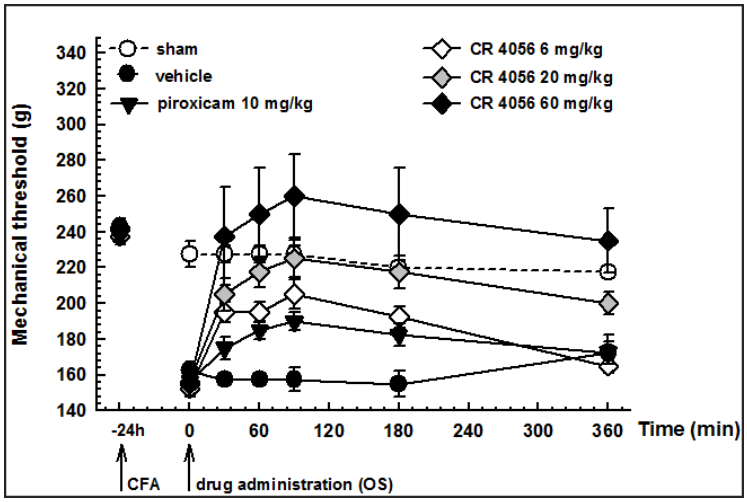

Figure 4*:* Antinociceptive effects of increasing doses of CR4056 on CFA-induced inflammatory pain in rats (Randall- Selitto test). CR4056 was orally administered 24h after CFA injection in the right paw of the rats. Piroxicam (10 mg/kg; p.o.) was used as positive control *[Ferrari et al., 2011].*

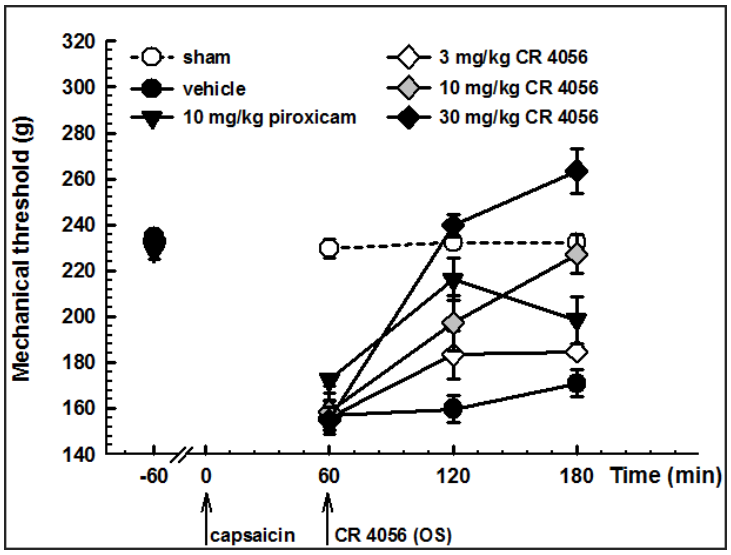

***Figure 5**:* Antinociceptive effect of increasing doses of CR4056 on capsaicin-induced inflammatory pain (Randall-Selitto test). CR4056 was orally administered 1h after the sub-plantar injection of capsaicin in the rats right paw. Piroxicam (10 mg/kg; p.o.) was used as positive control *[Ferrari et al., 2011].*

Moreover, the analgesic efficacy of a single oral administration of CR4056 was confirmed in the Brennan's model of postoperative pain (***Figure 6***). This animal model consists in a surgical incision through skin, fascia and muscle of the rat hind paw, which results in the development of secondary mechanical hyperalgesia, 24 hours after surgery *[Lanza et al., 2014].*

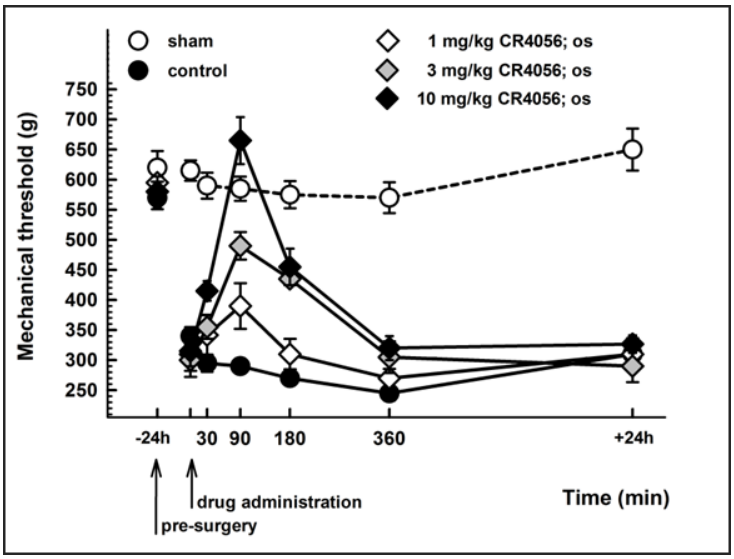

Figure 6: Anti-hyperalgesic effect of CR4056 on postoperative pain-induced mechanical hyperalgesia in rats (Randall-Selitto test). CR4056 was orally administered 24h after surgery *[Lanza et al., 2014].*

Both the capsaicin-induced neurogenic/inflammatory pain model and the Brennan's model of postoperative pain were employed to further investigate the pharmacological characterization of the analgesic activity of CR4056, given the *in vitro* evidence of a selective interaction of CR4056 with I2 receptors.

In particular, in the model of neurogenic inflammation obtained by capsaicin sub-plantar injection, several imidazoline and/or adrenergic receptors antagonists were administered 15 minutes before an effective analgesic dose of CR4056 (30 mg/kg). Efaroxan (a non-selective I1Rs and α2 adrenoceptors antagonist), yohimbine (a selective α2 antagonist) and prazosin (a selective α1 antagonist) did not influence the analgesic effect of CR4056 on capsaicin-induced mechanical hyperalgesia. Conversely, idazoxan (0.3, 1, 3 mg/kg; a non-selective antagonist of I2Rs and adrenergic α2 receptors) significantly and dose-dependently reduced the analgesic activity of CR4056. These results suggest that the binding with the I2 receptors is a primary requirement for CR4056 analgesic efficacy. Furthermore, naloxone (a μ-opioid receptors antagonist) was administered to capsaicin-treated rats, 15 minutes before CR4056 administration, in order to investigate the hypothesis of an indirect in vivo modulation of the opioid system by CR4056, given its hypoalgesic effect at high doses that could mimic the effect of some opioid agonists (i.e. morphine). Naloxone antagonized the slight hypoalgesic effect previously reported but not the analgesic effect induced by CR4056. Therefore, the hypoalgesic component of CR4056 analgesic activity may be due to the release of endogenous endorphins, as observed with other I2 ligands *[Ferrari et al., 2011].*

The analgesic effect of CR4056 seems to be mechanism-related (i.e. due to its interaction with I2 binding sites) even in Brennan's model of postoperative pain. As a matter of fact, idazoxan completely suppressed the analgesic activity of CR4056. Efaroxan and naloxone were unable to alter the analgesic response induced by CR4056. On the other hand, in this model, yohimbine and atipamezole, an additional α2-adrenoceptors antagonist, partially but significantly reduced the effect of CR4056. A possible hypothesis regarding these data may be related to CR4056 allosteric inhibition of MAO-A, resulting in increased levels of endogenous NE in different areas of the CNS that could activate presynaptic α2 autoreceptors, which in turn are blocked by exogenous yohimbine and/or atipamezole. Nevertheless, the results obtained in both capsaicin-induced and postoperative pain models support the hypothesis that CR4056 exerts its analgesic effects mainly through a mechanism strictly related to I2 receptors *[Lanza et al., 2014].*

A similar analgesic activity of CR4056 was detected in rat models of non-inflammatory muscular pain (i.e. acid-induced fibromyalgia-like pain) and both diabetes-induced (i.e. streptozotocin-induced) and chemotherapy-induced (i.e. bortezomib-induced) neuropathic pain. In particular, CR4056 dose-dependently decreased both streptozotocin-induced diabetic pain (i.e. secondary mechanical hyperalgesia) (***Figure 7***) and acidic saline-induced fibromyalgia-like pain (i.e. bilateral mechanical allodynia) (***Figure 8***) in rats, after single oral administration *[Ferrari et al., 2011].*

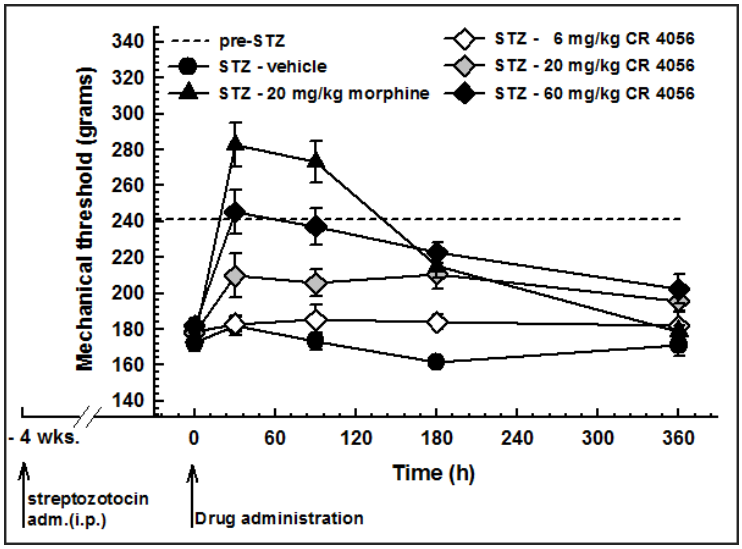

Figure 7: Streptozotocin (STZ)-induced neuropathic (diabetic, type I) pain in rats: effects of increasing oral doses of CR4056 (Randall–Selitto test). Diabetes was induced in rats by administration of a single dose of STZ (intraperitoneal [i.p.]). CR4056 was orally administered four weeks after the STZ injection. Morphine (20 mg/kg; subcutaneous [s.c.]) was used as positive control *[Ferrari et al., 2011].*

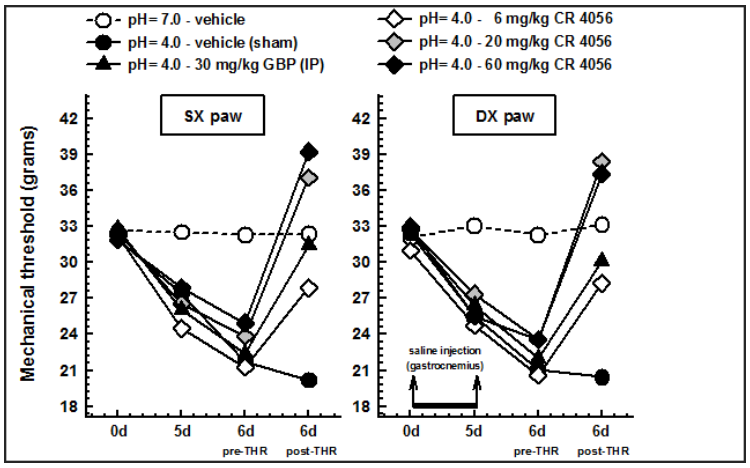

Figure 8: Antiallodynic effects of CR4056 in the acid-induced muscle allodynia model in rats (Dynamic Plantar Aesthesiometer). Right gastrocnemius muscle was injected with acidic saline (pH = 4). Five days later (d5), the same gastrocnemius muscle was re-injected using an identical injection protocol. Control animals were injected with sterile saline. Six days after the first acidic saline injection, CR4056 was orally administered two hours before testing. Gabapentin (GBP; 30 mg/kg; i.p.) was used as positive control *[Ferrari et al., 2011].*

Moreover, the efficacy of the compound was extensively investigated in the rat model of neuropathic pain induced by bortezomib, the frontline treatment for multiple myeloma, characterized by peripheral neurotoxicity as major adverse effect. This model was used to establish the minimal effective dose of CR4056 p.o. (0.6 mg/kg), its optimal dose (6 mg/kg), and the possible optimal scheme of treatment. In particular, the optimal dose of 6 mg/kg completely reversed mechanical allodynia without inducing tolerance, for an administration period up to 3 consecutive weeks. Moreover, the suspension of CR4056 treatment after 21 days did not induce any signs of withdrawal syndrome (***Figure 9***) *[Meregalli et al., 2012].*

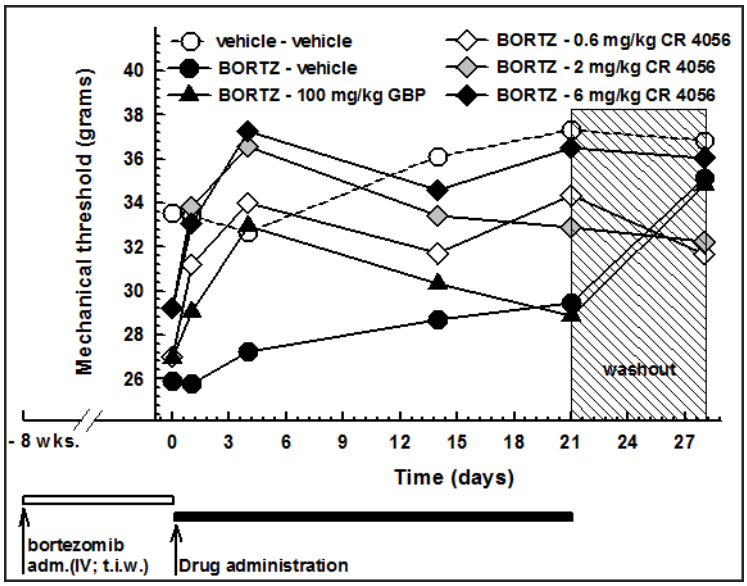

Figure 9: Bortezomib-induced neuropathic pain in rats: effect of increasing oral doses of CR4056 (0.6, 2, 6 mg/kg) on mechanical allodynia (Dynamic Plantar Aesthesiometer). CR4056 was administered once daily for 3 weeks, starting after the treatment with bortezomib (BORTZ; 0.2 mg/kg intravenous [i.v.]; three times a week for 8 weeks). Gabapentin (GBP; 100 mg/kg p.o.) was used as positive comparator *[Meregalli et al., 2012].*

Finally, the interaction between CR4056 and the opioid system was further investigated both in the model of neurogenic inflammation obtained by capsaicin sub-plantar injection and in the postoperative pain model, given several evidences of I2 receptors ligands modulation of the opioid system. Both experimental protocols highlighted a relevant synergy between CR4056 and morphine. The combination of the two drugs was clearly synergic, being more effective than predicted on the basis of a simple additive effect *[Ferrari et al., 2011; Lanza et al., 2014].*

Moreover, the effect of CR4056 on the development of tolerance to morphine analgesia was recently investigated in the inflammatory pain model induced by the sub-plantar injection in the rat paw of CFA, in comparison with the I2Rs selective ligand 2-BFI. Not-analgesic doses of CR4056 (range 0.1–1 mg/kg p.o.) and 2-BFI (range 0.003–0.03 mg/kg i.p.) were administered 15 minutes before each administration of a robust analgesic dose of morphine (5 mg/kg s.c.), given twice a day for 3 days, and once on day 4, to induce morphine analgesic tolerance. On day 4, a robust decrease in morphine analgesic efficacy on secondary mechanical hyperalgesia was evidenced in rats administered with repeated doses of morphine alone. On the other hand, both I2Rs ligands dose-dependently reduced morphine tolerance. In particular, 1 mg/kg CR4056 and 0.03 mg/kg 2-BFI completely restored morphine analgesic effect.

3.5.3 Safety pharmacology

Despite CR4056 effects on catecholamine levels in the CNS, no neurobehavioural changes were associated with the compound during preclinical safety pharmacology studies in rats (i.e. the behavioural Irwin test, the rotarod test for neuromuscolar coordination, and open field test for locomotor activity) *[Ferrari et al., 2011; Lanza et al., 2014].*

CR4056 effects on the cardiovascular and respiratory system seen in safety pharmacology studies may be explained by the activity of CR4056 on the catecholamine system, probably via interaction with I2 binding sites. In the conscious dog, CR4056 induced hypertensive effects associated with tachycardia at doses higher than 30 mg/kg. Tachypnea was observed in the conscious rat at and above a dose of 50 mg/kg. Interestingly, all these effects on cardio-respiratory functions can be produced by excitation of afferent cardiac sympathetic nerve fibers and are functionally opposite to what is generally observed after the administration of opioids.

Moreover, pharmacologically relevant doses of CR4056 induced a dose-dependent diuretic effect in rats. Notably, several imidazoline receptors ligands are characterized by a diuretic effect *[Ferrari et al., 2011].* Overall, these data have been proved the pharmacological safety of CR4056 in the species examined.

3.5.4 Animal pharmacokinetics

CR4056 was rapidly absorbed in rats and dogs after oral administration, with absolute bioavailability around 50%. After single oral administration in rats, the pharmacokinetics of the compound was virtually dose-independent (linear) in the dose range of 10 to 50 mg/kg. Similar results were observed in dogs at doses ranging from 0.3 to 10 mg/kg. The bioavailability of CR4056 administered as capsules was approximately 60-80% of the one obtained with the same dose solution, indicating that the selected formulation is suitable for use in clinical studies.

CR4056 was found to be highly bound to plasma proteins with an even distribution in plasma and blood cells from mice, rats, dogs and humans. Therefore, its exposure can be compared directly across species.

The ability of CR4056 to cross the blood-brain barrier, in agreement with its putative central analgesic effect, was demonstrated. The volume of distribution after intravenous administration was moderate in dogs to extensive in rats.

CR4056 was found to be an inhibitor of the activity of human cytochrome P450 (CYP450) enzymes, while a weak inducer of the same enzymes. Thus, drug interactions due to metabolic inhibition are possible with co-administered drugs metabolized by the CYP450 system, whereas drug interactions resulting from metabolic induction are unlikely.

Metabolic studies in rats and dogs indicated that these two species are suitable for the assessment of the toxicological profile of CR4056, since they are exposed to both the parent compound and its metabolites.

CR4056 was characterized by a high clearance after i.v. administration in rats and dogs; elimination occurred mainly through feces after both oral and intravenous administration, suggesting extensive biliary excretion.

4. AIM

Osteoarthritis (OA) is a disabling and painful condition, very common in the elderly, which affects several million individuals worldwide. Therefore, OA represents a massive worldwide healthcare and financial burden *[Poulet et al., 2016].*

In particular, knee osteoarthritis is the most common type of OA *[Michael et al., 2010].*

OA is a heterogeneous degenerative chronic disease that involves the whole synovial joint in a pathologic dynamic process, resulting in the disruption of the normal homeostasis of the joint *[Loeser et al., 2012].* OA development and progression can be considered the product of the interplay between systemic and local risk factors *[Zhang et al., 2010].*

Pain is the earliest and most disabling symptom for OA patients. OA pain results from a complex interaction between local tissue damage, inflammation, and the peripheral and central nervous systems. Moreover, OA pain is driven by both nociceptive and neuropathic mechanisms *[Salaffi et al., 2014].*

Although important advances in understanding OA pathophysiological processes have been accomplished, to date there are still no curative drugs for this condition. Moreover, the chronic use of first-line pharmacological treatments to handle OA pain (i.e. acetaminophen and non-steroidal anti-inflammatory drugs [NSAIDs]) is frequently associated with adverse effects *[Sofat et al., 2014].*

No ideal animal model for human OA has been described so far. Instead, different OA animal models are used to mimic different features of the human pathology *[McCoy, 2015].*

The first aim of my project was to analyze and compare the time-related progression of several OA pain-like behaviours in two commonly used OA animal models in rats, the MIA model and the MMT model. Both these OA animal models are able to mimic the painful and structural components of the human pathology. In particular, knee OA was induced either by single intra-articular injection of 1 mg/50 µl monosodium iodoacetate (MIA) or by medial meniscal tear (MMT) in the right knee of male rats. Moreover, in both OA models, the expression of several pain-related proteins was assessed in either lumbar spinal cord or L4 and L5 dorsal root ganglia (DRGs), in order to investigate potential markers of both chronic pain state and OA disease. In particular, I evaluated the activation of both mitogen-activated protein kinases (MAPKs) (i.e. the neuronal ERKs and the glial p38) and microglia (i.e. Iba-1 positive morphologically activated cells) in lumbar L4-L5 spinal cord and the activation of satellite glial cells (i.e. GFAP expression) in L4 and L5 DRGs, given their pivotal role in the establishment and maintenance of central sensitization [*Takeda et al., 2009; Lee at al., 2011; Sagar et al., 2011*].

My second purpose was to evaluate in these OA models the efficacy of CR4056, a novel analgesic compound, in comparison with naproxen, a NSAID often prescribed for human OA pain.

CR4056, an imidazoline-2 receptors ligand, is a promising analgesic drug that has been reported to be effective in several animal models of inflammatory, chronic and neuropathic pain *[Ferrari et al., 2011; Meregalli et al., 2012; Lanza et al., 2014].*

5. MATERIALS AND METHODS

5.1 ANIMAL SUBJECTS

Male Wistar rats (Harlan Italy, Correzzana, Italy) weighing 150-175 g and male Sprague Dawley rats (Charles River Laboratories Italy, Calco, Italy) weighing 300-325 g were housed with ad libitum access to food and water, in a temperature-controlled room with a 12 h light/dark cycle, at least 1 week before the surgical procedure. All the experimental procedures described herein were in compliance with national and international laws and policies (Italian Legislative Decree of 4th March 2014, which transposed the European Union Directive 2010/63/EU on the protection of animals used for scientific purposes) and were approved by the Rottapharm Biotech review board. All studies involving animals are reported in accordance with the Animal Research: Reporting of In Vivo Experiments (ARRIVE) guidelines for reporting experiments involving animals *[Kilkenny et al., 2010; McGrath et al., 2010].*

5.2 MIA MODEL OF OSTEOARTHRITIS

Unilateral knee OA was induced by a single intra-articular (i.a.) injection of monosodium iodoacetate (MIA; Sigma Aldrich, Milan, Italy) in the infrapatellar area of the right knee of male Wistar rats. 6 animals per group were used in each experiment. The experimental procedure was performed according to the method first proposed by Kalbhen *[Kalbhen, 1987],* and later revised by Sagar et al. *[Sagar et al., 2011].* The dose of MIA was selected for the present study based on a combination of preliminary results and literature data. In particular, our research group noticed that 1 mg/ 50 µl MIA was the minimum dose required to detect secondary allodynia and primary hyperalgesia associated with joint damage. On day 1, rats were anaesthetized with 2% isoflurane in pure oxygen inside an induction chamber. Once unconscious, rats were removed and placed on a non-rebreathing anaesthetic circuit with mask delivery of isoflurane in pure oxygen throughout the procedure. The right leg skin was sterilized with 75% ethyl alcohol and the knee was located by palpation. A 26-gauge needle was inserted vertically to penetrate the skin and turned distally for insertion into the articular cavity until a distinct loss of resistance was detected. 1 mg of MIA in 50 µl saline was then delivered into the articular cavity. Control rats received instead 50 µl of saline solution. All animals were sacrificed 21 days after the i.a. injection of either MIA or saline solution.

5.3 MMT MODEL OF OSTEOARTHRITIS

Unilateral knee OA was induced by the transection of both the medial collateral ligament and the medial meniscus of the right knee of male Sprague Dawley rats, which results in a progressive cartilage degeneration characterized by several changes typical of OA *[Janusz et al., 2002].* 9 rats per group were used in each experiment. On day 1, rats were anaesthetized with 2% isoflurane in pure oxygen inside an induction chamber. Once unconscious, rats were placed on a non-rebreathing anaesthetic circuit with mask delivery of isoflurane in pure oxygen throughout the procedure. The right leg was shaved and the skin was sterilized with 75% ethyl alcohol. The medial collateral ligament was exposed by blunt dissection and transected to reflect the meniscus toward the femur. The joint space was visualized and the meniscus was cut through the full thickness at its narrowest point to simulate a complete tear, taking care not to damage the tibial surface. The connective tissue layer and skin were closed with Vicryl 6.0 suture and a skin glue (3M Vetbond), respectively. For sham animals, the medial collateral ligament was exposed, but not transected, as previously reported *[Bove et al., 2006].* After surgery, rats were housed in Tecniplast Eurostandard type IV cages, measuring 595x380x200 mm, three per cages. Furthermore, starting from a week post-surgery, rats cages were changed twice a day to stimulate movement and an anti-stress enrichment was added. All animals were sacrificed 6 weeks after MMT surgery, an experimental period sufficient to create severe cartilage lesions that mimic late-stage OA, as demonstrated by several previous studies *[Janusz et al., 2002; Bove et al., 2006].*

5.4 PHARMACOLOGICAL TREATMENTS

CR4056 (2-phenyl-6-(1H-imidazol-1yl) quinazoline; Rottapharm Biotech, Monza, Italy) was suspended in 0.5% hydroxyl-propyl-carboxymethyl cellulose (HPMC) and administered orally in 5 ml/kg administration volume. Naproxen sodium salt (Sigma Aldrich, Milan, Italy) was dissolved in distilled water and administered orally in 5 ml/kg administration volume.

As regards MIA model, CR4056 (2, 6 and 20 mg/kg) and naproxen (10 mg/kg) were administered p.o., as single treatment on day 7 (i.e. early phase of the pathology) and as sub-acute treatment from day 14 to day 21, once a day. Sham and control animals were orally administered with HPMC (vehicle) following the same schedule. Similarly, MMT rats were treated p.o. with CR4056 (6 and 20 mg/kg) and naproxen (10 mg/kg) from day 28 (i.e. early phase of the pathology) to day 42, once

daily. Sham and control animals were orally administered with vehicle following the same schedule.

In particular, the experimental schedule was selected based on the literature related to pain evaluation in these two animal models of osteoarthritis *[Kalbhen, 1987; Mapp et al., 2013].* CR4056 doses were selected based on the previous experience with this compound in other animal models of pain *[Ferrari et al., 2011; Meregalli et al., 2012; Lanza et al., 2014].*

5.5 BEHAVIOURAL ASSESSMENTS

The behavioural assessments were selected according to previous reports related to pain evaluation in animal models of osteoarthritis *[Fernihough et al., 2004; Mapp et al., 2013].* Several behavioural tests were used to determine the alterations in pain perception related to MIA i.a. injection. In particular, we assessed the effect of CR4056 versus naproxen by evaluating both the allodynic and the primary hyperalgesic responses to mechanical stimuli. Moreover, static and dynamic hind paw weight bearing distribution and locomotor activity were assessed. The behavioural measures were performed on day 0 before MIA injection and on day 7, 14 and 21 after MIA injection. On days 14 and 21, behavioural tests were performed prior and 90 minutes after the drug administration, since in-house preliminary experiments have selected this time as the optimal time to observe reversal of pain behaviour after the oral drug administration. As regards MMT model, changes in pain behaviour were measured by assessing both mechanical allodynia and secondary hyperalgesia. Besides, joint discomfort perception was evaluated as changes in static and dynamic hind paw weight bearing distribution, locomotor activity and motor function. The behavioural measures were generally performed on day 0 before MMT surgery and on day 14, 28, 35 and 42 after the induction of OA, before and 90 minutes after the drug administration.

5.5.1 Mechanical allodynia

Mechanical withdrawal threshold of both the ipsilateral and contralateral hind paw was assessed in MIA model using a Dynamic Plantar Aesthesiometer (Ugo Basile S.r.l., Gemonio, VA, Italy) (***Figure 10***), which generates a linearly increasing mechanical force *[Malfait et al., 2013b].* On each

day of testing, rats were placed in a Plexiglas chamber (28 × 40 × 35 cm) equipped with a wire mesh floor, 20 cm above the bench, for a one-hour acclimatization period followed by testing. After the habituation period, a servo-controlled mechanical stimulus, represented by a pointed metallic filament of 0.5 mm diameter, was positioned under the plantar surface of the hind paw, exerting a progressively increasing punctate pressure, reaching up to 50 g within 20 seconds. A clear spontaneous hind paw withdrawal response caused by the punctuate pressure was recorded automatically. The results defined the minimum pressure (in grams) required to elicit a robust and immediate withdrawal reflex of the paw. Stimuli were applied alternately on each posterior paw every 2 minutes on three repeated measures to obtain a mean value representing the mechanical allodynic threshold.

Conversely, mechanical allodynia of the ipsilateral and contralateral paws was assessed in MMT model using a set of calibrated von Frey monofilament hairs (Stoelting Co., Wood Dale, IL, USA), according to previous studies in literature concerning this osteoarthritis model *[Fernihough et al., 2004; Bove et al., 2006].* On each day of testing, animals were placed in a Plexiglas chamber with a wire mesh floor and allowed to acclimatise for one hour prior to the start of the experiment. The von Frey hairs were applied from below to the plantar surface of both the ipsilateral and contralateral hind paw alternately to determine the 50% force withdrawal threshold, according to the up-and-down method described by Chaplan and colleagues *[Chaplan et al., 1994].* Briefly, nine von Frey filaments with bending force of 0.4-15 g were applied with enough pressure to buckle for up to 6 s, beginning with the 4 g filament. A positive response was noted if the paw was sharply withdrawn or a flinching occurred upon application of the hair. If no response was observed, the filament with the next highest force was applied, while the filament with the next lowest force was applied upon a positive response. Five consecutive filaments application was performed for each posterior paw. The sequence of flinch/no-flinch responses was used to calculate the actual paw withdrawal threshold.

In both models, mechanical allodynia was always assessed first on the ipsilateral paw, in order to avoid any bias in the animal response to evoked pain.

Figure 10: Dynamic Plantar Aesthesiometer.

5.5.2 Primary mechanical hyperalgesia

In MIA model mechanical hyperalgesia was assessed directly on both the ipsilateral and contralateral knees using PAM device (Pressure Application Measurement - Ugo Basile S.r.l., Gemonio, VA, Italy), a force transducer (range of 0-1500 g and 8 mm diameter) mounted on a unit fitted to the operator's thumb and connected to a recording base unit (***Figure 11***) *[Barton et al., 2007].* Animals were lightly, but securely held and the operator placed the thumb unit on one side of the animal's knee joint and the forefinger on the other. A progressive quantified squeeze force was then applied across the joint at a rate of approximately 300 grams per second (5 s as maximum test duration). The force that elicits the animal response, normally limb withdrawal or any behavioural signs of discomfort or distress, such as freezing of whiskers movement or wriggling, was recorded. In particular, the peak gram force applied immediately prior to limb withdrawal, designated as limb withdrawal threshold, represents the mechanical hyperalgesic threshold.

Mechanical hyperalgesia was always assessed first on the ipsilateral knee, in order to avoid any bias in the animal response to evoked pain.

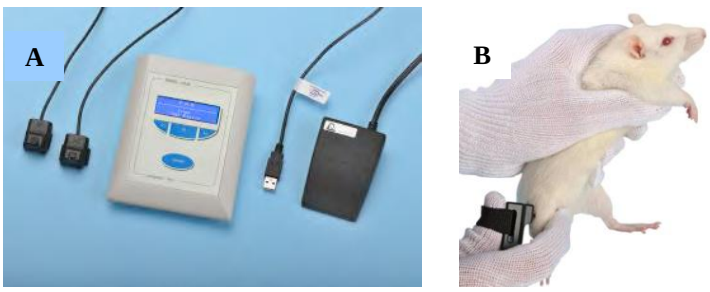

Figure 11: PAM device ***(panel A);*** force transducer on the operator's thumb (***panel B***).

5.5.3 Secondary mechanical hyperalgesia

In MMT model mechanical hyperalgesia of the ipsilateral paw was assessed by measuring the paw withdrawal threshold to an increasing pressure stimulus placed on the dorsal surface of the hind paw, using a Randall-Selitto electronic analgesymeter (Ugo Basile S.r.l., Gemonio, VA, Italy) (***Figure 12***) *[Santos-Nogueira et al., 2012].* Each animal was briefly handled to get used to manipulation and then securely held while the operator placed the hind paw tested on a small plinth under a cone-shaped pusher with a rounded tip. An increasing mechanical force was then applied on the medial portion of the dorsal surface of the hind paw, by the depression of a pedal-switch on behalf of the operator, until either a limb withdrawal response or vocalization occurred. The grams of the force exerted is continuously monitored by a counterweight moving along a linear mechanical scale. In this study, the maximum force applied was 750g (cut-off), after previous demonstration that no skin damage occurred.

Figure 12: Randall-Selitto electronic analgesymeter.

5.5.4 Static weight bearing

Changes in static hind paw weight distribution (HPWD) between the right (osteoarthritic) and left (contralateral control) limbs were assessed, in both MIA and MMT models, as index of joint discomfort in the osteoarthritic knee *[Bove et al., 2003].* HPWD was evaluated using an incapacitance tester (2Biological Instruments, Besozzo, VA, Italy) (***Figure 13***). The apparatus consists of two force transducers capable of measuring the body weight that the animal places on each hind limb. Animals were placed in an angled Plexiglas chamber, positioned so that each hind paw rested on a separate force-transducing plate; the force exerted by each hind limb (in grams)

was calculated over a 3-s period. The measurement was repeated two times and the results were averaged for each rat. The change in static HPWD was calculated by determining the difference in the amount of weight (g) between the contralateral and ipsilateral limbs.

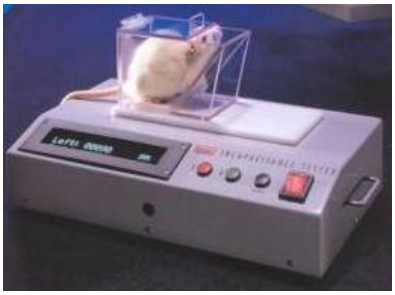

Figure 13: Incapacitance tester.

5.5.5 Dynamic weight bearing

The Dynamic Weight Bearing (DWB) system (Bioseb, Boulogne, France) (***Figure 14***) is a non-invasive method used to obtain the weight distribution and surface area of all four paws in a freely moving animal, as indirect index of spontaneous pain during movement *[Im et al., 2010; Bagi et al., 2015a].* The system consists of a Plexiglas enclosure (22 × 22 × 30 cm) with a floor sensor composed of 44 × 44 sensors. A camera is affixed to the top of the enclosure to align the sensor directionally during the analysis phase. Raw pressure and live video recordings are transmitted to a tablet PC via a USB interface at a sampling frequency of 10 Hz. The data were analysed using the DWB software, version 1.4.2. Zone parameters were set for the analysis as follows: ≥ 1.5 g for one sensor and a minimum of two adjacent sensors ≥ 1 g (to be considered a valid zone). For each time segment that was stable for more than 1 second, zones meeting the above criteria were validated and assigned as either right or left and front or rear paws. Mean values for the weight of each zone were calculated over the entire testing period based on the length of time for each validated segment. For each testing period, the animals were placed into the chamber and the data were collected over a period of 5 minutes. The animals were subjected to the test without previous adaptation, since exploratory movements improve data capture. The operator manually "validated" each test period by ensuring that each paw print corresponded to the appropriate paw, using the video footage as reference. The following parameters were measured for each limb separately and for both the front and hind limb combined: body weight (g), weight put on the limb (g) and percentage of weight placed on the limb. The change in dynamic HPWD was calculated in

both MIA and MMT model by determining the percentage of the weight placed on the ipsilateral hind limb (g) in relation to the total weight of the animal (g).

Figure 14: Dynamic weight bearing system.

5.5.6 Locomotor activity

The animals' spontaneous locomotor activity was measured in both MIA and MMT models as indirect index of spontaneous pain during movement, using an open field test system *[Walsh et al., 1976].* The testing arena consists of a grey-painted industrial plastic, square in shape with 45-cm-high walls. Two pairs of arena settings were set up side by side in order to allow the runs of four animals at the same time. For data acquisition, an overhead video camera coupled to a microcomputer by an image analyzer (EthoVision, Noldus Information Technology, Sterling, VA, USA) was used to track movement of rats in the maze. A remote switch was used to start and stop tracking.

Each individual trial started with the rat being placed in one corner of the maze and continued for 20 minutes, at which point the rat was promptly removed and returned to the housing colony. The distance travelled (cm) by each animal during the 20 minutes-period of the test was measured.

5.5.7 Motor function

In MMT model, the animals' motor function was additionally assessed, using the walking track analysis, a measure of overall coordinated distal motor function requiring intact motor and

sensory function. Walking track analysis, first described by de Medinaceli et al. *[de Medinaceli et al., 1982]*, combines gait analysis and the temporal and spatial relationship of one footprint to another during walking *[Sarikcioglu et al., 2009].* Animals were tested in a confined walkway (13 x 49cm) with a dark shelter at the end of the corridor. White paper cut to the appropriate dimensions was placed on the bottom of the track. The rats hind paws were dipped in a specific type of paint, and the animal was permitted to walk down the track, leaving its hind footprints on the paper *[Varejao et al., 2001].* For the calculation of the index SFI, the following ipsilateral (E) and contralateral (N) footprints parameters were measured: the distance from the heel to the third toe, the print length (PL), the distance from the first to the fifth toe, the toe spread (TS) and the distance from the second to the fourth toe, the intermediary toe spread (ITS) (***Figure 15***) SFI was calculated according to the formula revised by Hare et al. *[Hare et al., 1992]:* SFI = - 38.3 x PLF + 109.5 x TSF + 13.3 x ITF - 8.8; where PLF (print length factor)=(EPL-NPL)/NPL, TSF (toe spread factor) = (ETS - NTS)/NTS and ITF (intermediary toe spread factor) = (EIT- NIT)/NIT. Normal SFI is defined as 0±10 while a SFI of -100 represents total impairment, such as would result from a complete transection of the sciatic nerve *[Varejao et al., 2001].*

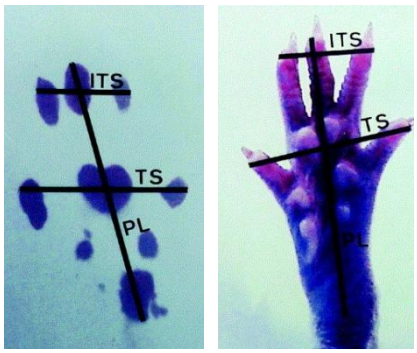

Figure 15: Footprints parameters measured for SFI index determination [*Varejao et al., 2001*].

5.6 LUMBAR DRGs AND SC COLLECTION.

For western blot analysis, all rats were sacrificed by decapitation, either 21 days after MIA i.a. injection or 42 days after MMT surgery. A longitudinal incision was made through the skin, abdominal viscera and the musculature along the spine were then removed and discarded. In order to open the spinal column several laminectomies were performed. After the exposure of the

spinal cord, L4 and L5 lumbar dorsal root ganglia (DRGs) and the respective L4-L5 lumbar spinal cord (SC) segments were removed, collected in eppendorf and stored at -80 °C. DRGs or SC samples were lysated by mechanical lysis (potter) in ice-cold buffer Tissue Protein Extraction Reagent (T-PER; Pierce, Rockford, IL, USA #78510) plus both phosphatases (Sigma-Aldrich S.r.l., Milan, Italy #p5726) and proteases inhibitors (Sigma-Aldrich S.r.l., Milan, Italy # p8340), followed by brief sonication, according to a fully reported standard protocol. The homogenate was centrifuged at 4°C at 14000 × g for 15 minutes. The protein concentration of the supernatant was evaluated by Bradford assay (Sigma-Aldrich S.r.l., Milan, Italy #B6916), using bovine serum albumin (BSA) as standard.

Conversely, for immunofluorescence staining, either 21 days after MIA injection or 42 days after MMT surgery, rats were deeply anesthetized with an overdose of urethane (1.5 g/kg, i.p.) and then transcardially perfused with 250 ml 0.9% saline containing 1% heparin (5000 UI/ml), followed by 500 ml 10% formalin (4% paraformaldehyde, Bio-Optica Spa, Milan, Italy). After a T13-L1 laminectomy, the L4-L5 segment of the lumbar spinal cord was exposed, dissected, and post-fixed in the same fixative (10% formalin) for 24 hours at 4 °C.

For the MIA model, SC segments were then kept in 30% sucrose with 0.01% sodium azide in 0.01 M phosphate-buffered saline (PBS, pH 7.4) for cryoprotection. The contralateral side of each L4-L5 SC segment was identified with a small cut in the ventral horn, before sectioning. Each SC segment was embedded in Tissue-Tek OCT compound (Sakura Finetek Europe, Alphen aan den Rijn, The Netherlands) and serially sliced in 20 µm transverse sections, using a cryostat (MTC, SLEE medical GmbH, Mainz, Germany), with every eighth section collected in the same SuperFrost Plus slide (Thermo Fisher Scientific, Waltham, MA, USA). Each SC segment was cut transversally yielding 16 sections per slide, on average. The slides were stored at -80 °C, before immunofluorescence staining.

For the MMT model, SC segments were then kept in 0.01% sodium azide in 0.01 M PBS (pH 7.4). The contralateral side of each post-fixed L4-L5 SC segment was identified with a small cut in the ventral horn. Each SC segment was then dehydrated through a graded series of ethanol solutions, cleared in xylene (BioClear, Bio-Optica Spa, Milan, Italy), and embedded in paraffin blocks for sectioning. Spinal cord transverse sections were sliced with a fully automated rotary microtome (RM2255, Leica Microsystem Srl, Milan, Italy) at 5 µm thickness and mounted on poli-L-lysine coated slides (Thermo Fisher Scientific, Waltham, MA, USA), six sections per slide. The slides were kept at room temperature (RT), before immunofluorescence staining.

Notably, a different tissue processing method was used for the MMT model lumbar SC samples, compared with the MIA ones, due mainly to technical issues encountered with the cryostat. Previous in-house studies have proved the suitability of paraffin-embedded tissue sectioning for rat spinal cord samples. In addition, this method seems to allow a better preservation of tissue morphology in comparison with cryostat sectioning. Moreover, preliminary in-house studies have demonstrated the suitability of 10 mM citrate buffer (pH 6.0) heating as antigens retrieval method for immunofluorescence staining of SC fixed sections, as previously suggested by several literature reports [*Al-Shamsi et al., 2015; Wen et al., 2015; Hu et al., 2016*].

5.7 WESTERN BLOT ANALYSIS OF DRGs AND SC SAMPLES.

Western blot analysis was employed to evaluate the protein expression levels of both phospho-extracellular receptor kinase 1/2 (pERK1/2) and phospho-p38 (pp38) in ipsilateral lumbar spinal cord in MIA model and glial fibrillary acidic protein (GFAP) in ipsilateral and contralateral L4 and L5 DRGs in MMT model.

As regards the assessment of ERK1/2 and p38 phosphorylation levels, equal amount of protein of each sample of lysated ipsilateral L4-L5 lumbar SC was separated by electrophoresis on NuPAGE™ Novex™ 4-12% Bis-Tris glycine precast minigel (Thermo Fisher Scientific, Waltham, MA, USA #NP0335) and transferred into a polyvinylidene difluoride (PVDF) membrane. Non-specific binding sites were blocked by 1 hour RT incubation in Starting Block Tris-buffered saline (TBS; Thermo Fisher Scientific, Waltham, MA, USA #37543). Subsequently the membrane was incubated overnight (ON) at 4°C with a rabbit anti phospho-p38 (Thr180/Tyr182) polyclonal antibody (Cell Signaling Technology Inc., Danvers, MA, USA #4511) diluted 1:2000 in Tris-buffered saline with Tween 20 (TBST: 150mM NaCl, 20mM Tris HCl pH 7.5 and Tween 20 0.05%) plus 5% BSA. The unbound antibody was removed by TBST washing and the membrane was subsequently incubated with horseradish peroxidase (HRP)-conjugated goat anti rabbit secondary antibody (AbCam, Cambridge, MA, USA #ab6721) diluted 1:20000 in TBST plus 5% BSA, for 1 hour at RT. Finally, the immune complexes were visualized using an enhanced chemiluminescence (ECL) system (ECL West Dura, Thermo Fisher Scientific, Waltham, MA, USA #34075). After blot scanning (LAS-3000 Imaging System, Fujifilm Medical Systems, Stamford, CT, USA), the densitometric analysis of the specific signals obtained was performed using the Image Quant TL Software. The same membrane was stripped through 30 minutes incubation at 37°C with StripAblotStripping Buffer (Euroclone Spa,

Pero, MI, Italy #EMP100500), in order to be subsequently incubated with a rabbit anti phospho-ERK1 (pT202/pY204) + ERK2 (pT185/pY187) polyclonal antibody (1:2000, AbCam, Cambridge, MA, USA #ab4819) and the HRP-conjugated goat anti rabbit secondary antibody (1:20000, AbCam, Cambridge, MA, USA #ab6721), following the same procedure.

As regards the evaluation of GFAP expression levels in ipsilateral and contralateral L4 and L5 DRGs, western blot was performed as described previously, using a goat anti GFAP polyclonal antibody (1:500, Sigma-Aldrich S.r.l., Milan, Italy #SAB2500462) and a HRP-conjugated donkey anti goat secondary antibody (dilution 1:20000, AbCam, Cambridge, MA, USA #ab97120).

To verify equal loading of proteins, both membranes were subsequently reprobed with primary rabbit polyclonal antibody against β-tubulin (1:5000, AbCam, Cambridge, MA, USA #ab6046). Results for each sample were then expressed as a relative optical density (OD), considering the ratio between the OD of the protein band of interest and the one of the corresponding β-tubulin band. Moreover, for GFAP expression, results for each sample are presented as the ratio between the normalized OD obtained for ipsilateral DRGs and the one of contralateral DRGs.

5.8 IMMUNOFLUORESCENCE STAINING OF LUMBAR SC SECTIONS

Immunofluorescence staining was employed to evaluate the expression of ionized calcium-binding adapter molecule 1 (Iba-1) as index of microglial cells activation in ipsilateral and contralateral lumbar spinal cord in both MIA and MMT model.

Slides containing every eighth frozen sections of L4-L5 spinal cord of animals injected with 1 mg/ 50 μl MIA or saline, and sacrificed 21 days after MIA injection, were used for immunofluorescence reaction for Iba-1. Briefly, frozen sections were air-dried, washed in 0.01 M PBS pH 7.4, followed by PBS containing 0.3% triton-X (PBST). In order to avoid unspecific bindings, sections were incubated in 10% normal horse serum (NHS) in PBST, for 90 minutes at RT. Sections were then incubated ON at 4°C with rabbit anti-Iba-1 (1:500, Wako Chemicals, Neuss, Germany #019-19741) primary polyclonal antibody, diluted in PBST containing 2% of NHS. After several washing with PBST containing 2% of NHS, sections were incubated with Alexa-Fluor 488 donkey anti-rabbit secondary antibody (1:400, Thermo Fisher Scientific, Waltham, MA, USA #A-21206) diluted in PBST with 2% of NHS, 1 h at RT. Slides were then washed in PBST followed by PBS and mounted with FluoroShield mounting medium with 4',6-diamidino-2-phenylindole (DAPI; Sigma-Aldrich S.r.l., Milan, Italy #F6057), to counterstain the nuclei.

Conversely, slides containing every sixth fixed sections of L4-L5 SC of MMT- or sham-operated animals, sacrificed 42 days post-surgery, were used for immunofluorescence reaction for Iba-1. Briefly, fixed sections were deparaffinized in xylene and rehydrated in 99%, 95% and then 70% ethanol solutions. Antigens were retrieved by heating in 10 mM citrate buffer (pH 6.0) for 20 min at 90 °C. After cooling at RT, the sections were then washed in PBS followed by PBST and then incubated in 10% NHS in PBST, for 90 minutes at RT, as previously. Afterwards, the sections were incubated ON at 4°C with rabbit anti-Iba-1 (1:350) primary polyclonal antibody. For secondary detection, sections were incubated for 1 h at RT with Alexa-Fluor 488 donkey anti-rabbit secondary antibody (1:400). Slides were briefly dehydrated in 95% and 99% ethanol solutions and then mounted with FluoroShield mounting medium with DAPI.

For both frozen and fixed sections negative controls were performed without the primary antibody.

Slides were visualized with Invitrogen EVOS FL Auto Cell Imaging System (Thermo Fisher Scientific, Waltham, MA, USA). A representative image of both the ipsilateral and contralateral laminae I-III of the spinal cord dorsal horns of each L4-L5 SC section was taken with a 20x magnification (selected frame of 578 μm x 434 μm area), using consistent exposure times across all sections. Laminae I-III were identified taking as reference the rat brain atlas of Paxinos and Watson *[Paxinos et al., 1st edition].* Quantification of microglia activation was performed in at least 6 sections of spinal cord dorsal horns at the level of L4-L5 per animal, according to previous methods *[Sagar et al., 2011; Yu et al., 2013]*. The number of Iba-1-positive microglial cells displaying clearly swollen cell bodies within the selected frame of 578 μm x 434 μm was determined in ipsilateral and contralateral superficial laminae of L4-L5 dorsal horns.

5.9 STATISTICAL ANALYSIS

GraphPad Prism 7 (GraphPad Software, Inc., La Jolla, CA, USA) was used for the data statistical analysis. Animals were randomly assigned to each group. Behavioural data were analyzed by repeated measures two-way analysis of variance (ANOVA), with $p<0.05$ accepted as significant. Differences between two experimental groups were assessed by Sidak's multiple comparisons test, while multiple inter-group differences were assessed by Dunnett's multiple comparisons test. Time-related profiles of treatments were presented as the mean ± standard error of the mean (SEM). The pharmacological effect of drugs was calculated as percentage reversal as follows: %

reversal = (post-dose threshold - pre-dose threshold)/(baseline threshold - pre-dose threshold) x 100; using the mean thresholds of the different experimental groups. The correlation analysis between behavioural tests was performed in each experiment by using the Pearson correlation test on end-point values**.**

Molecular data on end-point levels of expression of pain-related proteins were presented as the mean ± SEM. The statistical analysis between two experimental groups was conducted with Student's t-test, while inter-group differences between more than two experimental groups were evaluated by one-way ANOVA with Tukey's multiple comparisons test ($p<0.05$ accepted as significant).

6. RESULTS

CR4056 is a central analgesic drug. Moreover, CR4056 analgesic effect is mediated primarily by its interaction with imidazoline-2 binding sites *[Ferrari et al., 2011; Meregalli et al., 2012; Lanza et al., 2014].*

Therefore, based also on the assumption that CR4056 is not an osteoarthritis (OA) disease-modifying drug (DMOAD), pain-like behavioural assessments were the primary objective of this research work.

For this reason, histomorphological analysis of the injured knee joints of both MIA and MMT rats were conducted only in the preliminary in-house studies regarding these OA model to confirm the development of OA disease after both induction procedures. The solid data regarding the reliability and reproducibility of both MIA intra-articular injection and MMT surgery in inducing OA development (i.e. histological features of the disease) are not matter of discussion of this research work.

6.1. MIA MODEL OF OSTEOARTHRITIS

No differences in body weight gain were noted between MIA-injected animals and age-matched control group at any time point during all the studies on MIA model.

The single intra-articular injection of 1 mg/ 50µl MIA induced a significant development of mechanical allodynia of the ipsilateral paw, compared with either saline controls or the contralateral paw. MIA group maintained this significant decrease of the withdrawal mechanical threshold in the ipsilateral paw up to 21 days after MIA i.a. injection (***Figure 16, panel A***). No variation of the mechanical withdrawal threshold of the contralateral paw was observed in both sham and MIA group, throughout the course of the study (***Figure 16, panel B***).

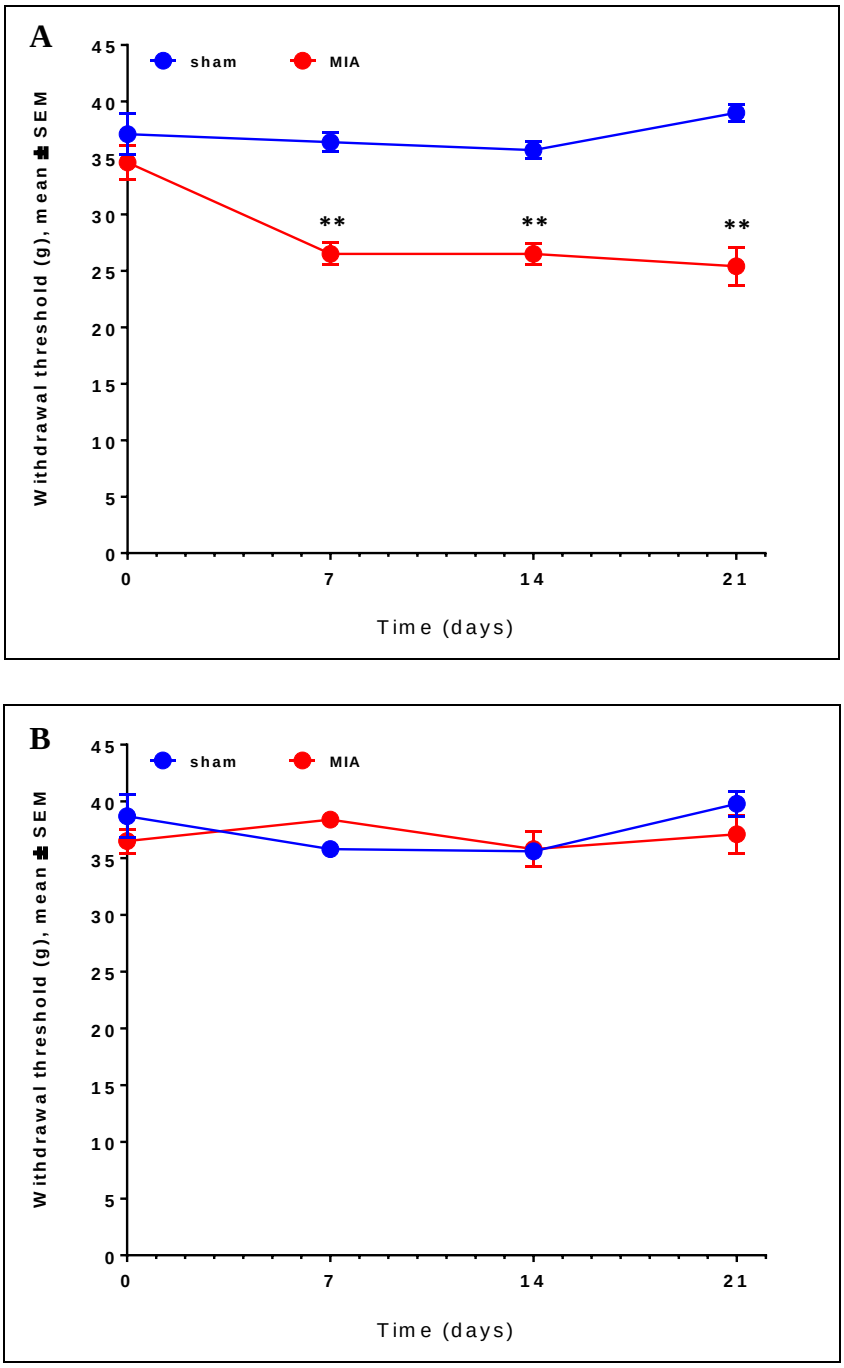

Figure 16: Time course of mechanical allodynia of ipsilateral ***(panel A)*** and contralateral ***(panel B)*** paws in sham and MIA-injected rats. Mechanical withdrawal threshold (in grams) was evaluated by von Frey test, using a Dynamic Plantar Aesthesiometer, prior (time 0) and 7, 14 and 21 days after MIA injection. Data represent the mean of 6 animals/group. **P<0.01 vs. sham rats (Two-way RM ANOVA, Sidak's post-hoc test).

Similar results were obtained with the assessment of primary mechanical hyperalgesia. MIA injection caused a long-lasting decrease of the withdrawal mechanical threshold in the ipsilateral limb compared with either saline controls or the contralateral limb (***Figure 17, panel A***). Limb

withdrawal threshold detected in the contralateral knee had no variation in both sham and MIA group, throughout the study period (***Figure 17, panel B***).

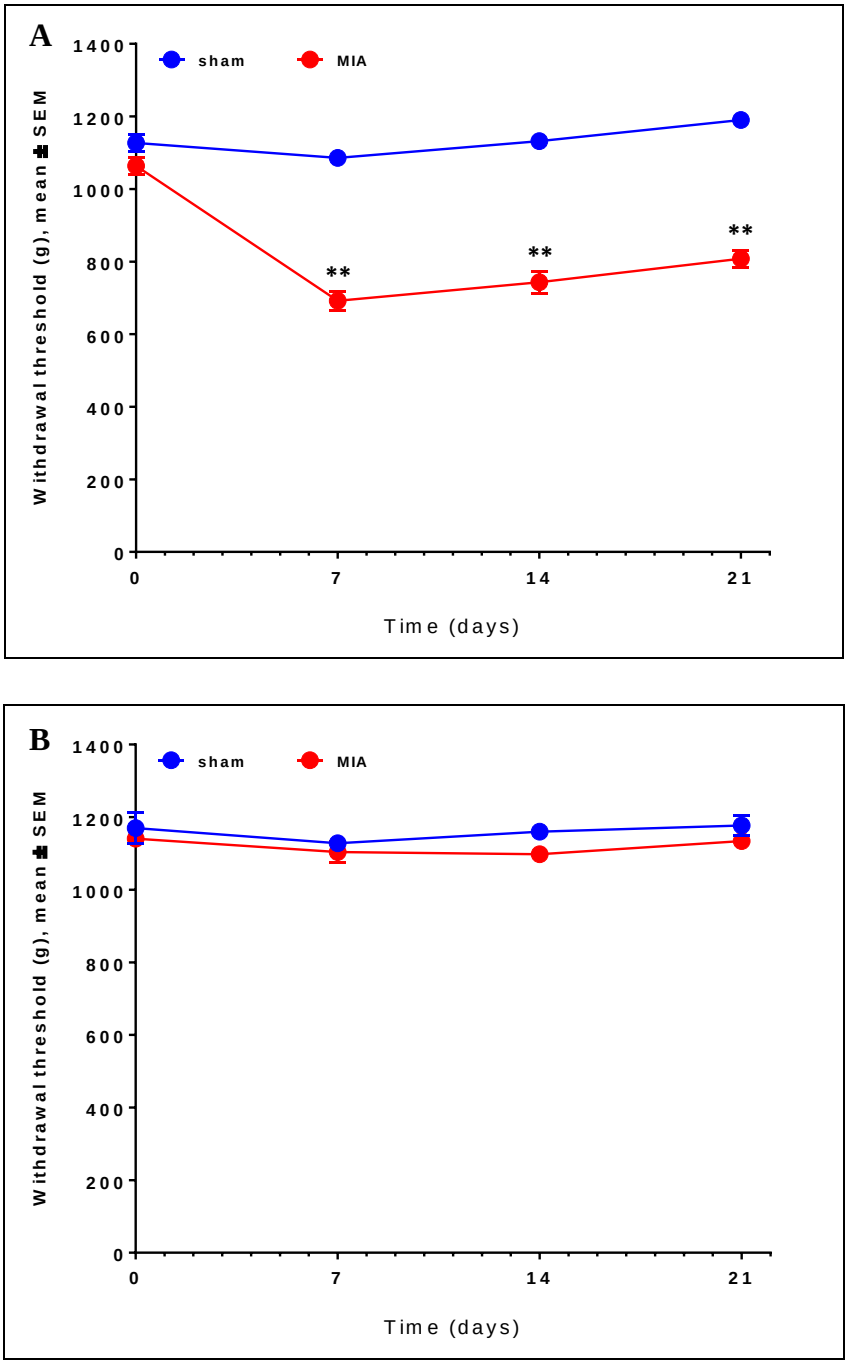

Figure 17: Time course of primary mechanical hyperalgesia of ipsilateral ***(panel A)*** and contralateral ***(panel B)*** knees in sham and MIA-injected rats. Mechanical withdrawal threshold (in grams) was evaluated using PAM (pressure application measurement) device, prior (time 0) and 7, 14 and 21 days after MIA injection. Data represent the mean of 6 animals/group. **P<0.01 vs. sham rats (Two-way RM ANOVA, Sidak's post-hoc test).

In addition, MIA i.a. injection induced a significant and long-lasting development of both static (***Figure 18, panel A***) and dynamic (***Figure 18, panel B***) hind paw left-right weight bearing imbalance, compared with saline controls. In particular, the significant changes in hind paw weight distribution (HPWD), expressed as the percentage of the weight placed on the ipsilateral hind limb in relation to the total weight of the animal, exhibited by MIA rats during movement (dynamic weight bearing), could be considered an indirect index of spontaneous pain during movement.

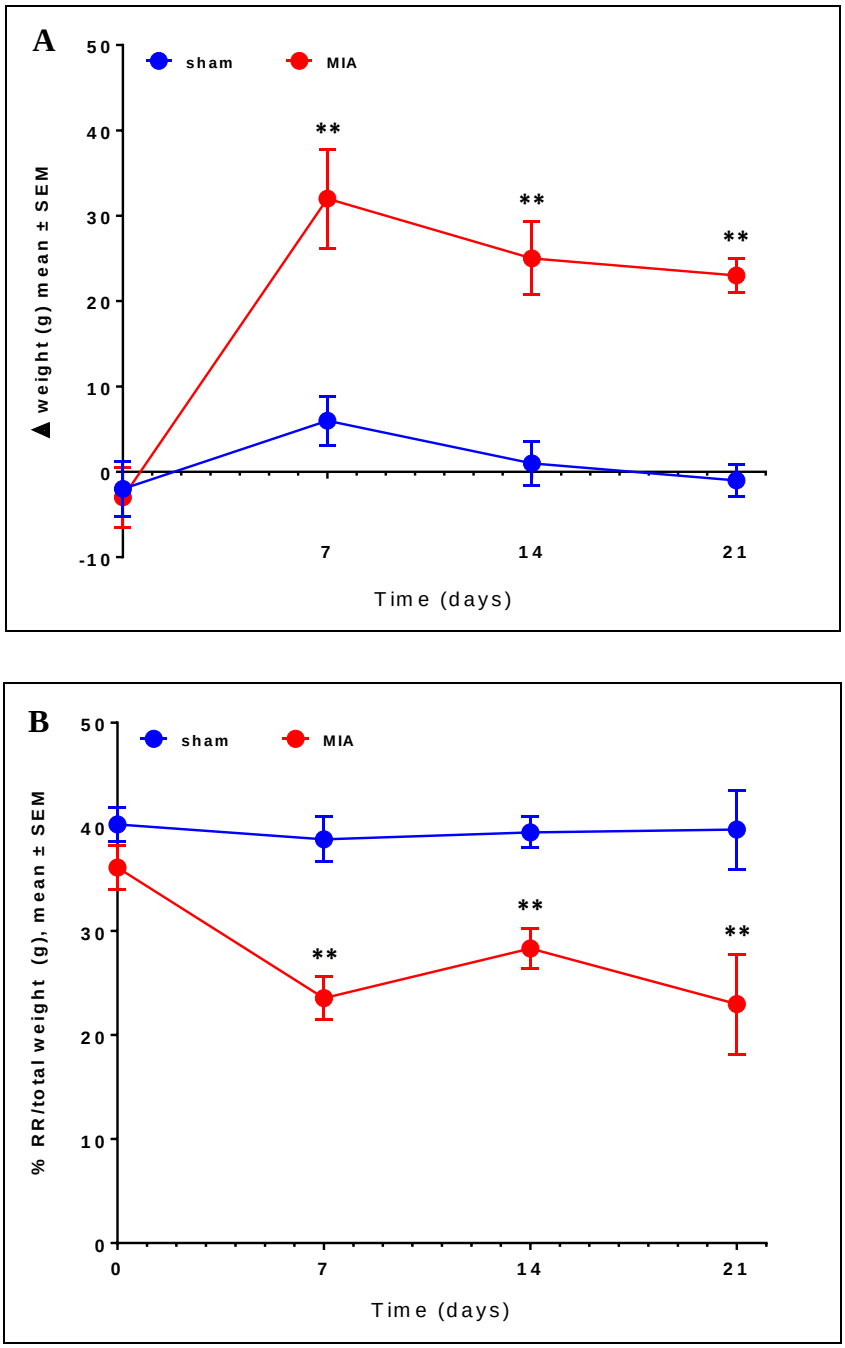

Figure 18: Time course of changes in static (***panel A***) and dynamic (***panel B***) HPWD in sham and MIA-injected rats. Weight bearing asymmetry was evaluated prior (time 0) and 7, 14 and 21 days after MIA injection, using the incapacitance tester or the dynamic weight bearing system, respectively. Static HPWD data are expressed as the difference in hind paw weight distribution (Δ) between the contralateral and ipsilateral limbs (in grams). Conversely, dynamic HPWD data are expressed as the percentage of the weight placed on the ipsilateral hind limb (RR) in relation to the total weight of the animal (in grams). Data represent the mean of 6 animals/group. **P<0.01 vs. sham group (Two-way RM ANOVA, Sidak's post-hoc test).

On the other hand, no significant difference was detected in locomotor activity, 14 and 21 days post MIA injection, between sham and MIA group (***Figure 19***).

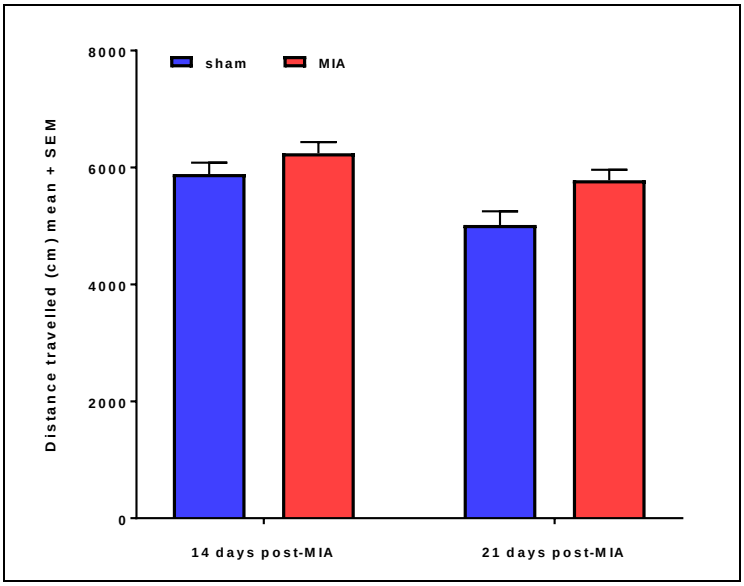

Figure 19: Locomotor activity in sham and MIA-injected rats, 14 and 21 days after MIA injection. Locomotor activity was evaluated using open field test and determined as distance travelled (cm) by the rats during the 20 minutes-period of the test. Data represent the mean of 6 animals/group (Two-way RM ANOVA, Sidak's post-hoc test).

Moreover, the correlation analysis between these pain-like behaviour assessments, 21 days after MIA i.a. injection, showed that the highest Pearson's correlation coefficient was observed between mechanical allodynia and primary mechanical hyperalgesia (PCC = 0.97). The correlation between either allodynia or hyperalgesia and static or dynamic HPWD was weaker, but still significant (/PCC/ > 0.7).

6.1.1 Effect of CR4056 acute administration

The assessment of mechanical allodynia showed a dose-dependent increase of the ipsilateral paw withdrawal threshold after acute oral treatment with 6 and 20 mg/kg CR4056, compared with MIA group treated with vehicle, 7 days after MIA injection (***Figure 20, panel A***). However, this effect did not reach the statistical significance. The percentage of reversal of mechanical threshold obtained with 6 mg/kg and 20 mg/kg CR4056 versus the basal pre-MIA injection of these groups

was 40 % and 58 %, respectively. Neither 2 mg/Kg CR4056 nor naproxen exerted a noticeable analgesic effect.

Conversely, the assessment of mechanical hyperalgesia showed that the acute p.o. administration of CR4056 induced a significant and dose-dependent increase of the ipsilateral limb withdrawal threshold, compared with MIA group treated with vehicle (***Figure 20, panel B***). The percentage of reversal of mechanical threshold obtained with 6 and 20 mg/kg CR4056 versus the basal pre-MIA injection of these groups was 35 % and 53 %, respectively. 2 mg/kg CR4056 and naproxen were devoid of noticeable effect. The pharmacological treatments did not influence the withdrawal threshold of the contralateral paw or knee (data not shown).

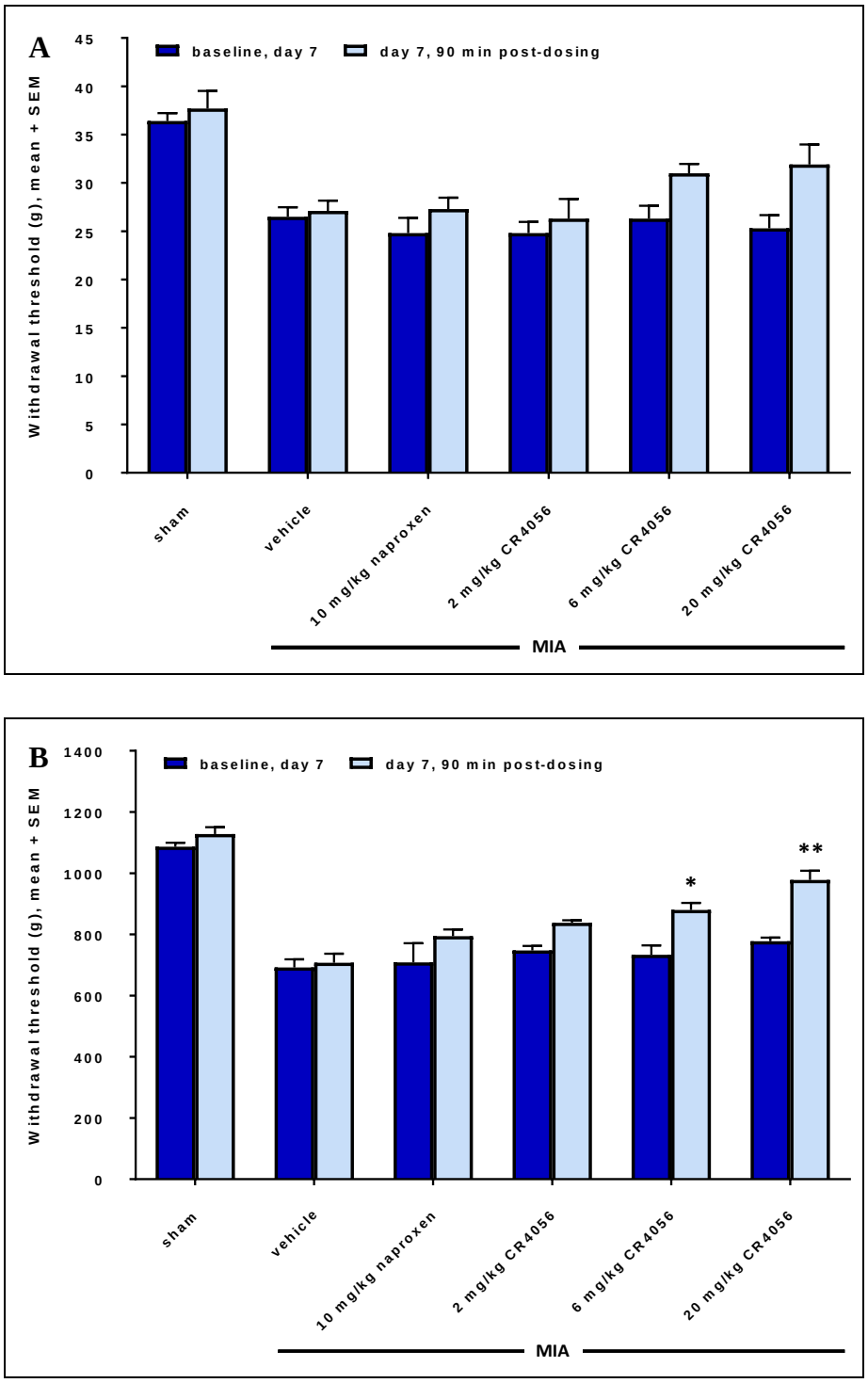

Figure 20: Effect of 2, 6 and 20 mg/kg CR4056 and 10 mg/kg naproxen, single oral treatment, on mechanical allodynia of the ipsilateral paw (***panel A***), and mechanical hyperalgesia of the ipsilateral knee (***panel B***). Withdrawal thresholds (in grams) were evaluated 7 days post-MIA injection by von Frey test and PAM device, respectively. Data representing the mean of 6 animals/group were collected before (baseline value) and 90 minutes after the drug administration. *P<0.05 and **P<0.01 vs. MIA vehicle-treated group (Two-way RM ANOVA, Dunnett's post-hoc test).

Moreover, 7 days after MIA i.a. injection, the single administration of 6 and 20 mg/kg CR4056 induced a dose-dependent decrease of the difference in static hind paw weight distribution between the contralateral and ipsilateral limbs, compared with MIA group (***Figure 21***). The percentage of reversal of left-right weight bearing imbalance obtained with 6 and 20 mg/kg CR4056 versus their basal pre-MIA injection was 29 % and 36 %, respectively. Nevertheless, this effect did not reach the statistical significance.

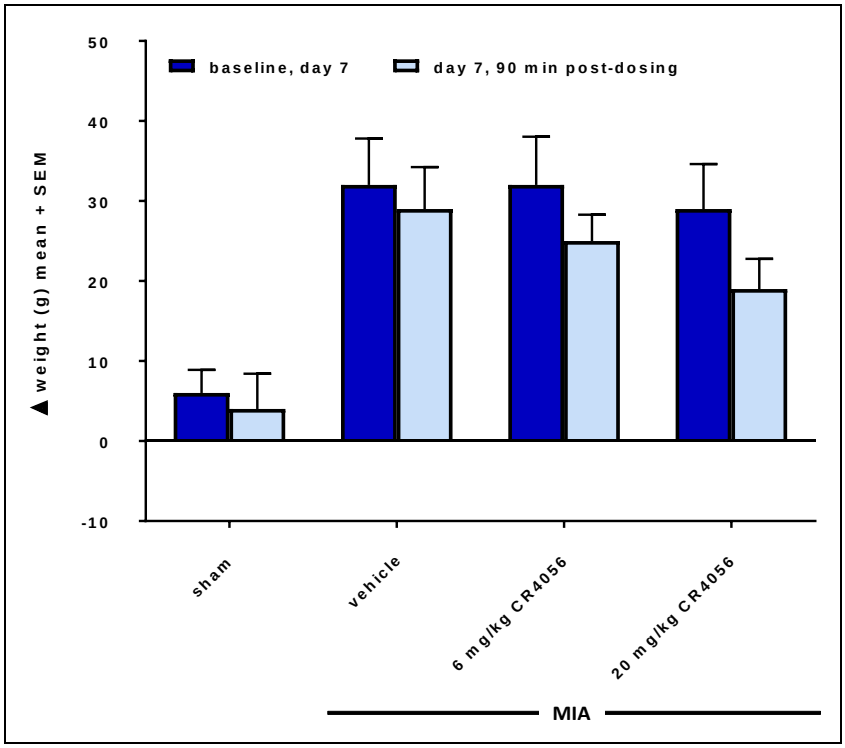

Figure 21: Effect of 6 and 20 mg/kg CR4056 single oral treatment on static HPWD. The difference in hind paw weight distribution (Δ) between the contralateral and ipsilateral limbs (in grams) was assessed 7 days after MIA injection, before (baseline value) and 90 minutes post-drug administration, using an incapacitance tester. Data represent the mean of 6 animals/group (Two-way RM ANOVA, Dunnett's post-hoc test).

14 days after MIA injection, the analgesic efficacy of the single oral administration of 6 and 20 mg/kg CR4056 on both mechanical allodynia and hyperalgesia was further confirmed (***Figure 22***). In particular, the percentages of reversal of both allodynic and hyperalgesic mechanical threshold for either 6 or 20 mg/kg CR4056 versus their basal pre-MIA injection were either 52% and 39% or 89% and 42%, respectively. Moreover, a statistically significant anti-allodynic effect was produced by naproxen single administration, 14 days post-MIA (percentage of reversal of mechanical allodynia of 38%). Conversely, 2 mg/kg CR4056 was devoid of noticeable effect.

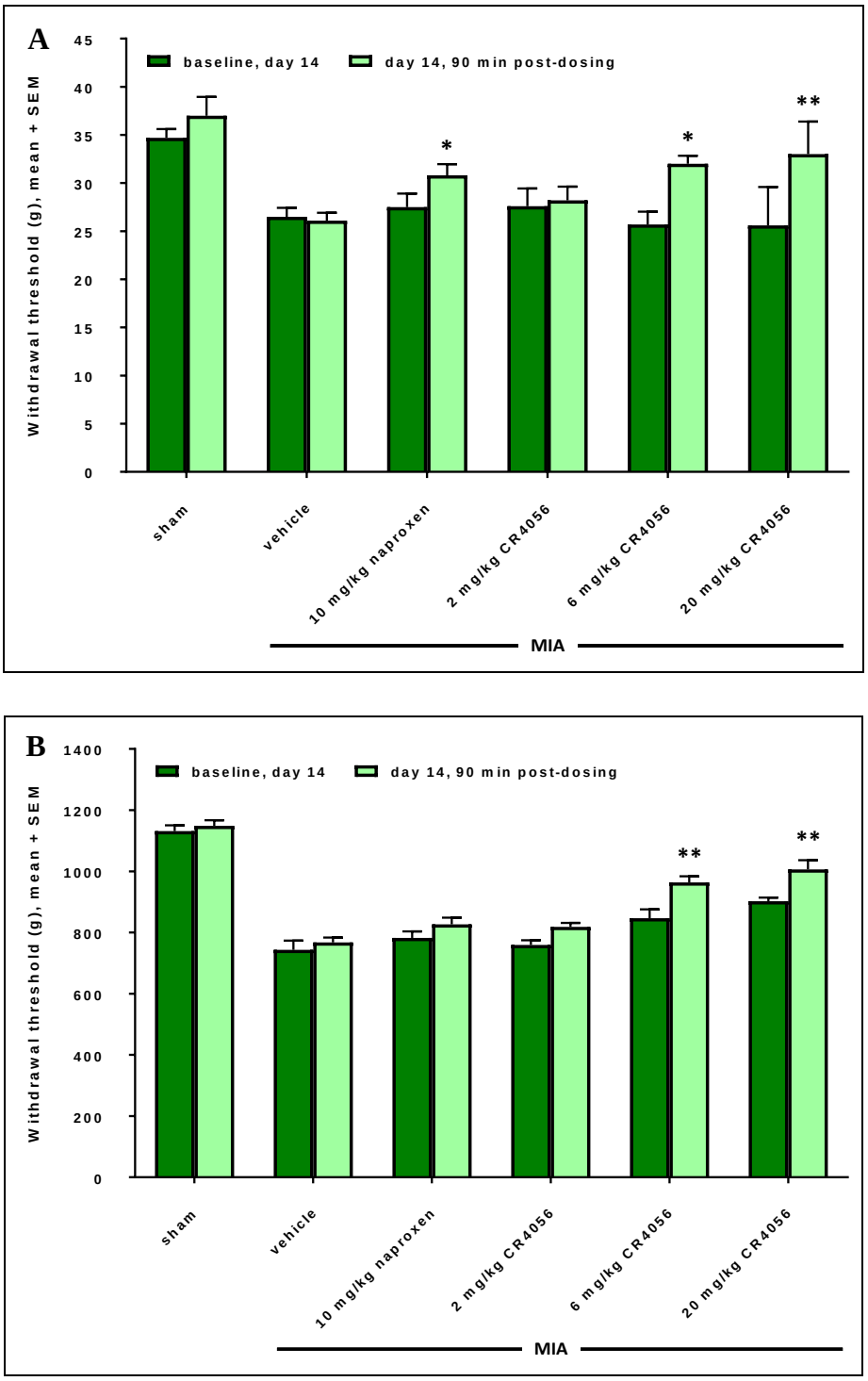

Figure 22: Effect of 2, 6 and 20 mg/kg CR4056 and 10 mg/kg naproxen, single oral treatment, on mechanical allodynia of the ipsilateral paw (***panel A***), and mechanical hyperalgesia of the ipsilateral knee (***panel B***). Withdrawal thresholds (in grams) were evaluated 14 days post-MIA injection by von Frey test and PAM device, respectively, before (baseline value) and 90 minutes post-drug administration. Data represent the mean of 6 animals/group. *P<0.05 and **P<0.01 vs. MIA vehicle-treated group (Two-way RM ANOVA, Dunnett's post-hoc test).

The single administration of 6 and 20 mg/kg CR4056, 14 days after MIA injection, confirmed the results on static weight bearing imbalance obtained 7 days post-MIA, after a single dose of the compound. In particular, 20 mg/kg CR4056 acute administration induced a reduction of left-right HPWD asymmetry (percentage of reversal versus the basal pre-MIA injection of 65%), which however did not reach the statistical significance, mostly due to the data high variance (i.e. standard error), especially within the group treated with 20 mg/kg CR4056 (***Figure 23***).

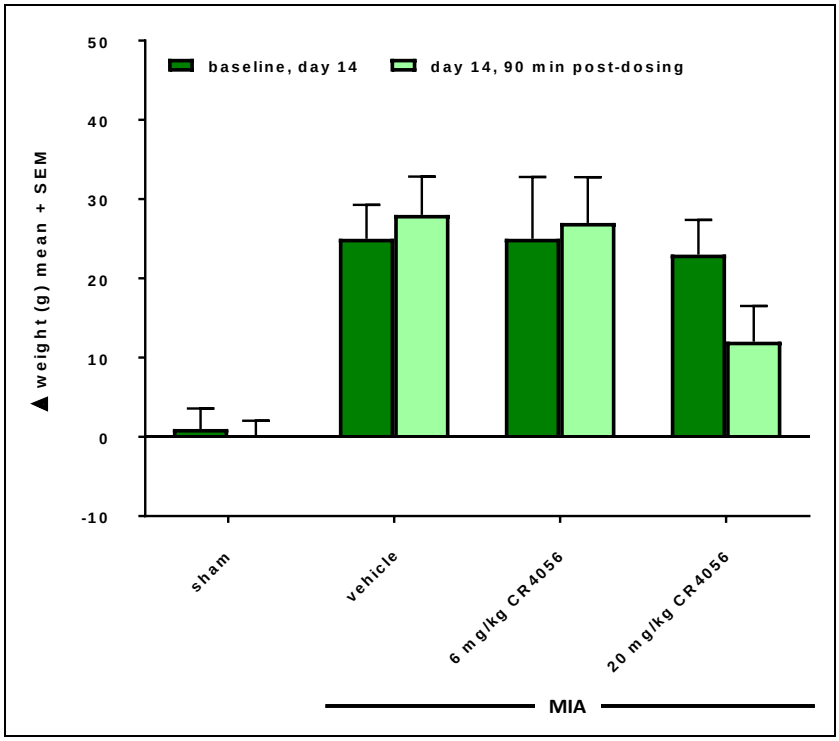

Figure 23: Effect of 6 and 20 mg/kg CR4056 single oral treatment on static HPWD. The difference in hind paw weight distribution (Δ) between the contralateral and ipsilateral limbs (in grams) was assessed 14 days after MIA injection, before (baseline value) and 90 minutes post-drug administration, using an incapacitance tester. Data represent the mean of 6 animals/group (Two-way RM ANOVA, Dunnett's post-hoc test).

Moreover, 14 days after MIA, the analgesic effect of a single administration of 6 mg/kg CR4056 and 10 mg/kg naproxen on dynamic weight bearing imbalance was evaluated. CR4056 was devoid of noticeable effects on dynamic HPWD, while naproxen induced a slight but not significant improvement of weight bearing asymmetry (i.e. the percentage of the weight placed on the ipsilateral hind limb in relation to the total weight of the animal) (***Figure 24***).

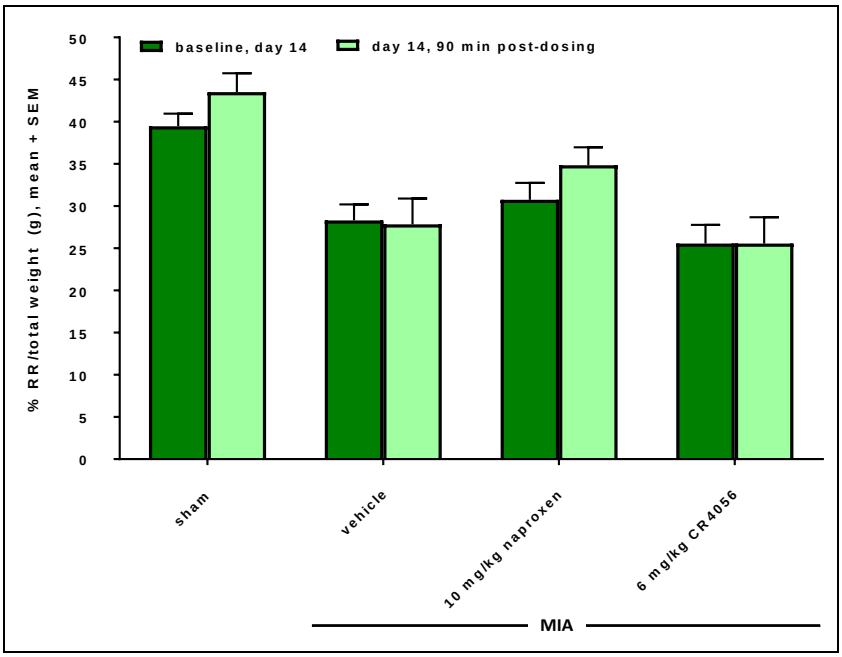

Figure 24: Effect of 6 mg/kg CR4056 and 10 mg/kg naproxen single oral treatment on dynamic weight bearing. Dynamic HPWD was evaluated 14 days post-MIA injection, using the dynamic weight bearing system, before (baseline value) and 90 minutes post-drug administration. Data representing the mean of 6 animals/group are expressed as the percentage of the weight placed on the ipsilateral hind limb (RR) in relation to the total weight of the animal (in grams) (Two-way RM ANOVA, Dunnett's post-hoc test).

6.1.2 Effect of CR4056 sub-acute treatment

The analgesic effect on both mechanical allodynia (***Figure 25, panel A***) and primary mechanical hyperalgesia (***Figure 25, panel B***) of 6 and 20 mg/kg CR4056 p.o. was further confirmed after sub-acute treatment, from day 14 to day 21 after MIA injection, QD. In particular, 21 days after MIA, both CR4056 doses induced a similar significant increase of both the ipsilateral paw and limb withdrawal thresholds, compared with MIA group. The percentages of reversal of both allodynic and hyperalgesic mechanical threshold for either 6 or 20 mg/kg CR4056 versus their basal pre-MIA injection were either 64% and 73% or 61% and 70%, respectively. At this time point, after 8-days repeated treatment, the statistical significance was reached also by 2 mg/kg CR4056 on mechanical hyperalgesia, while naproxen was significantly effective on both parameters (percentage of reversal of mechanical allodynia and hyperalgesia of 63% and 49%, respectively). Furthermore, 6 mg/kg CR4056 repeated doses induced a significant increase of both the allodynic and hyperalgesic threshold values even when assessed immediately before the dosing on day 21, i.e. 24 hours after the last administration.

Therefore, the overall analgesic activity, proved by 6 and 20 mg/kg CR4056 either on mechanical allodynia or mechanical hyperalgesia, appeared more significant and relevant compared with 10 mg/kg naproxen. Nevertheless, both CR4056 (6 and 20 mg/kg) and naproxen showed a greater analgesic efficacy on both behavioural assessments after 8-days repeated treatment, rather than a single administration.

The pharmacological treatment with both compounds was devoid of noticeable effect, at the considered time points, on both the allodynic and the hyperalgesic mechanical withdrawal thresholds of the contralateral paw or knee, respectively (data not shown).

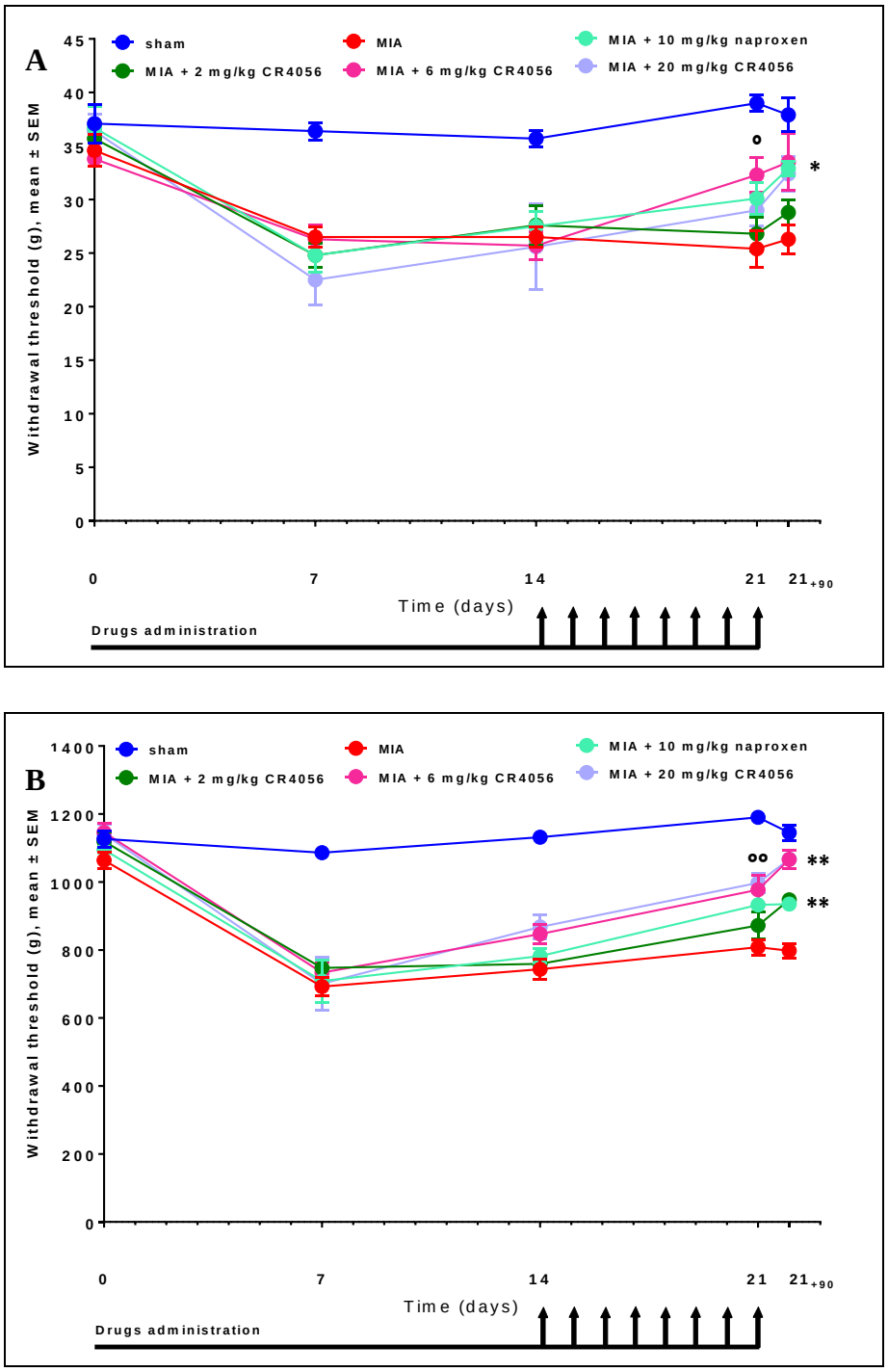

Figure 25: Effect of 2, 6 and 20 mg/kg CR4056 and 10 mg/kg naproxen 8-days sub-acute oral treatment, on mechanical allodynia of the ipsilateral paw (***panel A***), and mechanical hyperalgesia of the ipsilateral knee (***panel B***). Withdrawal thresholds (in grams) were evaluated by von Frey test and PAM device, respectively, prior (time 0), 7, 14 and 21 days after MIA (on day 21, before and 90 minutes post-drug administration). Data represent the mean of 6 animals/group. *P<0.05 and **P<0.01 vs. MIA vehicle-treated group; °P<0.05 and °°P<0.01 pre-drug basal in treated rats vs. basal of MIA vehicle-treated group (Two-way RM ANOVA, Dunnett's post-hoc test).

Moreover, after 8-days sub-acute treatment both 6 and 20 mg/kg CR4056 induced a similar decrease of the difference in static hind paw weight distribution between the contralateral and ipsilateral limbs, compared with MIA group. The percentage of reversal of HPWD asymmetry for either 6 or 20 mg/kg CR4056 versus their basal pre-MIA injection was 21% or 43%, respectively. However, as previously, this effect did not reach the statistical significance (***Figure 26***).

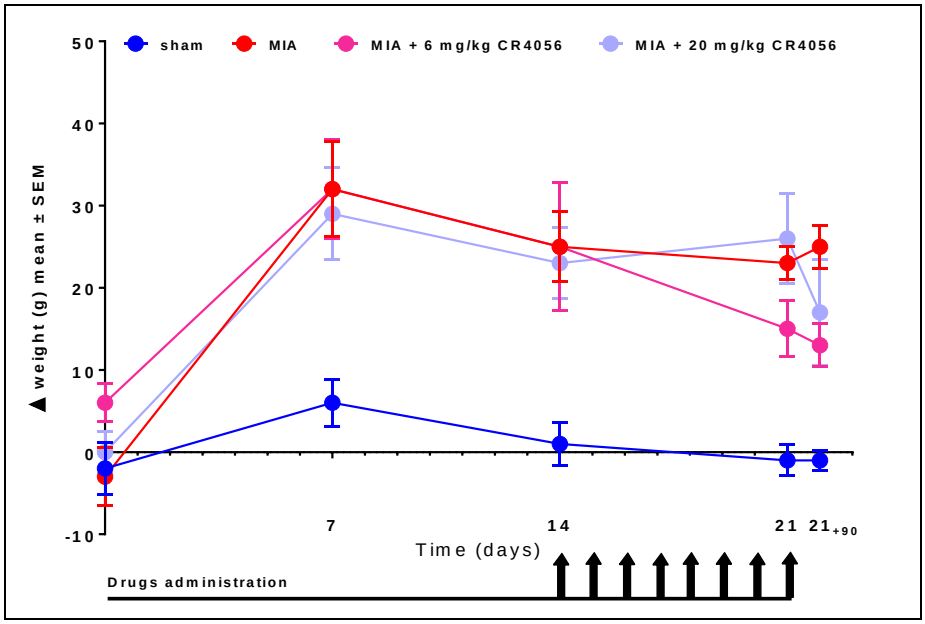

Figure 26: Effect of 6 and 20 mg/kg CR4056 8-days sub-acute oral treatment on static HPWD. The difference in hind paw weight distribution (Δ) between the contralateral and ipsilateral limbs (in grams) was assessed, using an incapacitance tester, prior (time 0), 7, 14 and 21 days after MIA injection (on day 21, both before and 90 minutes post-drug administration). Data represent the mean of 6 animals/group (Two-way RM ANOVA, Dunnett's post-hoc test).

Finally, the effect of 6 mg/kg CR4056 and 10 mg/kg naproxen on dynamic weight bearing imbalance remained unchanged after 8-days sub-acute treatment, i.e. CR4056 was devoid of noticeable effect, while naproxen induced a slight but not significant improvement of HPWD asymmetry (***Figure 27***).

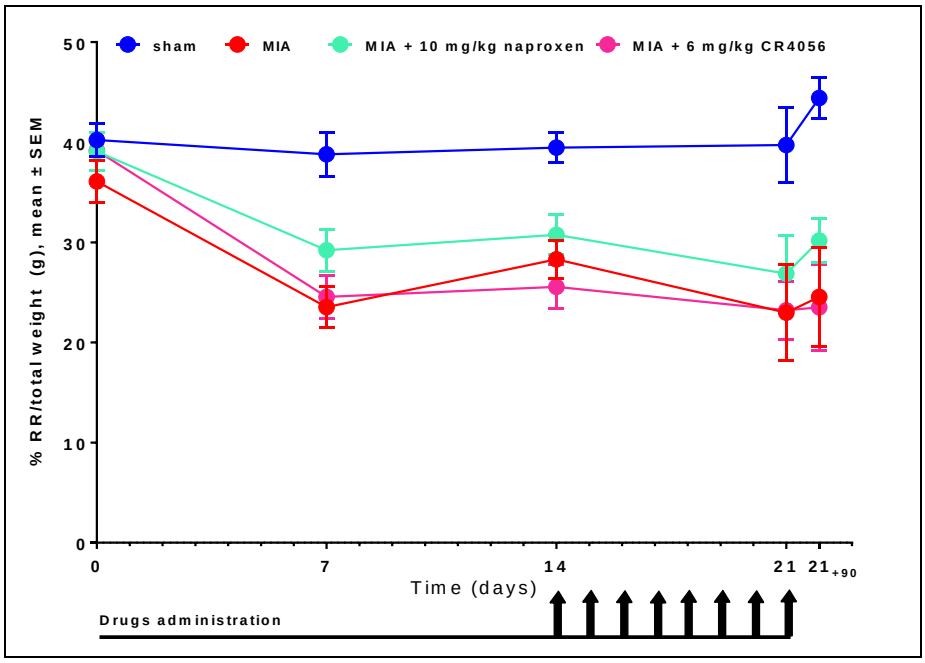

Figure 27: Effect of 6 mg/kg CR4056 and 10 mg/kg naproxen 8-days repeated oral treatment on dynamic weight bearing. Dynamic HPWD was evaluated prior (time 0), 7, 14 and 21 days after MIA injection (on day 21, both before and 90 minutes post-drug administration), using the dynamic weight bearing system. Data representing the mean of 6 animals/group are expressed as the percentage of the weight placed on the ipsilateral hind limb (RR) in relation to the total weight of the animal (in grams) (Two-way RM ANOVA, Dunnett's post-hoc test).

6.1.3 Neuronal and glial MAPKs activation in lumbar spinal cord

The densitometric analysis of the specific signals obtained by western blot analysis for both pERK1/2 and pp38 showed no significant difference in the phosphorylation levels of these MAPKs in ipsilateral L4-L5 lumbar spinal cord, between sham and MIA-injected rats, 21 days post MIA (***Figure 28***). Therefore, the effect of 8-days repeated treatment with either CR4056 or naproxen on ERK1/2 and p38 phosphorylation was not further analyzed.

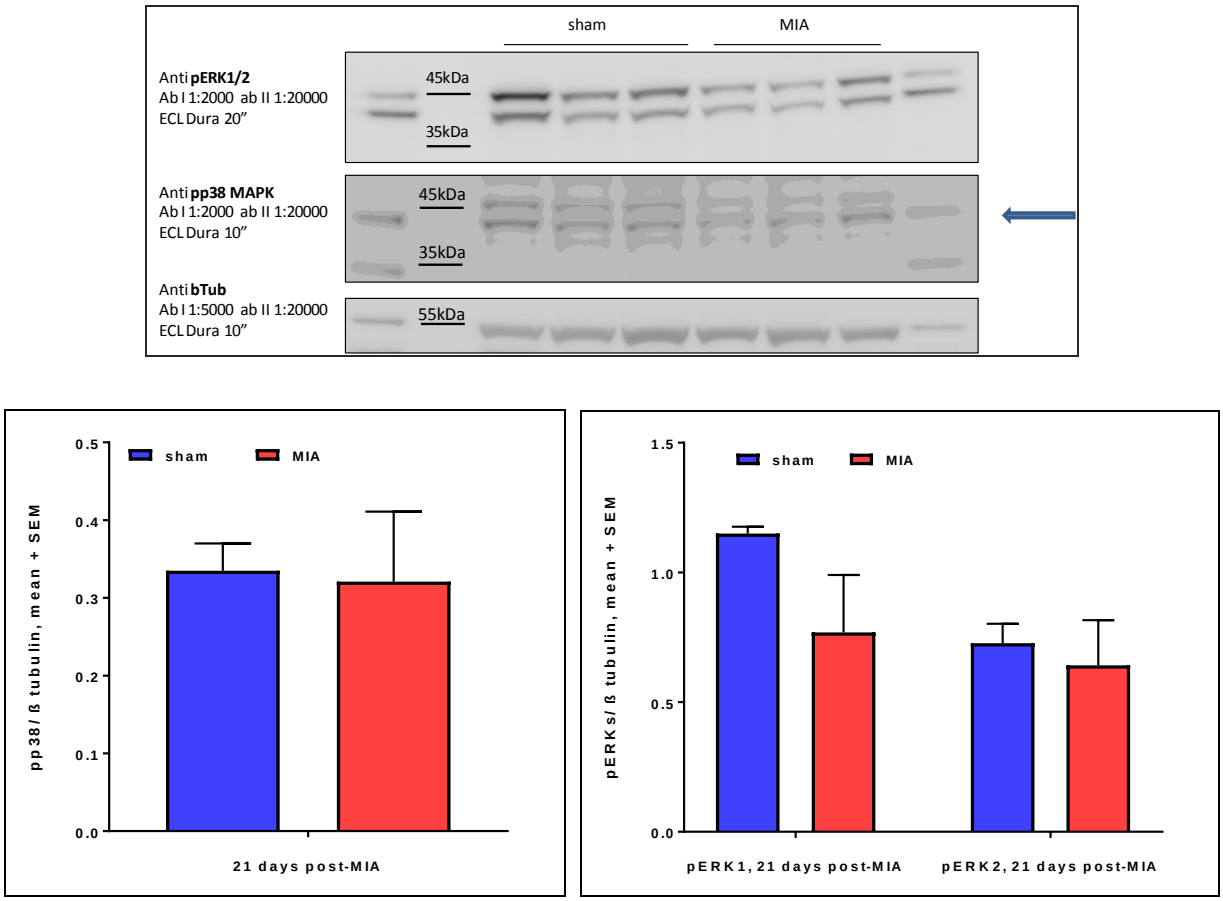

Figure 28: Western blot analysis of phosphorylation levels of ERK1/2 and p38 in ipsilateral lumbar spinal cord of sham and MIA-injected rats, 21 days after MIA injection. Results are expressed as relative optical density (OD), i.e. the ratio between the OD of the protein band of interest and the one of the corresponding β-tubulin band. Data represent the mean of 3 animals/group (Student's t-test).

6.1.4 Microglial cells activation in lumbar spinal cord

A representative image, for each experimental group, of both the entire L4-L5 SC section and the analyzed selected frame of the laminae I-III of the L4-L5 SC ipsilateral dorsal horn, stained for Iba-1 and counterstained for DAPI, is shown in ***Figure 29, panel A***. The number of Iba-1 positive, morphologically identified, activated microglial cells significantly increased in laminae I-III of the L4-L5 SC ipsilateral dorsal horn of MIA-injected animals, compare with sham group, 21 days after MIA i.a. injection. Moreover, 8-days sub-acute oral treatment with either 6 mg/kg CR4056 or 10 mg/kg naproxen significantly reversed microglia activation (i.e. the upregulation of Iba-1) in the superficial laminae of L4-L5 ipsilateral dorsal horn, compared with MIA group treated with vehicle (***Figure 29, panel B***). Conversely, no difference was detected in the number of Iba-1 positive

microglia between the ipsilateral and contralateral L4-L5 dorsal horns, 21 days post-MIA, among each experimental group.

A

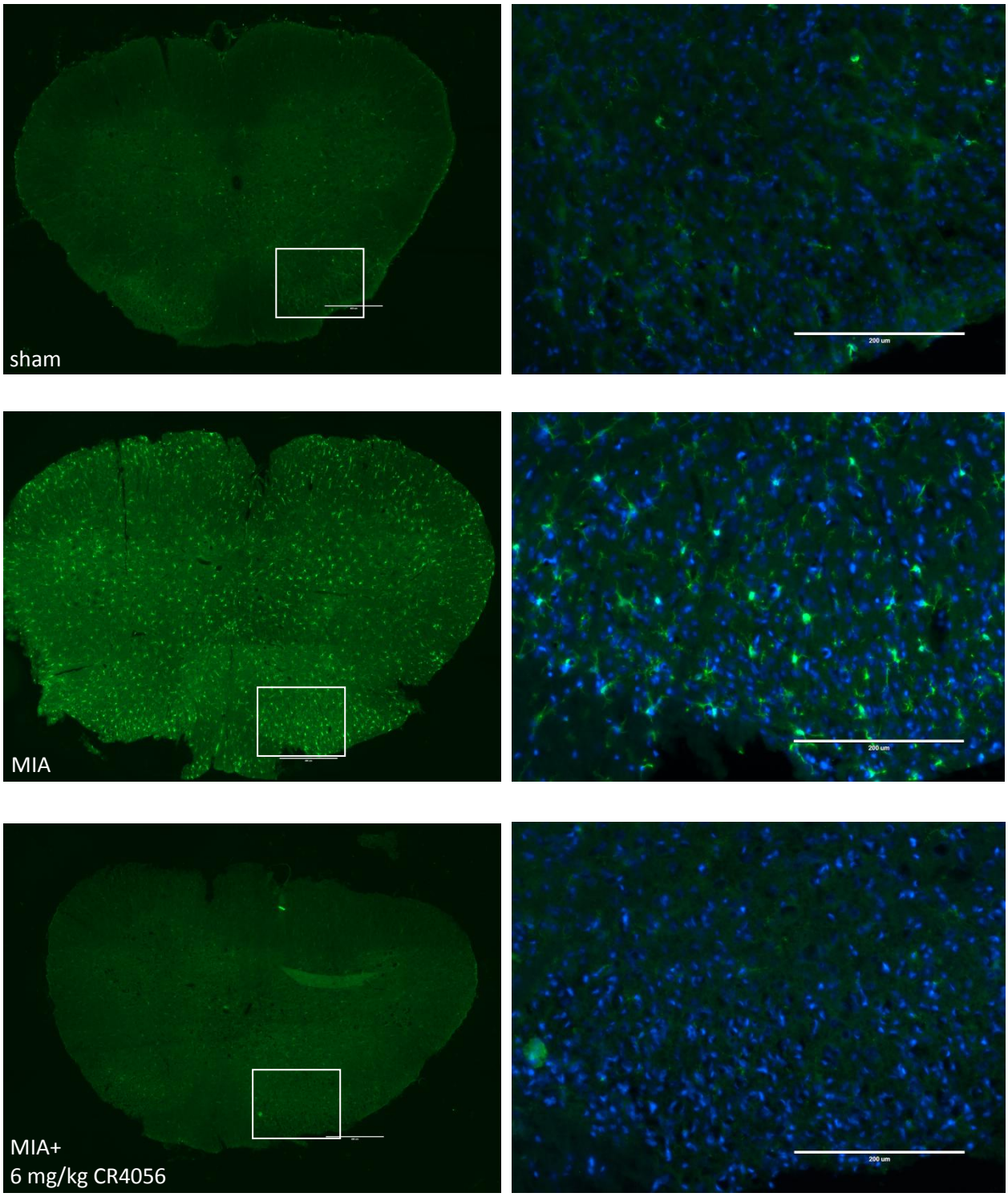

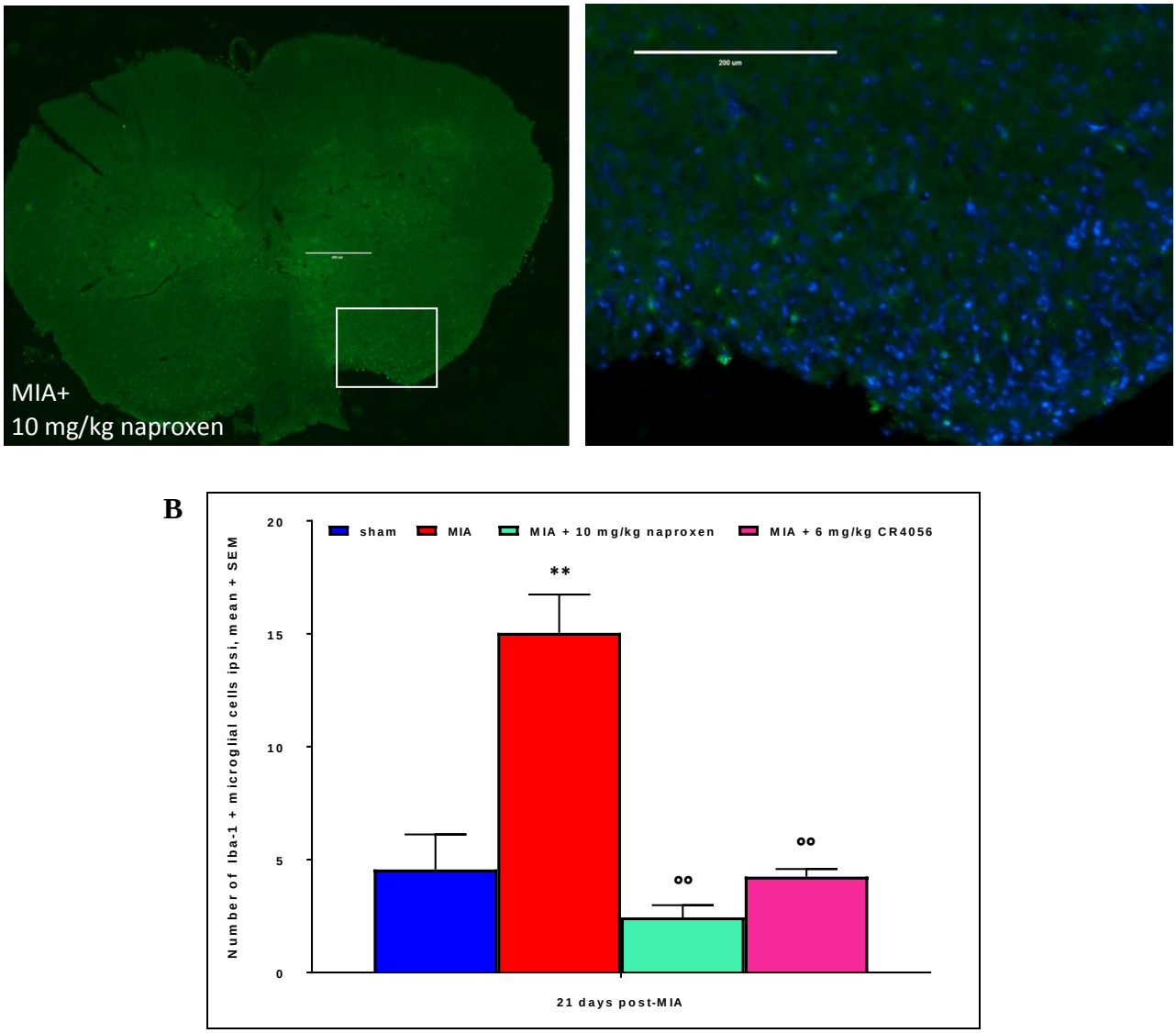

Figure 29: Spinal microglia activation 21 days after MIA injection. Representative images of both immunofluorescence staining for Iba-1 of the L4-L5 SC sections (scale bar 400 μm) (***left column,* panel A**) and the selected frame (capturing area of 578 μm x 434 μm at 20x magnification; scale bar 200 μm) of the laminae I-III of the L4-L5 SC ipsilateral dorsal horn stained for Iba-1 and DAPI (***right column, panel A***), in sham and MIA animals, treated either with vehicle, 6 mg/kg CR4056 or 10 mg/kg naproxen. The contralateral side of each L4-L5 SC segment was identified with a small cut in the ventral horn, before sectioning. The quantification of microglia activation in ipsilateral L4-L5 SC dorsal horn was determined as the number of Iba-1-positive microglia, displaying a clearly swollen cell body with reduced processes, within the analyzed selected frame of the superficial laminae (***panel B***). Data represent the mean of 4 animals/group. **P<0.01 vs. sham rats, °°P<0.01 vs. MIA vehicle-treated group (One-way ANOVA, Tukey's post-hoc test).

6.2. MMT MODEL OF OSTEOARTHRITIS

No differences in body weight gain were noted between MMT-operated animals and age-matched control groups at any time point during all the studies on MMT model.

MMT surgery induced a decrease of the withdrawal mechanical threshold (i.e. mechanical allodynia) of the ipsilateral paw, compared with sham group, which however did not reach the statistical significance (***Figure 30, panel A***). No variations of the mechanical withdrawal threshold of the contralateral paw were observed in both sham and MMT group, throughout the course of the study, especially after the induction of the disease (***Figure 30, panel B***).

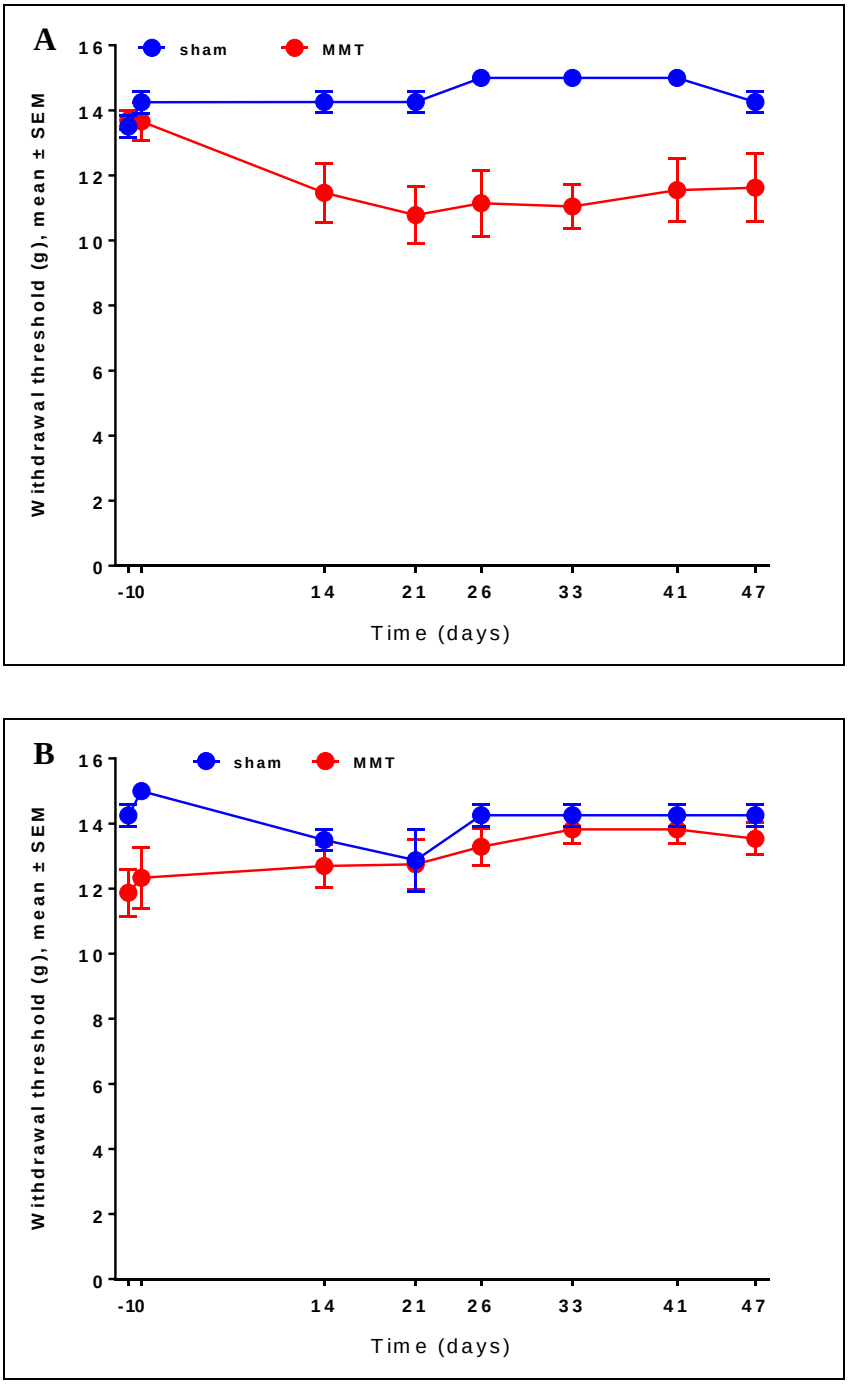

Figure 30: Time course of mechanical allodynia of ipsilateral ***(panel A)*** and contralateral ***(panel B)*** paws in sham and MMT-operated rats. Mechanical withdrawal threshold (in grams) was evaluated using von Frey hairs (nine filaments in the range 0.4-15 g), according to the up-and-down method described by Chaplan and colleagues *[Chaplan et al., 1994*]. Mechanical allodynia was assessed prior (time -1 and 0) and 14, 21, 26, 33, 41 and 47 days after MMT surgery. Data represent the mean of 9 animals/group (Two-way RM ANOVA, Sidak's post-hoc test).

Conversely, the transection of both the medial collateral ligament and the medial meniscus of the right knee induced a significant development of mechanical hyperalgesia of the ipsilateral paw,

compared with sham controls. MMT-operated animals maintained this significant decrease of the withdrawal mechanical threshold of the ipsilateral paw up to 42 days post-surgery (***Figure 31***).

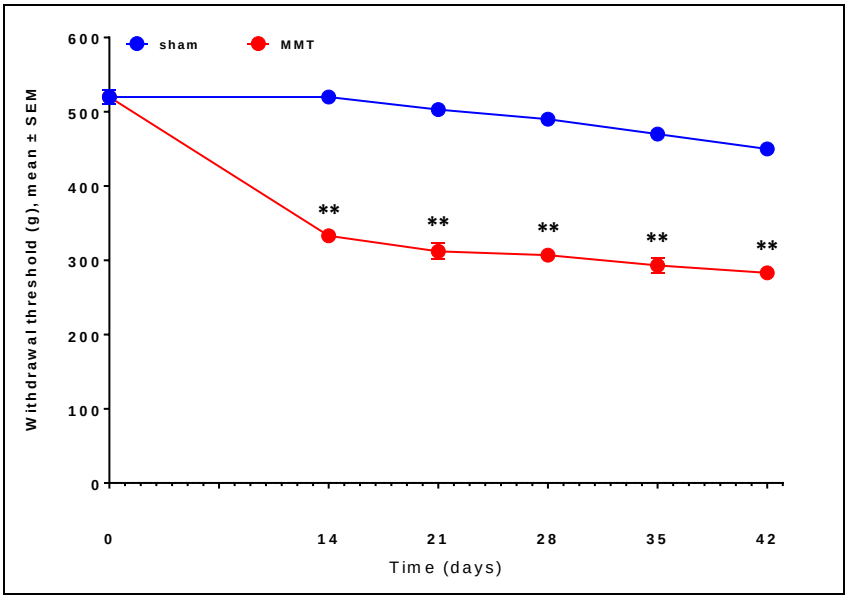

Figure 31: Time course of secondary mechanical hyperalgesia of ipsilateral paw in sham and MMT-operated rats. Mechanical withdrawal threshold (in grams) was evaluated by Randall-Selitto test, prior (time 0) and 14, 21, 28, 35 and 42 days after MMT surgery. Data represent the mean of 9 animals/group. **P<0.01 vs. sham rats (Two-way RM ANOVA, Sidak's post-hoc test).

Moreover, MMT surgery induced a significant and progressive development of static left-right weight bearing imbalance, compared with sham-operated rats (***Figure 32, panel A***). On the other hand, no change occurred in the dynamic HPWD (i.e. the percentage of the weight placed on the ipsilateral hind limb in relation to the total weight of the animal) after MMT surgery, compared with sham group, throughout the course of the study (***Figure 32, panel B***).

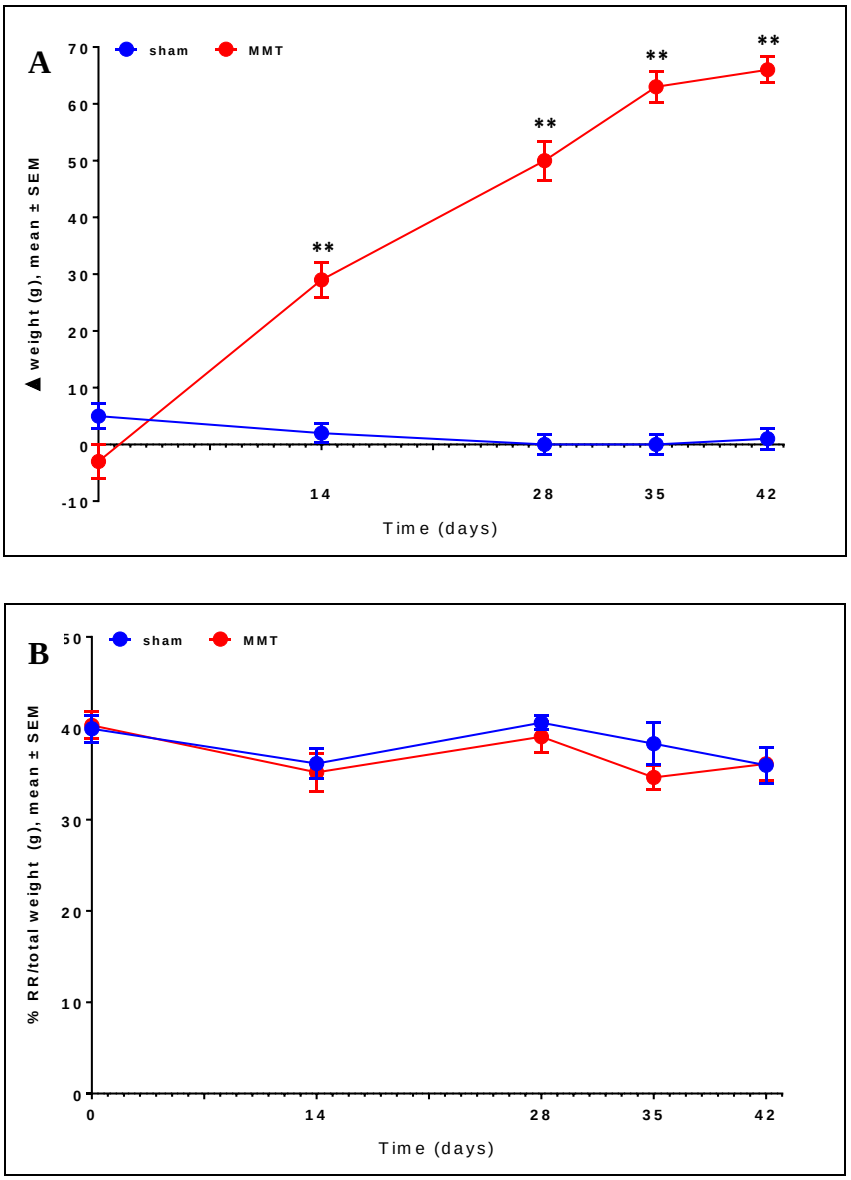

Figure 32: Time course of changes in static (***panel A***) and dynamic (***panel B***) HPWD in sham and MMT-operated rats. Weight bearing asymmetry was evaluated prior (time 0) and 14, 28, 35 and 42 days after MMT surgery, using the incapacitance tester or the dynamic weight bearing system, respectively. Static HPWD data are expressed as the difference in hind paw weight distribution (Δ) between the contralateral and ipsilateral limbs (in grams). Conversely, dynamic HPWD data are expressed as the percentage of the weight placed on the ipsilateral hind limb (RR) in relation to the total weight of the animal (in grams). Data represent the mean of 9 animals/group. **P<0.01 vs. sham group (Two-way RM ANOVA, Sidak's post-hoc test).

Furthermore, no significant difference was detected between sham and MMT group in locomotor activity, 42 days after MMT surgery *(**Figure 33, panel A***).

In the light of the negative outcomes of both DWB and locomotor activity assessments as indirect index of movement-induced spontaneous pain in MMT model, the walking track analysis was

performed as additional behavioural test to assess motor function, in order to further investigate the spontaneous pain component during movement after MMT surgery. However, no significant difference was detected between sham and MMT group even in motor function, throughout the study period (with the exception of 32 days post-surgery) (***Figure 33, panel B***).

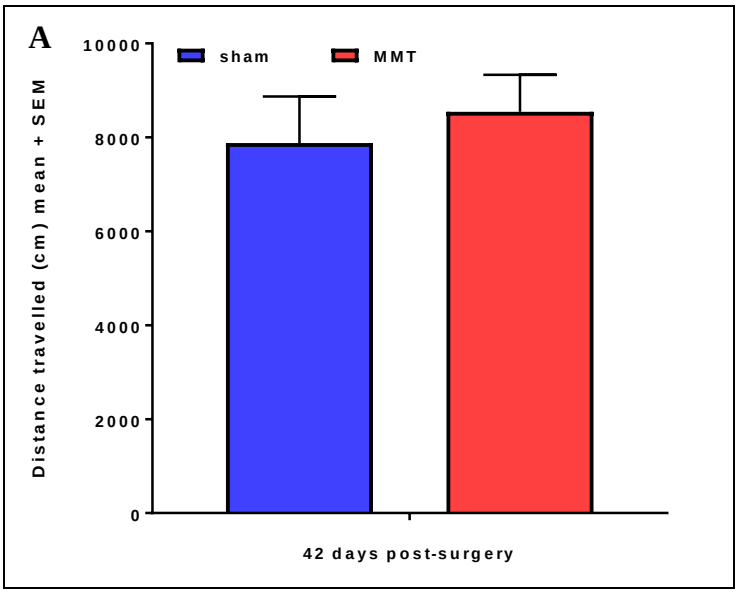

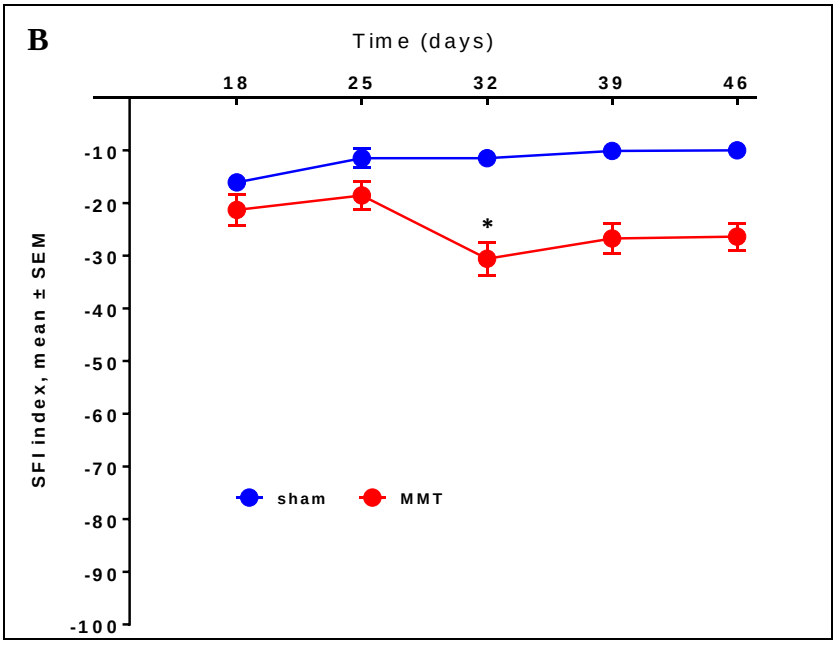

Figure 33: Locomotor activity (***panel A***) and motor function (***panel B***) in sham and MMT-operated rats. Locomotor activity was evaluated 42 days post-surgery, using open field test, and determined as distance travelled (cm) by the rats during the 20 minutes-period of the test. The time course of motor function was assessed using the walking track analysis, 18, 25, 32, 39 and 46 days post-surgery. Data are expressed as SFI index, calculated according to the formula revised by Hare et al. [*Hare et al., 1992*]. Data represent the mean of 9 animals/group. *P<0.05 vs. sham group (Two-way RM ANOVA, Sidak's post-hoc test).

Finally, secondary mechanical hyperalgesia and static HPWD asymmetry assessments were characterized by a significant correlation 42 days post-surgery, as shown by the Pearson's correlation coefficient (PCC = - 0.94).

6.2.1 Effect of CR4056 acute administration

The assessment of secondary mechanical hyperalgesia showed a significant increase of the ipsilateral paw withdrawal threshold, compared with MMT group treated with vehicle, after acute oral treatment, 28 days post-surgery, with 20 mg/kg CR4056 and 10 mg/kg naproxen, only. 6 mg/kg CR4056 was devoid of noticeable effect (***Figure 34***). The percentage of reversal of mechanical threshold obtained with 20 mg/kg CR4056 and naproxen versus their basal pre-MMT surgery was 26 % and 25 %, respectively.

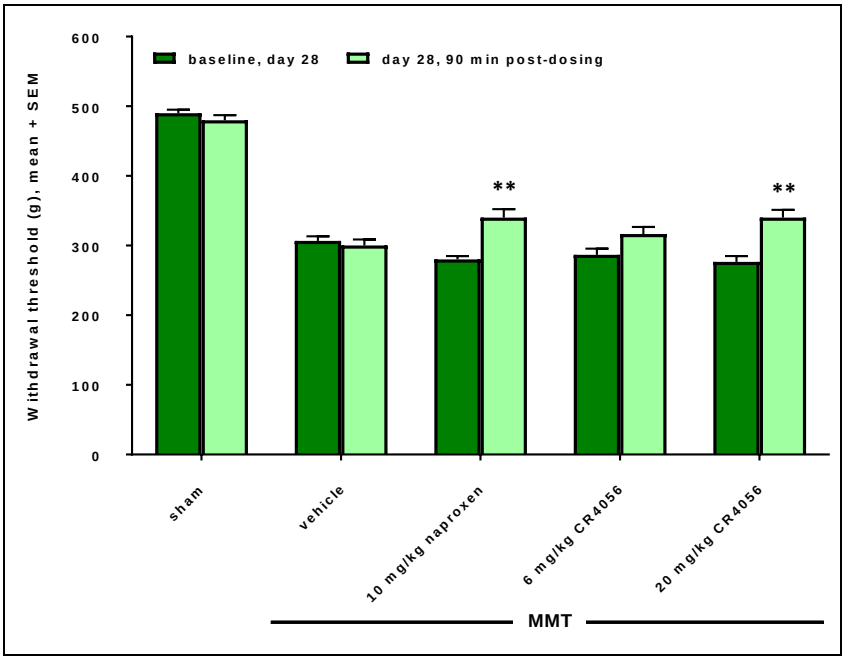

Figure 34: Effect of 6 and 20 mg/kg CR4056 and 10 mg/kg naproxen single oral treatment on mechanical hyperalgesia of the ipsilateral paw. Withdrawal threshold (in grams) was evaluated 28 days post-surgery, by Randall-Selitto test. Data representing the mean of 9 animals/group were collected before (baseline value) and 90 minutes after the drug administration. **P<0.01 vs. MMT vehicle-treated group (Two-way RM ANOVA, Dunnett's post-hoc test).

On the other hand, the single oral treatment with either 6 mg/kg CR4056 or naproxen, 28 days after MMT surgery, did not exerted a noticeable analgesic effect on static left-right weight bearing imbalance (***Figure 35***).

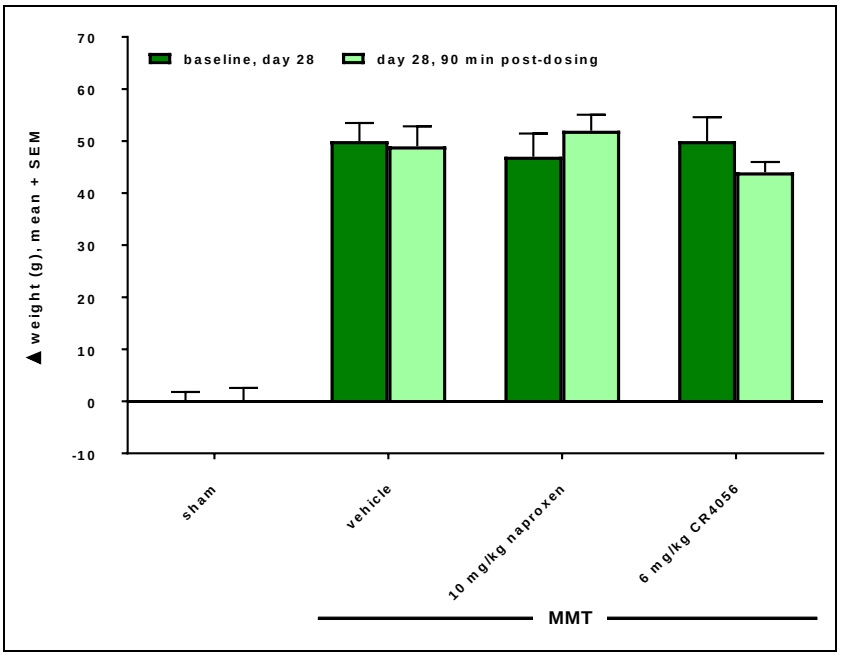

Figure 35: Effect of 6 mg/kg CR4056 and 10 mg/kg naproxen single oral treatment on static HPWD. The difference in hind paw weight distribution (Δ) between the contralateral and ipsilateral limbs (in grams) was assessed 28 days after MMT surgery, before (baseline value) and 90 minutes post-drug administration, using an incapacitance tester. Data represent the mean of 9 animals/group (Two-way RM ANOVA, Dunnett's post-hoc test).

6.2.2 Effect of CR4056 sub-acute treatment

After 15-days, QD repeated treatment both compounds did no longer exerted a significant analgesic effect on mechanical hyperalgesia of the ipsilateral paw, compared with MMT group (***Figure 36***).

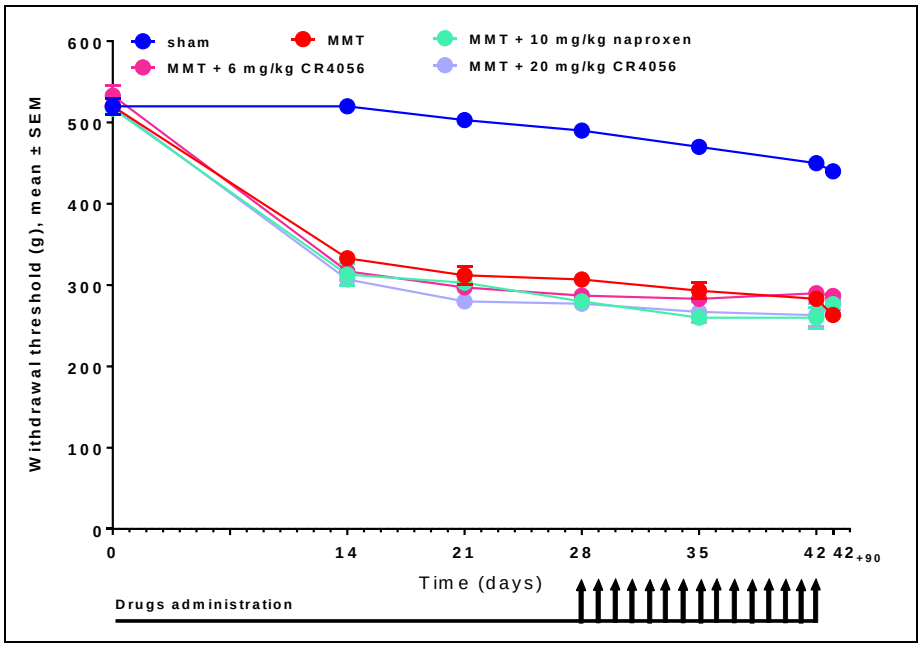

Figure 36: Effect of 6 and 20 mg/kg CR4056 and 10 mg/kg naproxen 15-days sub-acute oral treatment, on mechanical hyperalgesia of the ipsilateral paw. Withdrawal threshold (in grams) was evaluated by Randall-Selitto test, prior (time 0), 28, 35 and 42 days after MMT surgery (42 days both before and 90 minutes post-drug administration). Data represent the mean of 9 animals/group (Two-way RM ANOVA, Dunnett's post-hoc test).

Conversely, the assessment of static HPWD seven days after the beginning of the repeated treatment (day 35 post-surgery) showed a significant reduction of the left-right weight bearing asymmetry in rats treated with 6 mg/kg CR4056, compared with MMT group treated with vehicle (***Figure 37***). On the other hand, no difference was detected in MMT rats treated for seven days (day 35) with 10 mg/kg naproxen, compared with MMT group. After 15-days repeated treatment (day 42) HPWD results confirmed those obtained 7 days before, i.e. 6 mg/kg CR4056 treatment significantly reduced the left-right weight bearing imbalance (percentage of reversal of 21%), while naproxen showed only a non-significant tendency towards this reduction. Notably, the weight bearing asymmetry of animals treated with CR4056, 42 days post-surgery, was statistically lower than the one of the same animals assessed before starting the treatment (day 28). This last result may suggest that CR4056 is not only able to counteract the progression of the symptom seen between day 28 and 42 after surgery, but even to reduce it. Therefore, the analgesic activity, proved by 6 mg/kg CR4056, after sub-acute treatment, on joint discomfort defined as static weight bearing asymmetry, appeared more significant and relevant compared with 10 mg/kg naproxen.

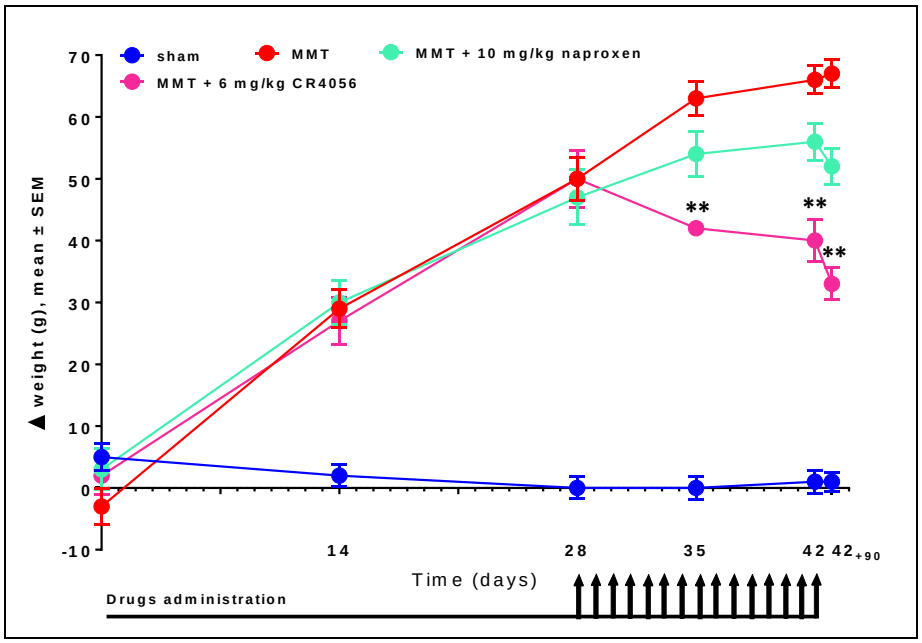

Figure 37: Effect of 6 mg/kg CR4056 and 10 mg/kg naproxen 15-days sub-acute oral treatment on static HPWD. The difference in hind paw weight distribution (Δ) between the contralateral and ipsilateral limbs (in grams) was assessed, using an incapacitance tester, prior (time 0), 14, 28, 35 and 42 days after MMT surgery (on day 42, both before and 90 minutes post-drug administration). Data represent the mean of 9 animals/group. **P<0.01 vs. MMT vehicle-treated group (Two-way RM ANOVA, Dunnett's post-hoc test).

6.2.3 Satellite glial cells activation in L4 and L5 DRGs

The densitometric analysis of GFAP specific signal obtained by western blot analysis showed a slight but not statistically significant increase of GFAP expression in L4 and L5 DRGs in MMT-operated rats, compared with sham group, 42 days post-surgery (***Figure 38***).

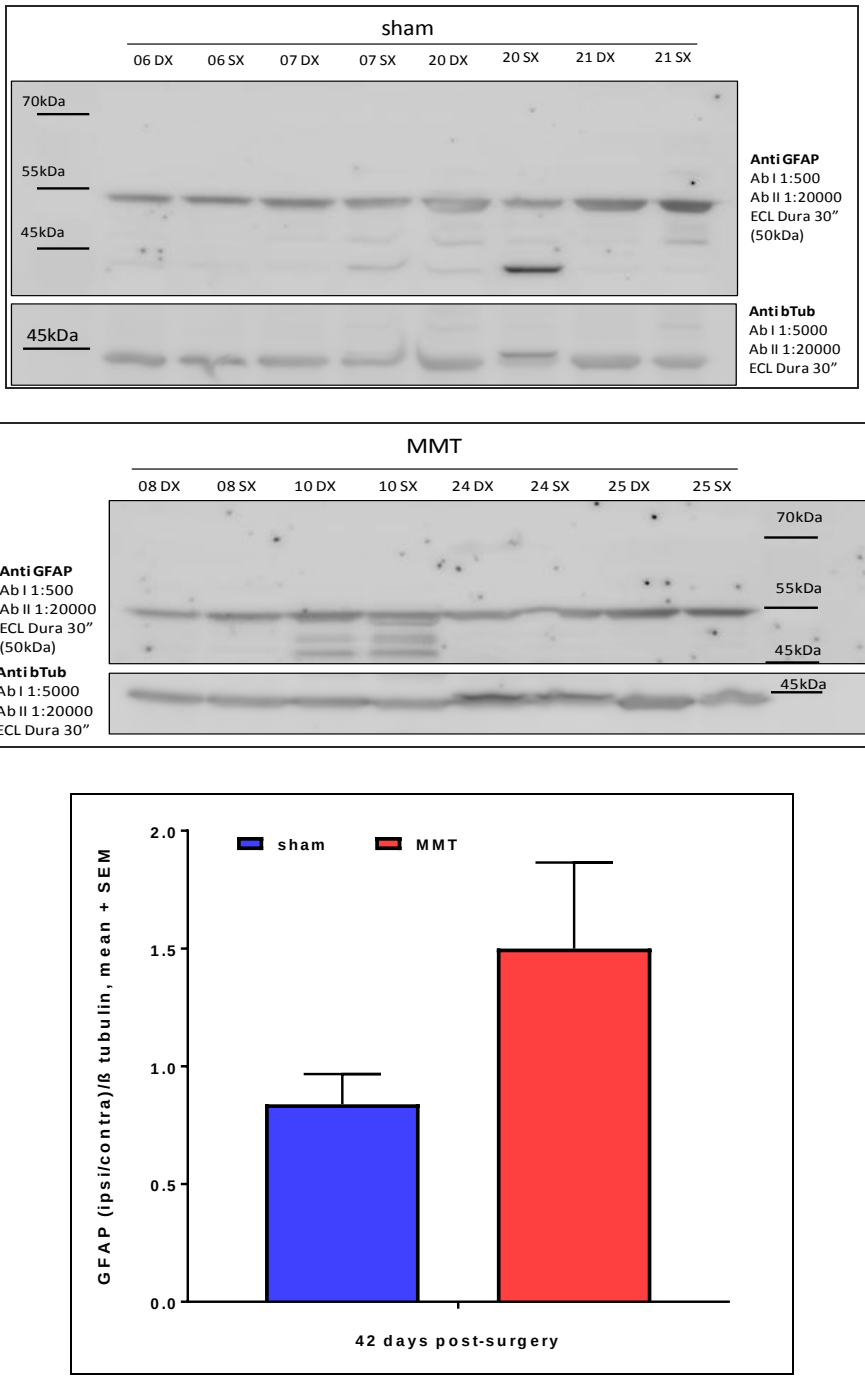

Figure 38: Western blot analysis of expression levels of GFAP in L4 and L5 DRGs of sham and MMT-operated rats, 42 days post-surgery. Results are expressed as the relative optical density (OD) (i.e. the ratio between the OD of the protein band of interest and the one of the corresponding β-tubulin band) of GFAP in ipsilateral L4 and L5 DRGs in relation to the relative OD of GFAP in contralateral L4 and L5 DRGs. Data represent the mean of 4 animals/group (Student's t-test).

6.2.4 Microglial cells activation in lumbar spinal cord

A representative image, for each experimental group, of both the entire L4-L5 SC section and the analyzed selected frame of the laminae I-III of the L4-L5 SC ipsilateral dorsal horn, stained for Iba-1 and counterstained for DAPI, is shown in ***Figure 39, panel A***. No significant difference was detected in the number of Iba-1 positive, morphologically identified, activated microglia in laminae I-III of the L4-L5 SC ipsilateral dorsal horn, among each experimental group, 42 days after MMT surgery (***Figure 39, panel B)***. Moreover, no difference was detected in the number of Iba-1 positive microglia between the ipsilateral and contralateral L4-L5 dorsal horns, 42 days post-surgery, among each experimental group.

A

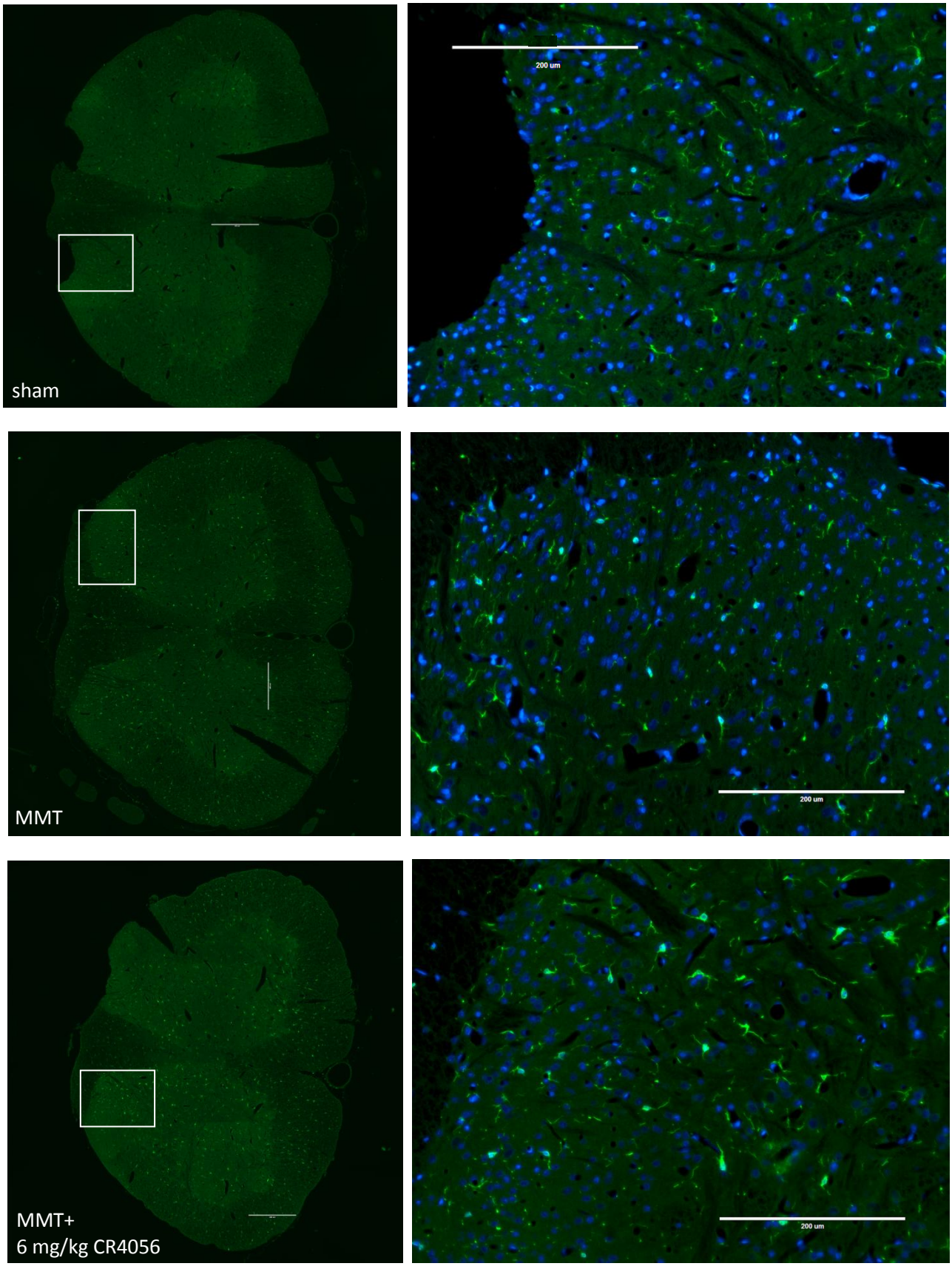

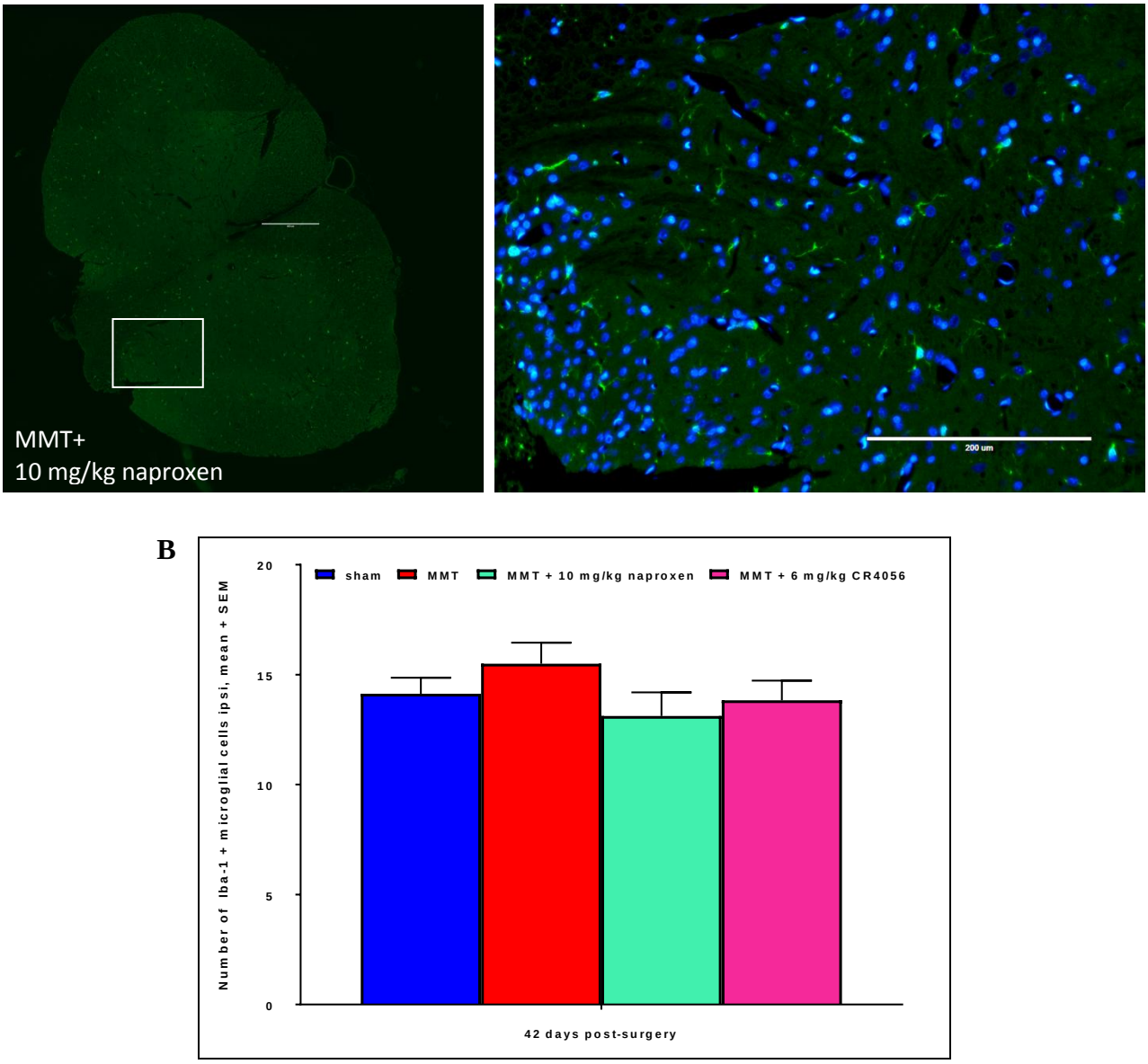

Figure 39: Spinal microglia activation 42 days after MMT surgery. Representative images of both immunofluorescence staining for Iba-1 of the L4-L5 SC sections (scale bar 400 μm) (***left column, panel A***) and the selected frame (capturing area of 578 μm x 434 μm at 20x magnification; scale bar 200 μm) of the laminae I-III of L4-L5 ipsilateral SC dorsal horn stained for Iba-1 and DAPI (***right column, panel A***), in sham and MMT animals, treated either with vehicle, 6 mg/kg CR4056 or 10 mg/kg naproxen. The contralateral side of each L4-L5 SC segment was identified with a small cut in the ventral horn, before sectioning. The quantification of microglia activation in ipsilateral L4-L5 SC dorsal horn was determined as the number of Iba-1-positive microglia, displaying a clearly swollen cell body with reduced processes, within the analyzed selected frame of the superficial laminae (***panel B***). Data represent the mean of 4/5 animals/group (One-way ANOVA, Tukey's post-hoc test).

7. DISCUSSION AND CONCLUSIONS

Osteoarthritis (OA) is a degenerative chronic disease that affects several million individuals worldwide, thus representing a massive healthcare and financial burden *[Poulet et al., 2016]*.

In particular, knee osteoarthritis is the most common type of OA *[Michael et al., 2010].*

Knee OA involves the whole joint in a pathologic dynamic process that implies the local progressive degeneration of hyaline cartilage, subchondral bone thickening, osteophytes formation, synovitis, and degeneration of ligaments and the menisci *[Loeser et al., 2012].*

Pain is the earliest and most disabling symptom for OA patients. OA pain results from a complex interaction between local tissues damage, inflammation, and the peripheral and central nervous systems. OA pain is characterized by peripheral and central sensitization and is driven by both nociceptive and neuropathic mechanisms *[Salaffi et al., 2014].*

Given the heterogeneity of this disease, no ideal animal model for human OA has been described so far. Instead, different OA animal models are employed to mimic different features of the human pathology *[McCoy, 2015].*

Although important advances have been made in understanding the pathophysiological processes of OA, there are currently no approved pharmacological treatments able to modify the disease progression. At present, OA pharmacological therapies, along with physical treatments, still focus on improving symptoms and particularly joint pain *[Sofat et al., 2014].* However, the efficacy of "first-line" agents such as acetaminophen is limited. Moreover, the most common and effective pharmacological therapies, e.g. non-steroidal anti-inflammatory drugs (NSAIDs) and stronger analgesics such as opioids, are frequently associated with significant adverse effects *[Zhang et al., 2016].* Therefore, more effective approaches to the management of OA pain are needed.

Interestingly, chronic musculoskeletal pain is associated with a dysregulation of the descending inhibitory pathways that modulate pain sensations *[Fitzcharles et al., 2011].*

In this clinical field, the selective serotonin-norepinephrine reuptake inhibitor (SNRI) duloxetine has been recently approved in the USA for the treatment of chronic musculoskeletal pain, including OA. Duloxetine is thought to alleviate pain through the increase of the tonic activity of the descending inhibitory pain pathways in the central nervous system (CNS) *[Malfait et al., 2013a].* Nevertheless, the use of this drug is limited by its adverse effects (e.g. increased blood pressure, nausea, fatigue and constipation) *[McAlindon et al., 2014].*

Imidazoline-2 (I2) binding sites might represent a potentially more interesting target to affect pain descending inhibitory pathways. Indeed, I2 receptors (I2Rs) ligands have been associated, at cellular level, with an allosteric inhibition of monoamine oxidases (MAOs) activity, thus increasing

the synaptic levels of norepinephrine and serotonin, which in turn contribute to pain control, especially in the CNS regions related to pain *[Bektas et al., 2015].* I2Rs ligands have been proved effective for tonic inflammatory and neuropathic pain, but generally ineffective for acute phasic pain. Moreover, several studies have shown that I2Rs agonists can potentiate opioid-induced analgesia and attenuate the development of tolerance and dependence associated to opioids *[Li et al., 2011].*

CR4056 is a novel I2Rs ligand that binds to I2 binding sites with a sub-micromolar affinity, and via this interaction inhibits human recombinant as well as rat MAO-A activity, through an allosteric mechanism *[Ferrari et al., 2011]*. CR4056 has been reported to be effective in several animal models of inflammatory, chronic and neuropathic pain *[Ferrari et al., 2011; Meregalli et al., 2012; Lanza et al., 2014].* Moreover, a relevant synergy between CR4056 and morphine was detected in animal models of neurogenic inflammation and postoperative pain *[Ferrari et al., 2011; Lanza et al., 2014];* while a reduction of morphine tolerance on behalf of CR4056 was proved in a model of inflammatory pain.

7.1 PAIN BEHAVIOURS AND CENTRAL SENSITIZATION IN OA ANIMAL MODELS

In this research study, the time-related progression of several OA pain-like behaviours was analyzed and compared in two commonly used OA animal models in rats: the monosodium iodoacetate (MIA) model and the medial meniscal tear (MMT) model. These OA animal models are both able to mimic the painful and structural components of the human pathology, even if they address different clinical “phenotypes” of OA. Although these two OA animal models have been extensively characterized and compared, OA pain-like behaviours have been investigated to a lesser extent in MMT model, compared with the MIA one.

The majority of pain behavioural tests used in the laboratory, bearing any real relevance to arthritic pain in a clinical sense, consists in evoked-pain assessments employing some sort of evoked response to an external mechanical stimulus.

In particular, mechanical allodynia (i.e. pain in response to non-noxious stimuli) is the most common evoked-pain evaluation performed by von Frey test in OA animal models *[Malfait et al., 2013b].* Mechanical allodynia is recognized as a clinical expression of neuropathic pain or pain central sensitization component *[Otis et al., 2016].* Indeed, central sensitization is the

predominant mechanism underlying the lowering of mechanical threshold at sites distal to the damaged joint *[Mapp et al., 2013].*

An additional evoked-pain assessment often employed in OA and chronic pain models consists in mechanical hyperalgesia (i.e. heightened sensitivity to noxious stimuli). Evoked mechanical hyperalgesic responses typically involve applying the noxious stimulus to the hind paw, using Randall-Selitto test, thus measuring secondary mechanical hyperalgesia *[Malfait et al., 2013b].*

On the other hand, PAM (Pressure Application Measurement) device allows the application of a nociceptive pressure stimulus directly to the site of injury, i.e. the knee joint. PAM device has previously proved its reliability as quantitative measurement of localized mechanical hypersensitivity in the knee joint of rats in the inflammatory monoarthritis model, obtained by the i.a. injection of Complete Freund's adjuvant (CFA). Therefore, PAM device provides a quantitative, objective measure of limb mechanical withdrawal threshold, allowing the alignment of pre-clinical measures to those commonly used clinically, such as the pressure dolorimeter, which has been adopted in clinical studies assessing knee OA as well as the pain associated with fibromyalgia. Indeed, the dolorimeter uses a gradually increasing force, applied in a perpendicular plane across the joint margin, to assess localized hypersensitivity of a human joint *[Barton et al., 2007].*

To the best of our knowledge, no previous report has ever employed PAM device to assess mechanical withdrawal threshold of the knee joint in rodent models of OA *[Malfait et al., 2013b].*

In OA patients, stability, walking, stair climbing and weight-bearing symmetry are commonly altered, given the structural role of the medial femorotibial compartment of the knee, which is the part most often affected by knee OA. Therefore, the preclinical evaluation of OA-induced deficits in kinetic (static or dynamic weight distribution) or kinematic (ambulation evaluation or characterization) measurements, represents an additional clinically relevant pain-like behavioural assessment with the potential to provide better guidance for clinical translation of novel analgesic compounds *[Hummel et al., 2016].*

The static weight bearing paradigm is based on the behavioural tendency of animals to avoid pain by shifting the weight from the painful, injured limb to the contralateral limb, a phenomenon that also occurs in patients with knee OA *[Ishikawa et al., 2014].* Static hind paw weight distribution (HPWD) paradigm shows weight bearing alterations in a confined, immobilized position where the majority of the body weight is directed over the hind limbs.

Conversely, the dynamic weight bearing (DWB) system allows the assessment of weight bearing in an unrestricted and more natural position, by measuring plantar surface and pressure from both

front limbs and hind limbs. In addition, dynamic weight bearing assessment allows the detection of possible compensatory patterns in the front limbs and contralateral hind limb, due to unilateral OA induction in rodents. Therefore, the DWB paradigm could be considered an indirect index of spontaneous pain during movement.

Gregersen and colleagues suggested however that the restricted weight bearing, assessed with incapacitance tester, may represent a more sensitive pain indicator in OA animal models, compared with the unrestricted one (DWB) *[Gregersen et al., 2013].*

Indeed, spontaneous pain assessments at rest or during movement (e.g. DWB, open field test or walking track analysis), even if they may reflect more accurately the clinical features of OA, are less sensitive pain index and often more difficult to obtain in a reliable, reproducible and objective manner in animal models *[Ishikawa et al., 2014].*

In this study, the role of central sensitization in OA pain was also investigated in both MIA and MMT model, since neuropathic pain mechanisms, such as central sensitization, contribute to OA pain, for at least a subset of OA patients *[Dimitroulas et al., 2014].*

Both spinal glial cells and satellite glial cells within DRGs are involved in the establishment and maintenance of central sensitization and neuropathic pain *[Gosselin et al., 2010; Dublin et al., 2007].*

Moreover, the family of mitogen-activated protein kinases (MAPKs) (e.g. the neuronal ERKs and the glial p38) plays a key role in the development and maintenance of central pain sensitization.

Therefore, both spinal microglia activation and either MAPKs or satellite glial cells activation was assessed in either MIA or MMT model, respectively, based on previous literature reports *[Takeda et al., 2009; Lee at al., 2011; Sagar et al., 2011].*

7.1.1 MIA model of osteoarthritis

MIA model was induced by a single intra-articular (i.a.) injection in the infrapatellar area of the rat knee joint of 1 mg/ 50 μl MIA, an inhibitor of glycolisis that disrupts chondrocytes metabolism, leading to cartilage degeneration. MIA injection dose-dependently produces a transient inflammation, rapid erosion of joint cartilage and subchondral bone remodelling with osteophytes formation *[Bove et al., 2003].* In particular, previous studies have shown that 1 mg/ 50μl MIA i.a. injection leads first to chondrocytes degeneration with thinning and collapsing of the cartilage matrix, associated with synovitis, followed by bone remodelling and fibrosis of the subchondral

bone marrow, 21 days after MIA injection *[Guzman et al., 2003; Ivanavicius et al., 2007].* Therefore, this model replicates many of the histological changes observed in human OA, as well as a pain-behaviour, consistent with activity-related pain in OA patients *[Kelly et al., 2012].* Nevertheless, as a chemically-induced OA model, MIA model has a unique pathophysiology, which is quite distinct from human naturally occurring OA or post-traumatic OA (PTOA) *[McCoy, 2015].* Moreover, MIA model develops very rapidly, with a time frame significantly different from human OA. Nevertheless, this OA model is a technically straightforward reproducible method, which has proved to be predictive of the effects of anti-inflammatory and analgesic agents in humans *[Hummel et al., 2016].* Hence, MIA model is mainly used to study the mechanism of OA pain-related behaviours and for the screening of symptom-modifying OA drugs *[McCoy, 2015].*

In this study, both the allodynic and the primary hyperalgesic responses to mechanical stimuli were evaluated prior to MIA i.a. injection and 7, 14 and 21 days after MIA. Moreover, static and dynamic hind paw weight bearing distribution and locomotor activity were assessed, following the same experimental design.

MIA model is characterized by a significant, long-lasting and dose-dependent decrease of mechanical withdrawal threshold of the ipsilateral hind paw, i.e. mechanical allodynia, as reported by several previous studies *[Combe et al., 2004; Im et al., 2010; Thakur et al., 2012].*

The results of our work further showed that 1 mg/ 50 µl MIA i.a. injection was able to induce a significant and long-lasting development of mechanical allodynia of the ipsilateral paw, compared with saline injected animals, thus confirming the suitability of von Frey test as evoked-pain measurement in this OA model.

Our study demonstrated that MIA injection induced also a significant and long-lasting development of primary mechanical hyperalgesia, assessed using PAM device, compared with sham group. The evidence of primary mechanical hyperalgesia development after MIA i.a. injection constitutes an evoked-pain assessment more clinically relevant, also for the translation of novel analgesics from animal models of OA to human patients.

Previous in-house studies have demonstrated that the dose of 1 mg was the minimum dose of MIA required to observe distal mechanical allodynia and primary mechanical hyperalgesia, associated to joint damage.

Static weight bearing imbalance has been previously reported to be significant by several studies in MIA model *[Ivanavicius et al., 2007; Ishikawa et al., 2014],* although the hind paw weight distribution (HPWD) paradigm in MIA-injected animals appears more variable when compared

with MMT model. As a matter of fact, the same authors reported its insensitivity or its sensitivity in two different papers *[Mapp et al., 2013, Nwosu et al., 2016,* respectively].

Our experiments in MIA model showed a significant, albeit very variable, static HPWD asymmetry, compared with sham controls.

Moreover, our results demonstrated a significant and long-lasting development of dynamic weight bearing asymmetry in MIA model. Hence, we further support the report by Gregersen and colleagues, which have previously shown the occurrence in this OA model of significant changes in unrestricted hind limb weight bearing, assessed with a method virtually equal to the DWB system *[Gregersen et al., 2013].* Moreover, changes of weight bearing distribution during movement in MIA model were previously demonstrated also by Ferreira-Gomes and colleagues, using the CatWalk test, a method similar to the DWB system, proving its suitability to evaluate nonreflexive and nonreferred OA-induced nociception in a clinically relevant manner [*Ferreira-Gomes et al., 2008; Ferreira-Gomes et al., 2012a*].

Finally, the results of the present study demonstrated a significant increase in the number of Iba-1 positive, morphologically identified, activated microglia in laminae I-III of the dorsal horns of the lumbar L4-L5 segment of the spinal cord, 21 days after MIA injection, compared with sham controls.

Sagar and colleagues have previously obtained similar results, showing that MIA model of OA pain is associated with a time-dependent activation of microglia and a later activation of astrocytes in the spinal cord *[Sagar et al., 2011].*

Moreover, several previous reports have demonstrated a dose-dependent degree of neuronal injury and/or central sensitization after MIA injection *[Ivanavicius et al., 2007; Im et al., 2010; Orita et al., 2011; Ferreira-Gomes et al., 2012b; Thakur et al., 2012].*

In this work, the increased activation of microglia was detected in both ipsilateral and contralateral L4-L5 dorsal horns of MIA-injected animals, as opposed to several works in literature showing a significant activation in the ipsilateral side only *[Orita et al., 2010; Sagar et al., 2011].* However, is not unusual for many changes in the nervous system to occur bilaterally, even in the case of a unilateral disease. Further assessment aimed to verify if these results may be related to the investigated experimental time point, after MIA injection, will be performed in the future.

Notably, 21 days after MIA injection, no differences were noted, between sham and MIA group, in the phosphorylation-activation of either the glial MAPK p38 or the neuronal MAPK ERKs, in ipsilateral L4-L5 lumbar spinal cord. The different results obtained regarding these pain-related

proteins levels could be related to the different methodology (i.e. either immunofluorescence staining or western blot analysis) used to assess either Iba-1 or pp38 and pERKs expression, respectively.

Moreover, the involvement of ERKs and p38 activation in pain-induced central sensitization was previously reported in the MIA model, obtained with 3 mg/ 50 µl MIA i.a. injection only *[Lee at al., 2011].* Therefore, our results may be also ascribed to the inferior dose of MIA employed in our model, related to a less severe OA disease, compared with the one used by Lee and colleagues.

Further investigation on these matters will be conducted in future studies.

7.1.2 MMT model of osteoarthritis

MMT model was induced by the transection of both the medial collateral ligament and the medial meniscus of the femorotibial rat joint, which leads to joint destabilization, resulting in progressive degeneration of articular cartilage, synovitis, subsequent subchondral bone thickening and osteophytes formation *[Bove et al., 2006].* In particular, the initial chondropathy (e.g. chondrocytes degeneration and apoptosis, loss of proteoglycans and matrix fibrillation) progressively increases between 14 and 49 days after surgery, with the concurrent development of evident subchondral bone sclerosis, osteophytosis and synovitis, starting from 14 days post-surgery *[Mapp et al., 2013].* The impairment of joint stability and mechanical loading leads in turn to pain-related behaviour, defined mainly as joint discomfort *[Janusz et al., 2002]*. Therefore, MMT model, as a surgically-induced OA model, is particularly suited for studying the pathophysiology of human PTOA and is commonly used to evaluate potential disease- or symptom-modifying OA drugs *[Yu et al., 2015].*

As opposite to MIA model, the assessment of mechanical allodynia, using von Frey monofilaments, in MMT model has so far produced contradictory results. Several works have demonstrated the occurrence of mechanical allodynia after the transection of both the medial collateral ligament and the medial meniscus of rats knee, compared with sham-operated animals [*Fernihough et al., 2004; Kloefkorn et al., 2015].* On the other hand, an interesting report by Mapp and colleagues, comparing both structural and pain differences between MIA and MMT model, has demonstrated that allodynic withdrawal threshold decreased in MIA rats but not in MMT rats, after the induction of the pathology, compared with the corresponding sham controls *[Mapp et al., 2013].*

The surgery procedure as well as the method for mechanical allodynia evaluation in these research studies were equal to the ones used herein. This study showed only a non-significant tendency in the reduction of the withdrawal mechanical threshold of the ipsilateral paw, compared with sham group, up to 47 days after MMT surgery. Therefore, our results confirmed the relative insensitivity of MMT-induced pain evaluation by von Frey hairs that renders this paradigm unsuitable for testing analgesic compounds in this OA model.

Conversely, we reported a significant and long-lasting development of secondary mechanical hyperalgesia 14, 21, 28, 35 and 42 days after MMT surgery, compared with sham-operated animals. Mechanical withdrawal threshold of the hind paw was assessed using the Randall-Selitto test. In particular, according to the weight (i.e. 300-325 g) of the rats enrolled, the cut-off of the device was set at 750 grams. This range of weight did not cause cutaneous damage and the thresholds of sham-operated rats were unchanged throughout the 6-weeks study.

Similarly, a previous report by Fernihough and colleagues showed a decrease of the mechanical withdrawal threshold of the ipsilateral paw in MMT rats with an inferior weight, using Randall-Selitto analgesymeter with a cut-off of 250 grams [*Fernihough et al., 2004].*

In our studies in MMT model, primary hyperalgesia assessment, using PAM device, was not performed in order to avoid any bias related to postoperative pain and a possible worsening of the pathology due to the repeated application of pressure directly to the operated joint. A histopathological evaluation aimed to clarify this last hypothesis will be performed in the future.

Static weight bearing distribution, assessed using an incapacitance tester, is the main pain-like behaviour investigated in MMT model. As a matter of fact, several previous reports in literature have demonstrated that weight bearing asymmetry increases over time in this surgical model of OA *[Bove et al., 2006; Yu et al., 2012; Mapp et al., 2013].*

The results of our research work further confirmed the development of a significant and progressive static left-right weight bearing imbalance in MMT-operated animals, compared with sham controls. Conversely, no difference was detected between MMT- and sham-operated rats with DWB system, 14, 28, 35 and 42 days post-surgery. These results seem to further support the hypothesis that the restricted static weight bearing may represent a more sensitive pain indicator in OA animal models, compared with the unrestricted dynamic weight bearing *[Gregersen et al., 2013].*

To our knowledge, the study of Bagi and colleagues is the only one that has assessed dynamic weight bearing in MMT model so far. In particular, they demonstrated that MMT rats are

characterized by a mild but statistically significant difference in the weight bearing between the contralateral and ipsilateral hind limb, and an earlier shift in their body weight toward the front limbs, compared with sham rats *[Bagi et al., 2015b]*. The different results obtained in our study, compared with the one of Bagi and colleagues, could be ascribed to either the different rats strain and weight or the DWB analysis parameters employed, respectively.

As regard the role of central sensitization in MMT-induced OA pain, to the best of our knowledge, no previous reports have ever assessed either satellite glial cells (SGCs) or microglia activation, related to central sensitization development and maintenance, in MMT model.

Our results showed no changes in either GFAP or Iba-1 expression, in either ipsilateral L4 and L5 DRGs or ipsilateral L4-L5 dorsal horns of the spinal cord, compared with sham-operated animals, 42 days after MMT surgery. Therefore, neither the activation of SGCs in DRGs nor the activation of microglia in spinal cord seem to occur in this surgical model of OA. Hence, these results may indicate a marginal role of central pain mechanisms in OA pain-like behaviours development and maintenance in MMT model.

7.1.3 Conclusions

The results of this research study, regarding several pain-like behaviours evaluation in both MIA and MMT model (***Table 1***), further support the hypothesis first suggested by Mapp and colleagues *[Mapp et al., 2013]*, i.e. the relative contribution of peripheral and central pain mechanisms seems to differ significantly between these two OA models. Indeed, we demonstrated both a significant decrease of mechanical withdrawal threshold of the ipsilateral paw (i.e. mechanical allodynia) and the activation of microglia in the spinal cord dorsal horns, in MIA model only. Therefore, central sensitization mechanisms seem to be mostly involved in OA pain induced by MIA i.a. injection, rather than the one resulting from MMT surgery. Moreover, even the detection of a significant weight bearing asymmetry in MMT model, using the restricted and more sensitive measurement (i.e. incapacitance tester) only, could be related to the marginal role of central sensitization in this OA model. Furthermore, the suitability of the dynamic weight bearing paradigm as indirect index of spontaneous pain during movement was proved in MIA model only. Therefore, MIA model appears to be characterized by a major contribution of central sensitization mechanisms to OA pain, as well as a movement-evoked pain component (i.e. dynamic weight bearing asymmetry), as opposed to MMT model.

Finally, in this study, no changes were detected in locomotor activity and/or motor function after either MIA injection or MMT surgery, suggesting that both open field test and walking track analysis may not represent a suitable measure as indirect index of movement-induced spontaneous pain, in both these OA models.

In this regard, to further characterize OA pain-like behaviours in both MIA and MMT model, further analysis aimed to evaluate the spatiotemporal gait as indirect measure of spontaneous pain during movement *[Ishikawa et al., 2014; Kloefkorn et al., 2015]* will be performed in future studies.

In summary, this research study has further confirmed that MIA and MMT models display a pain-behaviour comparable to human OA. However, these animal models do not mimic identical aspects of OA pain of the human disease. These differences should be taken into account for future studies focusing on specific features of human osteoarthritis.

Further analysis of both astrocytes activation in spinal cord and pain-related neuropeptides (e.g. SP and CGRP) expression in DRGs will be performed in both MIA and MMT model, in order to further investigate the role of peripheral and central pain mechanisms in OA pain development and maintenance.

	MIA MODEL	**MMT MODEL**
Mechanical allodynia	yes	no
Primary mechanical hyperalgesia	yes	-
Secondary mechanical hyperalgesia	-	yes
Static weight bearing	yes	yes
Dynamic weight bearing	yes	no
Locomotor activity	no	no
Motor function	-	no
Microglial activation (central sensitization)	yes	no

Table 1: Results of our study regarding the presence or absence of several pain-like behaviours and central sensitization in either MIA or MMT model of OA.

7.2 CR4056 ANALGESIC EFFICACY IN OA PAIN ANIMAL MODELS

In the present study, CR4056 analgesic efficacy was investigated in both MIA and MMT model of osteoarthritis, in comparison with naproxen, a NSAID often prescribed for human OA pain.

Acute naproxen was previously found to alleviate the joint discomfort following MIA injection in the rat knee *[Bove et al., 2003; Ivanavicius et al., 2007].* Moreover, several authors have suggested a specific sensitivity to acute NSAIDs administration up to approximately 2 weeks post-MIA injection only *[Ivanaviucius et al. 2007, Gregersen et al. 2013, Ishikawa et al., 2014].* Conversely, to the best of our knowledge, no studies in literature have previously assessed the analgesic efficacy of naproxen in MMT model, while only few have used different NSAIDs *[Bove et al., 2006*; *Ashraf et al., 2011].*

7.2.1 CR4056 in MIA model of osteoarthritis

This study proved that 6 and 20 mg/kg CR4056 induced a significant and dose-dependent anti-hyperalgesic and anti-allodynic effect both following acute and repeated daily treatment from day 14 to day 21, after MIA injection, compared with vehicle-treated MIA controls. Conversely, acute 10 mg/kg naproxen exerted a significant effect on mechanical allodynia only, while the 8-days sub-acute treatment with this compound reduced both mechanical allodynia and primary mechanical hyperalgesia. This is in accordance with previous results showing that a sub-acute dosing of NSAIDs is necessary to improve, at least in part, MIA-induced behavioural deficits *[Pomonis et al., 2005].*

Therefore, our results suggested that the overall analgesic activity proved by 6 and 20 mg/kg CR4056 on either mechanical allodynia or primary mechanical hyperalgesia in MIA model, appeared more significant and relevant compared with 10 mg/kg naproxen. Nevertheless, both CR4056 doses and naproxen showed a greater analgesic efficacy on both behavioural assessments after 8-days sub-acute treatment, rather than a single administration.

It has to be noted that both compounds were devoid of noticeable effect on static and dynamic weight bearing asymmetry induced by MIA injection.

Future studies aimed to assess if stronger analgesics, such as morphine, may reverse MIA-induced changes in either static or dynamic weight bearing distribution will be conducted in the future. Notably, even in OA patients, alterations in weight bearing symmetry can persist even after a

significant reduction of pain is obtained with interventions, such as total knee arthroplasty *[Mizner et al., 2005].*

In addition, our results showed that 8-days sub-acute treatment with either 6 mg/kg CR4056 or 10 mg/kg naproxen significantly reversed MIA-induced microglia activation in ipsilateral dorsal horn of the lumbar L4-L5 segment of the spinal cord.

Glial cells within the spinal cord dorsal horns secrete, upon activation, inflammatory mediators, such as pro-inflammatory cytokines, BDNF and GDNF, which contribute to sensitization of the spinal neurons, furthering the development and maintenance of central sensitization. In turn, neurons can regulate the activation of microglia and astrocytes through multiple cellular pathways *[Gosselin et al., 2010; Dimitroulas et al., 2014]*. Moreover, an additional important mechanism in central sensitization is the upregulation of COX-2 *[Dimitroulas et al., 2014]*. Therefore, the reduction of microglial activation in spinal cord induced by naproxen sub-acute treatment in MIA model could be purely ascribed to its anti-inflammatory activity.

Recent reports have shown that spinal microglia and astrocytes, besides being involved in the establishment and maintenance of central sensitization in chronic pain states, play a pivotal role in the development of morphine hypersensitivity and decreased efficacy (i.e. tolerance) *[DeLeo et al., 2004; O'Callaghan et al., 2010].* In particular, chronic morphine exposure results in strong microglia activation, i.e. both upregulation of the microglia markers cluster of differentiation molecule 11b (CD11b) and Iba-1 and activation of the MAPK p38 *[Wen et al., 2011].* Notably, blocking microglia activation (e.g. with minocycline) prevents the development of morphine tolerance and hyperalgesia *[O'Callaghan et al., 2010; Wen et al., 2011].*

CR4056 has proved its efficacy in either reducing microglia activation related to central sensitization, in the MIA model of OA pain, or reversing the development of tolerance to morphine analgesia, in the inflammatory pain model induced by the sub-plantar injection of CFA. Therefore, in the light of the evidences of microglia role both in central sensitization and morphine tolerance, in addition to our results on this I2Rs ligand in MIA model, we may suggest a possible interplay between microglia and CR4056 activity in the central nervous system. Further investigations on this matter, aimed to obtain novel insights on CR4056 mode of action will be performed in the future.

7.2.2 CR4056 in MMT model of osteoarthritis

In MMT model, 20 mg/kg CR4056 and 10 mg/kg naproxen showed a significant anti-hyperalgesic effect after acute treatment only, 28 days post-surgery, compared with the vehicle-treated MMT controls.

On the other hand, 6 mg/kg CR4056 15-days sub-acute treatment, from 28 to 42 days post-surgery, significantly reduced the static left-right weight bearing imbalance, while naproxen showed only a non-significant tendency towards this reduction. Notably, the weight bearing asymmetry of animals treated with CR4056, 42 days post-surgery, was statistically lower than the one of the same animals assessed before starting the treatment (day 28). This last result may suggest that CR4056 is not only able to counteract the progression of the symptom seen between day 28 and 42 after surgery, but even to reduce it.

Therefore, the results of our study suggested that even in this OA model, the analgesic activity proved by 6 mg/kg CR4056, after sub-acute treatment, on MMT-induced joint discomfort (i.e. static HPWD asymmetry), appeared more significant and relevant compared with naproxen.

7.2.3 Conclusions

In summary, the present research work has demonstrated that the optimal dose of 6 mg/kg of CR4056 significantly reduced the progression of the characteristic pain-like behaviours (i.e. either mechanical allodynia and hyperalgesia in MIA model or static weight bearing imbalance in MMT model) in these two different rat models of OA, without apparent tolerance after repeated doses. Thus, given also CR4056 neurobiological, cardiovascular and respiratory safety previously established, this novel imidazoline-2 binding sites ligand could represent a new highly effective treatment option for OA pain.

As regards future perspectives, an additional study aimed to evaluate CR4056 analgesic efficacy, in comparison with duloxetine, and its interaction with microglia in the spinal cord, will be conducted in both these OA models in rats, in order to further elucidate CR4056 mode of action in relation to the activity of the descending inhibitory pain pathways.

8. REFERENCES

Al-Shamsi M, Shahin A, Ibrahim MF, Tareq S, Souid AK, Mensah-Brown EP. Bioenergetics of the spinal cord in experimental autoimmune encephalitis of rats. BMC Neuroscience. 2015; 16:37.

Arden N, Nevitt MC. Osteoarthritis: epidemiology. Best practice & research. Clinical Rheumatology. 2006; 20(1):3-25.

Ashraf S, Mapp PI, Walsh DA. Contributions of angiogenesis to inflammation, joint damage, and pain in a rat model of osteoarthritis. Arthritis and Rheumatism. 2011; 63(9):2700-2710.

Ayral X, Pickering EH, Woodworth TG, Mackillop N, Dougados M. Synovitis: a potential predictive factor of structural progression of medial tibiofemoral knee osteoarthritis - results of a 1 year longitudinal arthroscopic study in 422 patients. Osteoarthritis and Cartilage. 2005; 13(5)-361-367.

Bagi CM, Berryman E, Zakur DE, Wilkie D, Andresen CJ. Effect of antiresorptive and anabolic bone therapy on development of osteoarthritis in a posttraumatic rat model of OA. Arthritis Research & Therapy. 2015a; 17:315.

Bagi CM, Zakur DE, Berryman E, Andresen CJ, Wilkie D. Correlation between µCT imaging, histology and functional capacity of the osteoarthritic knee in the rat model of osteoarthritis. Journal of Translational Medicine. 2015b; 13:276-287.

Barton NJ, Strickland IT, Bond SM, Brash HM, Bate ST et al. Pressure application measurement (PAM): a novel behavioural technique for measuring hypersensitivity in a rat model of joint pain. Journal of Neuroscience Methods. 2007; 163(1):67-75.

Basbaum AI, Bautista DM, Scherrer G, Julius D. Cellular and molecular mechanisms of pain. Cell. 2009; 139(2):267-284.

Beaumont GH, Roman-Blas JA, Castaneda S, Jimenez SA. Primary osteoarthritis no longer primary: three subsets with distinct etiological, clinical and therapeutic characteristics. Seminars in Arthritis and Rheumatism. 2009; 39(2):71-80.

Bektas N, Nemutlu D, Arslan R. The imidazoline receptors and ligands in pain modulation. Indian Journal of Pharmacology. 2015; 47(5):472-478.

Bendele AM. Animal models of osteoarthritis. Journal of Musculoskeletal and Neuronal Interactions. 2001; 1(4):363-376.

Bennell KL, Hunter DJ, Hinman RS. Management of osteoarthritis of the knee. BMJ (Clinical Research Ed.). 2012; 345:e4934.

Bove SE, Calcaterra SL, Brooker RM, Huber CM, Guzman RE et al. Weight bearing as a measure of disease progression and efficacy of anti-inflammatory compounds in a model of monosodium iodoacetate-induced osteoarthritis. Osteoarthritis and Cartilage. 2003; 11(11):821-830.

Bove SE, Laemont KD, Brooker RM, Osborn MN, Sanchez BM et al. Surgically induced osteoarthritis in the rat results in the development of both osteoarthritis-like joint pain and secondary hyperalgesia. Osteoarthritis and Cartilage. 2006; 14(10):1041-1048.

Bruyère O, Cooper C, Pelletier JP, Branco J, Luisa Brandi M et al. An algorithm recommendation for the management of knee osteoarthritis in Europe and internationally: a report from a task force of the European Society for Clinical and Economic Aspects of Osteoporosis and Osteoarthritis (ESCEO). Seminars in Arthritis and Rheumatism. 2014; 44(3):253-263.

Buchanan WW, Kean WF. Osteoarthritis II: Pathology and pathogenesis. Inflammopharmacology. 2002; 10(1-2):23-52.

Chang CH, Wu HT, Cheng KC, Lin HJ, Cheng JT. Increase of beta-endorphin secretion by agmatine is induced by activation of imidazoline I(2A) receptors in adrenal gland of rats. Neuroscience Letters. 2010; 468(3):297-299.

Chaplan SR, Bach FW, Pogrel JW, Chung JM, Yaksh TL. Quantitative assessment of tactile allodynia in the rat paw. Journal of Neuroscience Methods. 1994; 53:55-63.

Chappell AS, Desaiah D, Liu-Seifert H, Zhang S, Skljarevski V et al. A double-blind, randomized, placebo-controlled study of the efficacy and safety of duloxetine for the treatment of chronic pain due to osteoarthritis of the knee. Pain Practice: the Official Journal of World Institute of Pain. 2011; 11(1):33-41.

Chappell AS, Ossanna MJ, Liu-Seifert H, Iyengar S, Skljarevski V et al. Duloxetine, a centrally acting analgesic, in the treatment of patients with osteoarthritis knee pain: a 13-week, randomized, placebo-controlled trial. Pain. 2009; 146(3):253-260.

Combe R, Bramwell S, Field MJ. The monosodium iodoacetate model of osteoarthritis: a model of chronic nociceptive pain in rats? Neuroscience Letters. 2004; 370(2-3):236-240.

Coutaux A, Adam F, Willer JC, Le Bars D. Hyperalgesia and allodynia: peripheral mechanisms. Joint Bone Spine. 2005; 72(5):359-371.

Cross M, Smith E, Hoy D, Nolte S, Ackerman I et al. The global burden of hip and knee osteoarthritis: estimates from the global burden of disease 2010 study. Annals of the Rheumatic Diseases 2014; 73(7):1323–1330.

de Medinaceli L, Freed WJ, Wyatt RJ. An index of the functional condition of rat sciatic nerve based on measurements made from walking tracks. Experimental Neurology. 1982; 77(3):634-643.

DeLeo JA, Tanga FY, Tawfik VL. Neuroimmune activation and neuroinflammation in chronic pain and opioid tolerance/hyperalgesia. Neuroscientist. 2004; 10(1):40-52.

Dimitroulas T, Duarte RV, Behura A, Kitas GD, Raphael JH. Neuropathic pain in osteoarthritis: a review of pathophysiological mechanisms and implications for treatment. Seminars in Arthritis and Rheumatism. 2014; 44(2):145-154.

Dray A, Read SJ. Future targets to control osteoarthritis pain. Arthritis and Pain. 2007; 9(3):212-225.

Dublin P, Hanani M. Satellite glial cells in sensory ganglia: their possible contribution to inflammatory pain. Brain, Behavior, and Immunity. 2007; 21(5):592-598.

Fang H, Beier F. Mouse models of osteoarthritis: modelling risk factors and assessing outcomes. Nature Reviews. Rheumatology. 2014; 10(7):413-421.

Felson DT, Lawrence RC, Dieppe PA, Hirsch R, Helmick CG et al. Osteoarthritis: new insight. Part 1: the disease and its risk factors. Annals of Internal Medicine. 2000; 133:635-646.

Felson DT. Clinical practice. Osteoarthritis of the knee. The New England Journal of Medicine. 2006; 354(8):841-848.

Ferland CE, Pailleux F, Vachon P, Beaudry F. Determination of specific neuropeptides modulation time course in a rat model of osteoarthritis pain by liquid chromatography ion trap mass spectrometry. Neuropeptides. 2011; 45(6):423-429.

Fernihough J, Gentry C, Malcangio M, Fox A, Rediske J et al. Pain related behaviour in two models of osteoarthritis in the rat knee. Pain. 2004; 112(1-2):83-93.

Ferrari F, Fiorentino S, Mennuni L, Garofalo P, Letari O et al. Analgesic efficacy of CR4056, a novel imidazoline-2 receptor ligand, in rat models of inflammatory and neuropathic pain. Journal of Pain Research. 2011; 4:111-125.

Ferreira-Gomes J, Adães S, Castro-Lopes JM. Assessment of movement-evoked pain in osteoarthritis by the knee-bend and CatWalk tests: a clinically relevant study. The Journal of Pain. 2008; 9(10):945-954.

Ferreira-Gomes J, Adães S, Mendonça M, Castro-Lopes JM. Analgesic effects of lidocaine, morphine and diclofenac on movement-induced nociception, as assessed by the Knee-Bend and CatWalk tests in a rat model of osteoarthritis. Pharmacology, Biochemistry, and Behavior. 2012a; 101(4):617-624.

Ferreira-Gomes J, Adães S, Sousa RM, Mendonça M, Castro-Lopes JM. Dose-dependent expression of neuronal injury markers during experimental osteoarthritis induced by monoiodoacetate in the rat. Molecular Pain. 2012b; 8:50.

Fitzcharles MA, Shir Y. Management of chronic pain in the rheumatic diseases with insights for the clinician. Therapeutic Advances in Musculoskeletal Disease. 2011; 3(4):179-190.

Garau C, Miralles A, García-Sevilla JA. Chronic treatment with selective I2-imidazoline receptor ligands decreases the content of pro-apoptotic markers in rat brain. Journal of Psychopharmacology (Oxford, England). 2013; 27(2):123-134.

Gentili F, Cardinaletti C, Carrieri A, Ghelfi F, Mattioli L et al. Involvement of I2-imidazoline binding sites in positive and negative morphine analgesia modulatory effects. European Journal of Pharmacology. 2006; 553(1-3):73-81.

Goldring MB, Otero M. Inflammation in osteoarthritis. Current Opinion in Rheumatology. 2011; 23(5):471-478.

Goldring MB. Articular cartilage degradation in osteoarthritis. HSS journal: the musculoskeletal journal of Hospital for Special Surgery. 2012; 8(1):7-9.

Gosselin RD, Suter MR, Ji RR, Decosterd I. Glial cells and chronic pain. Neuroscientist. 2010; 16(5):519-531.

Grainger R, Cicuttini FM. Medical management of osteoarthritis of the knee and hip joints. The Medical Journal of Australia. 2004; 180(5):232-236.

Gregersen LS, Røsland T, Arendt-Nielsen L, Whiteside G, Hummel M. Unrestricted weight bearing as a method for assessment of nociceptive behavior in a model of tibiofemoral osteoarthritis in rats. Journal of Behavioral and Brain Science. 2013, 3:306-314.

Guzman RE, Evans MG, Bove S, Morenko B, Kilgore K. Mono-iodoacetate-induced histologic changes in subchondral bone and articular cartilage of rat femorotibial joints: an animal model of osteoarthritis. Toxicologic Pathology. 2003; 31(6):619-624.

Hanani M. Satellite glial cells in sensory ganglia: from form to function. Brain Research Reviews. 2005; 48(3):457-476.

Hare GM, Evans PJ, Mackinnon SE, Best TJ, Bain JR et al. Walking track analysis: a long-term assessment of peripheral nerve recovery. Plastic and Reconstructive Surgery. 1992; 89(2):251-258.

Haseeb A, Haqqi TM. Immunopathogenesis of osteoarthritis. Clinical Immunology. 2013; 146:185-196.

Haviv B, Bronak S, Thein R. The Complexity of Pain around the Knee in Patients with Osteoarthritis. Israel Medical Association Journal. 2013; 15(4):178-181.

Hayashi D, Roemer FW, Guermazi A. Imaging for osteoarthritis. Annals of Physical and Rehabilitation Medicine. 2016; 59(3):161-169.

Helmick CG, Felson DT, Lawrence RC, Gabriel S, Hirsch R et al. Estimates of the prevalence of arthritis and other rheumatic conditions in the United States. Part I. Arthritis and Rheumatism 2008; 58(1):15–25.

Hill CL, Hunter DJ, Niu J, Clancy M, Guermazi A et al. Synovitis detected on magnetic resonance imaging and its relation to pain and cartilage loss in knee osteoarthritis. Annals of the Rheumatic Diseases. 2007; 66(12):1599-1603.

Hu J, Yang Z, Li X, Lu H. C-C motif chemokine ligand 20 regulates neuroinflammation following spinal cord injury via Th17 cell recruitment. Journal of Neuroinflammation. 2016; 13(1):162.

Hummel M, Whiteside GT. Measuring and realizing the translational significance of preclinical in vivo studies of painful osteoarthritis. Osteoarthritis and Cartilage. 2016; S1063-4584(16)30242-4 (epub ahead of print).

Hunter DJ, Guermazi A. Imaging Techniques in Osteoarthritis. The American Academy of Physical Medicine and Rehabilitation. 2012; 4:S68-S74.

Im HJ, Kim JS, Li X, Kotwal N, Sumner DR et al. Alteration of sensory neurons and spinal response to an experimental osteoarthritis pain model. Arthritis and Rheumatism. 2010; 62(10):2995-3005.

Ishikawa G, Nagakura Y, Takeshita N, Shimizu Y. Efficacy of drugs with different mechanisms of action in relieving spontaneous pain at rest and during movement in a rat model of osteoarthritis. European Journal of Pharmacology. 2014; 738:111-117.

Ivanavicius SP, Ball AD, Heapy CG, Westwood FR, Murray F et al. Structural pathology in a rodent model of osteoarthritis is associated with neuropathic pain: increased expression of ATF-3 and pharmacological characterisation. Pain. 2007; 128(3):272-282.

Janusz MJ, Bendele AM, Brown KK, Taiwo YO, Hsieh L et al. Induction of osteoarthritis in the rat by surgical tear of the meniscus: Inhibition of joint damage by a matrix metalloproteinase inhibitor. Osteoarthritis and Cartilage. 2002; 10(10):785-791.

Ji RR, Woolf CJ. Neuronal plasticity and signal transduction in nociceptive neurons: implications for the initiation and maintenance of pathological pain. Neurobiology of Disease. 2001; 8(1):1-10.

Jordan KJ, Arden NK, Doherty M. EULAR recommendations 2003: an evidence based approach to the management of knee osteoarthritis: report of a Task Force of the Standing Committee for International Clinical Studies Including Therapeutic Trials (ESCISIT). Annals of the Rheumatic Diseases. 2003; 62(12):1145-1155.

Kalbhen DA. Chemical model of osteoarthritis--a pharmacological evaluation. Journal of Rheumatology. 1987; 14:130-131.

Kean WF, Kean R, Buchanan WW. Osteoarthritis: symptoms, signs and source of pain. Inflammopharmacology. 2004; 12(1):3-31.

Kellgren JH, Lawrence JS. Radiological assessment of osteo-arthosis. Annals of the Rheumatic Diseases. 1957; 16(4):494-502.

Kelly S, Dunham JP, Murray F, Read S, Donaldson LF et al. Spontaneous firing in C-fibers and increased mechanical sensitivity in A-fibers of knee joint-associated mechanoreceptive primary afferent neurones during MIA-induced osteoarthritis in the rat. Osteoarthritis and Cartilage. 2012; 20(4):305-313.

Kilkenny C, Browne W, Cuthill IC, Emerson M, Altman DG. Animal research: reporting in vivo experiments: the ARRIVE guidelines. British Journal of Pharmacology. 2010; 160(7): 1577–1579.

Kloefkorn HE, Jacobs BY, Loye AM, Allen KD. Spatiotemporal gait compensations following medial collateral ligament and medial meniscus injury in the rat: correlating gait patterns to joint damage. Arthritis Research and Therapy. 2015; 17:287-301.

Kuyinu EL, Narayanan G, Nair LS, Laurencin CT. Animal models of osteoarthritis: classification, update, and measurement of outcomes. Journal of Orthopaedic Surgery and Research. 2016: 11-19.

Lane NE, Brandt K, Hawker G, Peeva E, Schreyer E, Tsuji W et al. OARSI-FDA initiative: defining the disease state of osteoarthritis. Osteoarthritis and Cartilage. 2011; 19(5):478-482.

Lanza M, Ferrari F, Menghetti I, Tremolada D, Caselli G. Modulation of imidazoline I2 binding sites by CR4056 relieves postoperative hyperalgesia in male and female rats. British Journal of Pharmacology. 2014; 171(15):3693-701.

Lee Y, Pai M, Brederson JD, Wilcox D, Hsieh G et al. Monosodium iodoacetate-induced joint pain is associated with increased phosphorylation of mitogen activated protein kinases in the rat spinal cord. Molecular Pain. 2011; 7:39-48.

Li JX, Zhang Y. Imidazoline I2 receptors: target for new analgesics? European Journal of Pharmacology. 2011; 658(2-3):49-56.

Litwic A, Edwards MH, Dennison EM, Cooper C. Epidemiology and burden of osteoarthritis. British Medical Bulletin 2013; 105:185–199.

Loeser RF, Goldring SR, Scanzello CR, Goldring MB. Osteoarthritis: a disease of the joint as an organ. Arthritis and Rheumatism. 2012; 64(6):1697-1707.

Lories RJ, Luyten FP. The bone-cartilage unit in osteoarthritis. Nature Reviews. Rheumatology. 2011; 7(1):43-49.

Lowry JA, Brown JT. Significance of the imidazoline receptors in toxicology. Clinical Toxicology (Philadelphia Pa.). 2014; 52(5):454-69.

Malfait AM, Little CB, McDougall JJ. A commentary on modelling osteoarthritis pain in small animals. Osteoarthritis and Cartilage. 2013b; 21(9):1316-26.

Malfait AM, Little CB. On the predictive utility of animal models of osteoarthritis. Arthritis Research and Therapy. 2015; 17:225.

Malfait AM, Schnitzer TJ. Towards a mechanism-based approach to pain management in osteoarthritis. Nature Reviews. Rheumatology. 2013a; 9(11):654-664.

Mantyh PW. The neurobiology of skeletal pain. European Journal of Neuroscience. 2014; 39(3):508-519.

Mapp PI, Sagar DR, Ashraf S, Burston JJ, Suri S et al. Differences in structural and pain phenotypes in the sodium monoiodoacetate and meniscal transection models of osteoarthritis. Osteoarthritis and Cartilage. 2013; 21(9):1336-1345.

Martel-Pelletier J, Wildi LM, Pelletier JP. Future therapeutics for osteoarthritis. Bone. 2012; 51(2):297-311.

Mason RM, Chambers MG, Flannelly J, Gaffen JD, Dudhia J, Bayliss MT. The STR/ort mouse and its use as a model of osteoarthritis. Osteoarthritis and Cartilage. 2001; 9(2):85-91.

McAlindon TE, Bannuru RR, Sullivan MC, Arden NK, Berenbaum F et al. OARSI guidelines for the non-surgical management of knee osteoarthritis. Osteoarthritis and Cartilage. 2014; 22(3):363-388.

McCoy AM. Animal Models of Osteoarthritis: Comparisons and Key Considerations. Veterinary Pathology. 2015; 52(5):803-818.

McDougall JJ, Linton P. Neurophysiology of arthritis pain. Current Pain and Headache Reports. 2012; 16(6):485-491.

McGrath J, Drummond G, McLachlan E, Kilkenny C, Wainwright C. Guidelines for reporting experiments involving animals: the ARRIVE guidelines. British Journal of Pharmacology. 2010; 160(7):1573–1576.

Merashly M, Uthman I. Management of knee osteoarthritis: an evidence-based review of treatment options. Le Journal Medical Libanais. 2012; 60(4):237-242.

Meregalli C, Ceresa C, Canta A, Carozzi VA, Chiorazzi A et al. CR4056, a new analgesic I2 ligand, is highly effective against bortezomib-induced painful neuropathy in rats. Journal of Pain Research. 2012; 5:151-167.

Merskey H, Bogduk N. Part III: Pain Terms, A Current List with Definitions and Notes on Usage. In Merskey H, Bogduk N, editors. Classification of Chronic Pain, second edition. Seattle: IASP Press. 1994; 209-214.

Michael JW, Schlüter-Brust KU, Eysel P. The epidemiology, etiology, diagnosis, and treatment of osteoarthritis of the knee. Deutsches Ärzteblatt international. 2010; 107(9):152-162.

Millan MJ. Descending control of pain. Progress in Neurobiology. 2002; 66(6):355-474.

Mizner RL, Snyder-Mackler L. Altered loading during walking and sit-to-stand is affected by quadriceps weakness after total knee arthroplasty. Journal of Orthopaedic Research. 2005; 23(5):1083-1090.

Nwosu LN, Mapp PI, Chapman V, Walsh DA. Blocking the tropomyosin receptor kinase A (TrkA) receptor inhibits pain behaviour in two rat models of osteoarthritis. Annals of the Rheumatic diseases. 2016; 75(6):1246-1254.

O'Callaghan JP, Miller DB. Spinal glia and chronic pain. Metabolism. 2010; 59(Suppl 1):S21-S26.

Orita S, Ishikawa T, Miyagi M, Ochiai N, Inoue G et al. Pain-related sensory innervation in monoiodoacetate-induced osteoarthritis in rat knees that gradually develops neuronal injury in addition to inflammatory pain. BMC Musculoskeletal Disorders. 2011; 12:134-145.

Otis C, Gervais J, Guillot M, Gervais JA, Gauvin D et al. Concurrent validity of different functional and neuroproteomic pain assessment methods in the rat osteoarthritis monosodium iodoacetate (MIA) model. Arthritis and Rheumatism. 2016; 18:150-165.

Palazzo C, Nguyen C, Lefevre-Colau MM, Rannou F, Poiraudeau S. Risk factors and burden of osteoarthritis. Annals of Physical and Rehabilitation Medicine. 2016; 59(3):134-138.

Palazzo C, Ravaud J-F, Papelard A, Ravaud P, Poiraudeau S. The burden of musculoskeletal conditions. PLoS One. 2014; 9(3):e90633.

Paxinos G, Watson C. The rat brain in stereotaxic coordinates. 1st edition, Academic Press.

Pertovaara A. Noradrenergic pain modulation. Progress in Neurobiology. 2006; 80(2):53-83.

Platzer W. Color atlas and textbook of human anatomy. Locomotor system, vol. I. 5th edition, Thieme Flexibook.

Pomonis JD, Boulet JM, Gottshall SL, Phillips S, Sellers R et al. Development and pharmacological characterization of a rat model of osteoarthritis pain. Pain. 2005; 114(3):339-346.

Poulet B, Staines KA. New developments in osteoarthritis and cartilage biology. Current opinion in pharmacology. 2016; 28:8-13.

Pritzker KP. Animal models for osteoarthritis: processes, problems and prospects. Annals of the Rheumatic Diseases. 1994; 53(6):406-420.

Punzi L, Galozzi P, Luisetto R, Favero M, Ramonda R et al. Post-traumatic arthritis: overview on pathogenic mechanisms and role of inflammation. RMD open. 2016; 2(2):e000279.

Qiu Y, He XH, Zhang Y, Li JX. Discriminative stimulus effects of the novel imidazoline I2 receptor ligand CR4056 in rats. Scientific Reports. 2014; 4:6605.

Raychaudhuri SP, Raychaudhuri SK, Atkuri KR, Herzenberg LA, Herzenberg LA. Nerve growth factor: A key local regulator in the pathogenesis of inflammatory arthritis. Arthritis and Rheumatism. 2011; 63(11):3243-3252.

Read SJ, Dray A. Osteoarthritic pain: a review of current, theoretical and emerging therapeutics. Expert Opinion on Investigational Drugs. 2008; 17(5):619-640.

Ren K, Dubner R. Interactions between the immune and nervous system in pain. Nature Medicine. 2010; 16(11):1267-1276.

Robinson WH, Lepus CM, Wang Q, Raghu H, Mao R et al. Low-grade inflammation as a key mediator of the pathogenesis of osteoarthritis. Nature reviews. Rheumatology. 2016; 12(10):580-592.

Rousseau JC, Garnero P. Biological markers in osteoarthritis. Bone. 2012; 51(2):265-277.

Ruiz-Durántez E, Ruiz-Ortega JA, Pineda J, Ugedo L. Effect of agmatine on locus coeruleus neuron activity: possible involvement of nitric oxide. British Journal of Pharmacology. 2002; 135(5):1152-1158.

Sagar DR, Burston JJ, Hathway GJ, Woodhams SG, Pearson RG et al. The contribution of spinal glial cells to chronic pain behaviour in the monosodium iodoacetate model of osteoarthritis pain. Molecular Pain. 2011; 7:88.

Salaffi F, Ciapetti A, Carotti M. The sources of pain in osteoarthritis: a pathophysiological review. Reumatismo. 2014; 66(1):57-71.

Sánchez-Blázquez P, Boronat MA, Olmos G, García-Sevilla JA, Garzón J. Activation of I(2)-imidazoline receptors enhances supraspinal morphine analgesia in mice: a model to detect

agonist and antagonist activities at these receptors. British Journal of Pharmacology. 2000; 130(1):146-152.

Santos-Nogueira E, Redondo Castro E, Mancuso R, Navarro X. Randall-Selitto Test: A New Approach for the Detection of Neuropathic Pain after Spinal Cord Injury. Journal of Neurotrauma. 2012; 29(5):898–904

Sarikcioglu L, Demirel BM, Utuk A. Walking track analysis: an assessment method for functional recovery after sciatic nerve injury in the rat. Folia Morphologica (Warsz). 2009; 68(1):1-7.

Sarzi-Puttini P, Cimmino MA, Scarpa R, Caporali R, Parazzini F et al. Osteoarthritis: an overview of the disease and its treatment strategies. Seminars in Arthritis and Rheumatism. 2005; 35(1 Suppl 1):1-10.

Scanzello CR, Goldring SR. The Role of Synovitis in Osteoarthritis pathogenesis. Bone. 2012; 51(2):249-257.

Siemian JN, Obeng S, Zhang Y, Zhang Y, Li JX. Antinociceptive Interactions between the Imidazoline I2 Receptor Agonist 2-BFI and Opioids in Rats: Role of Efficacy at the μ-Opioid Receptor. Journal of Pharmacology and Experimental Therapeutics. 2016; 357(3):509-519.

Sinusas K. Osteoarthritis: diagnosis and treatment. American Family Physician. 2012; 85(1):49-56.

Sofat N, Ejindu V, Kiely P. What makes osteoarthritis painful? The evidence for local and central pain processing. Rheumatology. 2011; 50(12):2157-2165.

Sofat N, Kuttapitiya A. Future directions for the management of pain in osteoarthritis. International Journal of Clinical Rheumatology. 2014; 9(2):197-216.

Sokolove J, Lepus CM. Role of inflammation in the pathogenesis of osteoarthritis: latest findings and interpretations. Therapeutic Advances in Musculoskeletal Disease. 2013; 5(2):77-94.

Stemkowski PL, Smith PA. Sensory neurons, ion channels, inflammation and onset of neuropathic pain. The Canadian Journal of Neurological Sciences. 2012; 39(4):416-435.

Suri P, Morgenroth DC, Hunter DJ. Epidemiology of osteoarthritis and associated comorbidities. PM & R: the journal of injury, function and rehabilitation. 2012; 4(5):S10-19.

Takeda M, Takahashi M, Matsumoto S. Contribution of the activation of satellite glia in sensory ganglia to pathological pain. Neuroscience and Biobehavioral Reviews. 2009; 33(6):784-792.

Thakur M, Dickenson AH, Baron R. Osteoarthritis pain: nociceptive or neuropathic? Nature Reviews Rheumatology. 2014; 10:374-380.

Thakur M, Rahman W, Hobbs C, Dickenson AH, Bennett DL. Characterisation of a peripheral neuropathic component of the rat monoiodoacetate model of osteoarthritis. PLoS One. 2012; 7(3):e33730.

Thorn DA, An XF, Zhang Y, Pigini M, Li JX. Characterization of the hypothermic effects of imidazoline I2 receptor agonists in rats. British Journal of Pharmacology. 2012; 166(6):1936-1945.

Vaishya R, Pariyo GB, Agarwal AK, Vijay V. Non-operative management of osteoarthritis of the knee joint. Journal of Clinical Orthopaedics and Trauma. 2016; 7(3):170-176.

Varejão AS, Meek MF, Ferreira AJ, Patrício JA, Cabrita AM. Functional evaluation of peripheral nerve regeneration in the rat: walking track analysis. Journal of Neuroscience Methods. 2001; 108(1):1-9.

Walsh RN, Cummins RA. The Open-Field Test: a critical review. Psychological Bulletin. 1976; 83(3):482-504.

Wen J, Sun D, Tan J, Young W. A consistent, quantifiable, and graded rat lumbosacral spinal cord injury model. Journal of Neurotrauma. 2015; 32(12):875-892.

Wen YR, Tan PH, Cheng JK, Liu YC, Ji RR. Microglia: a promising target for treating neuropathic and postoperative pain, and morphine tolerance. Journal of the Formosan Medical Association. 2011; 110(8):487-494.

Wu CL, Raja SN. Treatment of acute postoperative pain. Lancet. 2011; 377(9784):2215–2225.

Yu D, Liu F, Liu M, Zhao X, Wang X et al. The inhibition of subchondral bone lesions significantly reversed the weight-bearing deficit and the overexpression of CGRP in DRG neurons, GFAP and Iba-1 in the spinal dorsal horn in the monosodium iodoacetate induced model of osteoarthritis pain. PLoS One. 2013; 8(10):e77824.

Yu DG, Nie SB, Liu FX, Wu CL, Tian B et al. Dynamic Alterations in Microarchitecture, Mineralization and Mechanical Property of Subchondral Bone in Rat Medial Meniscal Tear Model of Osteoarthritis. Chinese Medical Journal. 2015; 128(21):2879-2886.

Yu DG, Yu B, Mao YQ, Zhao X, Wang XQ et al. Efficacy of zoledronic acid in treatment of teoarthritis is dependent on the disease progression stage in rat medial meniscal tear model. Acta Pharmacologica Sinica. 2012; 33(7):924-934.

Zhang W, Nuki G, Moskowitz RW, Abramson S, Altman RD et al. OARSI recommendations for the management of hip and knee osteoarthritis, Part II: OARSI evidence-based, expert consensus guidelines. Osteoarthritis and Cartilage. 2008; 16(2):137-162.

Zhang W, Ouyang H, Dass CR, Xu J. Current research on pharmacologic and regenerative therapies for osteoarthritis. Bone Research. 2016; 4:15040.

Zhang Y, Jordam JM. Epidemiology of Osteoarthritis. Clinics in Geriatric Medicine. 2010; 26(3):355-369.

9. ACKNOWLEDGEMENTS

"I can no other answer make but thanks, and thanks; and ever thanks." [William Shakespeare]

First, I would like to express my sincere gratitude to Dr. Lucio Rovati, for giving me the opportunity to carry out my PhD project within the laboratory and research facilities of the Pharmacology and Toxicology Department of Rottapharm Biotech.

My research would have been impossible without the financial support of Rottapharm Biotech S.r.l.

I would also like to thank Dr. Guido Cavaletti and his research group for giving me access to their laboratory instruments and equipment.

I am profoundly grateful to Dr. Gianfranco Caselli, my tutor Dr. Marco Lanza and Dr. Flora Ferrari for all the advice, moral support and patience in guiding me through this project and helping me to grow as a research scientist.

I would like to sincerely thank Luca, Dario, Chiara M., Francesca, Raffaella, Emanuele, Paolo, Marco, Silvia, Daniele, Mario, Sergio, Chiara G., Chiara S., Roberto, Rosanna and all my others colleagues. Each one of you have helped me and supported me in many ways in the last three years. Thank you for all the insightful discussions and laughs we have shared. You have been not only a source of good advice and collaboration, but friendship as well.

Special thanks to Alessia, Federica, Valentina, Lara and my others former fellow colleagues and friends for their precious friendship and support.

Infinite heartfelt thanks to Marina and Elena, my dearest Friends. You have always been there to advise me, encourage me, comfort me or just hug me, especially in the last three years. I deeply cherish our friendship.

Finally, I would like to thank my family, for its unconditional love and support throughout my life.

Last but not least, I would like to express my profound gratitude to Fabio, for always standing beside me and unremittingly encouraging me. You are my safe harbour. Thank you for making me more than I am. This journey would not have been possible without you.